

DISSERTATION

DONOR-APPENDED SENSITIZERS AND FURTHER EXPLORATION OF COBALT
POLYPYRIDYL MEDIATORS: BEHAVIOR AND CONSEQUENCES IN DYE-SENSITIZED
SOLAR CELLS

Submitted by

Lance Ashbrook

Department of Chemistry

In partial fulfillment of the requirements

for the Degree of Doctor of Philosophy

Colorado State University

Fort Collins, Colorado

Fall 2014

Doctoral Committee:

Advisor: Anthony Rappé

Martin Gelfand

Alan Kennan

Branka Ladanyi

Matthew Shores

Copyright by Lance Noel Ashbrook 2014

All Rights Reserved.

ABSTRACT

DONOR-APPENDED SENSITIZERS AND FURTHER EXPLORATION OF COBALT POLYPYRIDYL MEDIATORS: BEHAVIOR AND CONSEQUENCES IN DYE-SENSITIZED SOLAR CELLS

Dye-sensitized solar cells (DSCs) have been thoroughly investigated over the past two decades as viable alternatives to traditional silicon solar cells. Fueling this research is the potential for DSCs to exhibit comparable efficiencies to silicon but at a fraction of the cost due to the generally cheaper materials employed. This dissertation presents studies conducted with cobalt polypyridyl mediators as substitutes for the more commonly employed I^-/I_3^- . In addition, several novel sensitizers are synthesized incorporating electron donors in order to separate the injected electron and subsequent hole on the dye.

Chapter 1 reviews a brief history of DSC development and the relevant processes in an operational cell. The interplay of these processes is discussed. Commonly employed materials are presented as well as alternatives used in the literature and in the work throughout this dissertation. Instrumentation and methods utilized throughout this work are also discussed.

The use of copper polypyridyl dyes in DSCs is discussed in Chapter 2. While there is literature precedent for these materials as sensitizers, very few studies exist due to inherent issues to the sensitizers that are not shared with the more traditional ruthenium dyes. These problems are highlighted and discussed in the context of sensitizer design. One of the primary issues is the coordination of mediator additives to the oxidized copper center, rendering it unable to participate in further photoexcitation. Studies are presented that show the incorporation of a

phenothiazine-type electron donor into the sensitizer results in rapid reduction of the copper center and prevents additional coordination.

Electrochemical and cell testing studies are presented in Chapter 3 that partially explain why the addition of lithium ion to the mediator solution results in better DSC current values, particularly with cobalt mediators. The electrochemistry of the $\text{Co}^{2+/3+}$ couple on FTO appears to be highly dependent on cations present in solution. Li^+ present in solution results in current being “shut off” at the FTO surface. Thus, Li^+ addition leads to an additional charge transfer resistance at the anode which leads to a reduction in undesired electron scavenging.

Although platinum films or platinized FTO are the usual materials of choice for DSC cathodes, they generally perform better when used in conjunction with I^-/I_3^- . The cobalt complexes employed as alternative mediators tend to exhibit more reversible electrochemistry on gold, but gold cathodes have historically been difficult to fabricate reproducibly. Chapter 4 probes a sulfide modification technique that appears to improve gold cathode performance. Based on the data presented, the mediator additive *t*-butyl pyridine weakly adsorbs to the gold surface which disrupts the electronic coupling with an oxidized cobalt complex. Modification with sulfide ion results in a lower charge transfer resistance at the surface which translates to a better fill factor.

Finally, the last chapter further explores the use of incorporating a phenothiazine electron donor into the sensitizer. In this chapter, novel ruthenium dyes are synthesized and evaluated against some commonly employed sensitizers in the literature. The relevant processes are more difficult to elucidate in these systems than in the copper systems due to the similar absorption profiles of the $\text{Ru} \rightarrow \text{ligand}$ MLCT and oxidized phenothiazine. This makes the important technique of transient absorption more problematic to employ. Therefore, the effect of the donor

is evaluated based primarily off cell testing data. The de-convolution of mass transport and donor effects is attempted by comparing with Z-907, which is a commonly used sterically demanding sensitizer. Additional experiments are also suggested which would offer more insight into this competition.

ACKNOWLEDGEMENTS

The career of a graduate student begins long before one actually enters graduate school. The passion for a field must manifest, develop, and be stoked for years. In my case, although they will never know it, the likes of Mr. Wizard (Don Herbert), Beakman (Paul Zaloom), and Bill Nye were responsible for manifesting my love of science. My high school chemistry teachers, Ms. Dennis and Mrs. George, pointed me towards chemistry. The combined efforts of the entire Department of Chemistry at Virginia Tech, especially those of Dr. Brian Tissue and Dr. James Tanko, further convinced me to be a Ph.D. chemist.

My family deserves a lot of credit as well. My mother, Penny Ashbrook, has always pushed me to succeed, no matter the circumstances, from when I was a small child to last week. My father, Lance Ashbrook Sr., taught me never to take life too seriously, a lesson which has helped me immeasurably throughout graduate school work. The stubbornness I got from both of them. They both have my profound love and thanks. My wife, JonEll Ashbrook, and her two daughters Savannah and Rinoa, have been incredibly supportive throughout my entire graduate school career, even living an hour away from CSU. I especially have to thank my wife for the years of not killing me every night I got home late when we had plans.

Finally, I must thank my late advisor, C. Michael Elliott. He taught me nearly everything I know about chemistry, though it was not even a shade of his own knowledge. I cannot even begin to thank him for his mentorship over the past several years. Instead, I will thank him simply for not collecting on my substantial bill for stupid questions. Even though I never got to share it in full, I hope he knew how much I appreciated him, and how much I regret that I did not get to buy him that drink I owed.

TABLE OF CONTENTS

Chapter 1: Dye-Sensitized Solar Cells - History, Principles, and Techniques	1
A Brief History	1
The Grätzel Cell	2
DSC Component Selection	5
Replacing the Γ/I_3^- Mediator	9
Applied Techniques in Solar Cell Evaluation	13
Chapter 1 References	24
Chapter 2: Dye-Sensitized Solar Cell Studies of a Donor-Appended Bis(2,9-dimethyl-1,10-phenanthroline) Cu(I) Dye Paired with a Cobalt-Based Mediator	27
Introduction	27
Experimental	40
Results and Discussion	48
Conclusions	73
Chapter 2 References	75
Chapter 3: Tris(4,4'-di- <i>t</i> -butyl-2,2'-bipyridine)cobalt: Cation Effects on the Voltammetry at ITO and on Mediator Performance in Dye-Sensitized Solar Cells	79
Introduction	79
Experimental	81
Results and Discussion	82
Conclusions	91
Chapter 3 References	93
Chapter 4: Sulfide Modification of Dye-Sensitized Solar Cell Gold Cathodes for Use with Cobalt Polypyridyl Mediators	95
Introduction	95
Experimental	97
Results and Discussion	99

Conclusions	115
Chapter 4 References	117
Chapter 5: Donor-Appended N3-Type Sensitizers	120
Introduction	120
Experimental	122
Results and Discussion.....	127
Future Directions	139
Conclusions	141
Chapter 5 References	143

Chapter 1: Dye-Sensitized Solar Cells – History, Principles, and Techniques

A Brief History

Photovoltaics are generally classified into three main generations. The first generation is characterized by high cost, highly efficient cells. The traditional crystalline silicon cells fall under this class. Cells of the second generation attempt to cut costs by transitioning to thin film technologies such as CdTe or copper indium gallium selenide (CIGS) and have reached respectable efficiencies through years of research.¹ The third class, of which dye-sensitized solar cells (DSCs) are a part, attempts to maintain low costs while boosting efficiency.

The idea of “spectral sensitization” (i.e., dyeing materials) is, obviously, not a particularly new notion. Although the thought of adsorbing a dye to the surface of a semiconductor for solar harvesting is a relatively new notion, the concept has been around for more than a century. Histories of sensitization have been summed up quite nicely elsewhere.^{2,3} The notion could be said to be born in the work of Hermann Vogel, a German painter in the late 1800s who found that exposing photographic plates to yellow dye made them sensitive to green light. It then evolved over the course of ca. 100 years as the transition from photographic applications to photoelectric applications came to fruition.

In the early 1990s, Michael Grätzel and Brian O'Regan applied this concept to a new system based on a three-dimensional mesoporous TiO₂ substrate.^{4,5} Nanocrystalline TiO₂, a fairly cheap and common material used as a white pigment in paint, has a bandgap of 3.2 eV in its anatase form. This places its absorption λ_{max} in the UV. While the absorption of photons at these energies itself is not problematic, the solar flux at those wavelengths is fairly small due to atmospheric filtering (Fig. 1.1). This makes the material, by itself, a poor solar energy harvester.

However, by adsorbing a dye to the TiO_2 surface, Grätzel and O'Regan were able to red-shift the photoactive region sufficiently to harvest photons at the point close to maximum solar irradiance.^{4,5} Thus the idea of the DSC was born.

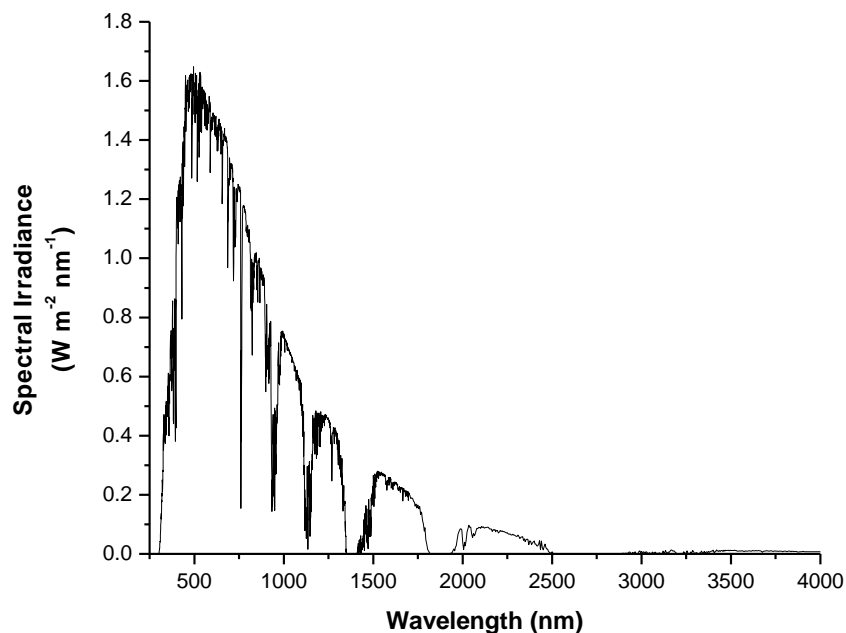


Figure 1.1. “1-sun” solar irradiance incident on Earth’s surface. Significant negative valleys in the spectrum are due to absorption by atmospheric gases (primarily CO_2 and H_2O).

The Grätzel Cell

The dyed semiconductor, while crucial for these devices, is only one component of the cell. When the dye absorbs a solar photon, an electron is promoted to a higher energy orbital within the dye (Fig. 1.2). If the dye molecule were free in solution, then the complex would relax back to the ground state. By adsorbing the dye to a semiconductor, the electron can be transported from the dye to the conduction band of the semiconductor. This results in a large population of electrons in the semiconductor, as well as a large population of oxidized surface-bound dye molecules. In the absence of any other redox options, the conduction band electrons

would eventually regenerate the ground state of the dye due to the large thermodynamic driving force borne from the energy difference between the semiconductor Fermi energy and the dye ground-state redox potential. Thus, to harvest the electron, additional components must be included to direct the electron through a load before it recombines with the hole on the dye.

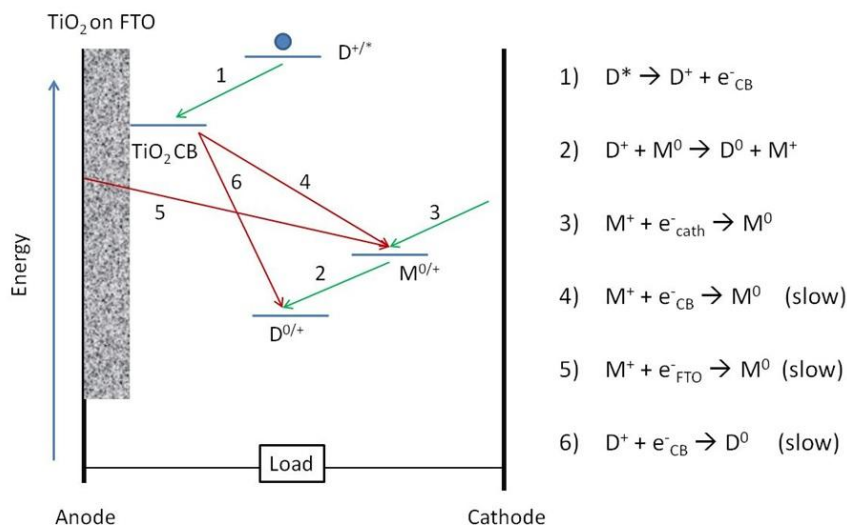


Figure 1.2. Diagram of relevant DSC processes post-excitation of dye. For maximum performance, electron transfer events depicted by red arrows should be slow.

On the semiconductor side, matters are fairly simple. If the main issue (at least, insofar as the current discussion is concerned) is recombination of already-injected electrons with a hole on the dye, then transport of the electrons away from the dye should suffice to mitigate this problem. This can easily be accomplished by mounting the nanocrystalline TiO₂ onto a substrate that supports rapid electron transport away from the dye. In principle this current collector could be one of many conductive materials, but for reasons that will be briefly discussed shortly and in more depth in Chapter 3, a conductive glass such as fluorine-doped tin oxide (FTO) or indium tin oxide (ITO) functions superbly for this task.

Matters are far more complicated on the sensitizer side. After photo-excitation and injection into the semiconductor, the dye is left in a formally oxidized state. In order for the dye

to return to photoactivity, it must be reduced back to its original oxidation form. Provided the injected electron has been transported away from the dye, another species (the mediator) is needed to donate an electron to the dye. The requirements on the mediator are that it must possess a redox potential at a higher energy (i.e., more negative potential) than the ground state of the dye, and that the electron transfer kinetics between it and the oxidized site on the dye (the metal center in the case of inorganic dyes) must be slower than electron injection from the excited state of the dye to the TiO_2 conduction band but faster than recombination of the dye ground state hole with the photoinjected TiO_2 electron.

To complete the circuit, the current-collecting substrate for the photoanode must be connected to a load and then to another electrode (the cathode) for the electron to be re-introduced back into the cell. This electron serves to regenerate the mediator used to reduce the metal center, returning all chemical species to their original oxidation states and effectively resetting the system for another photoexcitation. The cathode must be comprised of a material that efficiently catalyzes the reduction of the mediator, so the selection of one dictates the other to some extent.

Relevant electron transfer events and rate requirements are presented in Fig. 1.2. Green arrows indicate desired processes, while arrows in red indicate unwanted processes. To summarize the diagram, once the electron is elevated to an excited state it can relax back to the ground state, inject into the semiconductor, or recombine with a hole on an existing oxidized mediator species. The injection rate must then be faster than relaxation or mediator hole recombination. Once the electron is in the semiconductor, mobile mediator species can intercept it from the conduction band before it can diffuse through to the current collecting substrate. This

rate can be heavily influenced by the TiO₂ film thickness, dye coverage, and dye and/or mediator steric footprint. After the electron passes through the circuit, it must effectively reduce oxidized mediator at the cathode. Finally, the mediator must be capable of quickly regenerating the ground state of the dye for further photochemistry to occur.

The complex interplay of several interfacial chemistries results in a solar cell that can be terribly difficult to optimize. The selection of a single component largely dictates the possible range of other components. To capture the most light the dye must absorb strongly in the visible region, and the HOMO and LUMO energies will dictate what semiconductors and what mediators will be acceptable to maintain sufficient thermodynamic driving force for the desired electron transfers. For this reason it is frequently not a productive endeavor to only change one component of the system. Attempting to optimize a particular system has generally resulted in nominal increases in cell performance compared with the archetypal N3 dye (see Fig. 1.4 for structure), I/I₃⁻/Pt, TiO₂ system.⁵ For example, nearly two decades passed for an improvement from 10% efficiency to 12% to be realized.⁶ The shortcomings of this system will now be addressed, along with proposed alternatives that serve as the basis for the current work.

DSC Component Selection

For many years [Ru(bpy)₃]²⁺-based complexes have been studied for their impressive photophysical characteristics (bpy = 2,2'-bipyridyl, Fig. 1.3).⁷ When used as a dye, one bpy ligand is generally replaced by two SCN⁻ groups. This substitution red-shifts the λ_{max} and renders the complex net neutral.⁵ These complexes exhibit properties relevant to DSCs, including long excited-state lifetimes and relatively high (up to ca. 14,000 M⁻¹ cm⁻¹) molar

extinction coefficients at wavelengths near 530 nm.⁵ Subsequent research⁸⁻¹¹ yielded several ruthenium polypyridyl-based dyes, the most studied of which are shown in Fig. 1.4.

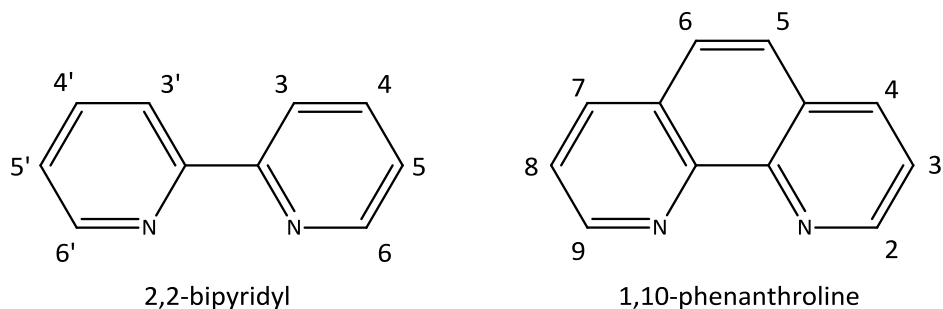


Figure 1.3. Structures of bpy and phen with ring substitution positions labeled.

Beyond the photophysical requirements briefly described above, the dye must have a pathway to electronically and physically couple with the semiconductor. Generally this is accomplished with carboxylic acids or their corresponding salts but other functional groups such as phosphonic acids can also be used.¹¹ In addition, regardless of where its λ_{max} lies, the LUMO needs to reside at a higher energy than the semiconductor conduction band for efficient electron injection.

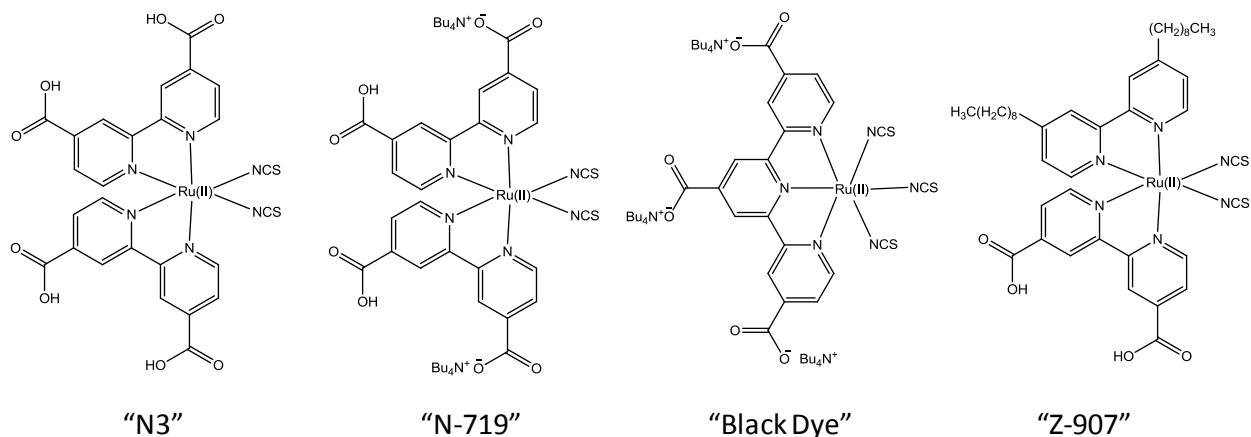


Figure 1.4. Structures of the more common Ru polypyridyl dyes.

While the $[\text{Ru}(\text{bpy})_3]^{2+}$ -based dyes satisfy all of these requirements, they are still based on a rare and expensive metal center. Since the main goal of DSCs is to provide a drastically cheaper option to expensive silicon processing, this remains a rather large issue. In order to address this problem, several of the dyes investigated in the current work are based on $[\text{Cu}(\text{phen})_2]^+$ complexes, where phen = 1,10-phenanthroline (see Fig. 1.3). These complexes exhibit some similar qualities to their ruthenium counterparts, but also require additional considerations that will be presented in depth in Chapter 2.

Organic sensitizers have also been a large focus of investigators in recent years since the report of “D5” by Sun and Hagfeldt in 2006.¹² Low processing costs satisfy the requirement of 3rd Generation photovoltaic technologies, though their overall power conversion efficiencies are typically lower than their inorganic counterparts.¹³ In an inorganic sensitizer, the electron is physically separated from the hole since the electron excitation is of MLCT nature. Since organic sensitizers are generally conjugated molecules, electron-hole recombination occurs at much faster rates. This shortcoming has been the primary focus of organic DSC improvement. Still, impressive progress has been made in the area in a relatively short amount of time.¹³

A very recent but intense category of DSC research has been focused on perovskites. Initially these were employed as traditional sensitizers in place of common ruthenium complexes.¹⁴ Further developments over a few years yielded surprisingly 15% efficient cells.¹⁵ Snaith and coworkers have recently reported the ability of these materials to operate in similarly efficient working cells without the use of a TiO_2 semiconducting layer.¹⁶ A recently published optimization study of this technology yielded a 19.3% efficient cell¹⁷, making it highly competitive with existing silicon cells if replicated on a commercial scale.

Although TiO_2 was (and still remains) the principal semiconductor of investigation for DSCs in most labs, the identity of the semiconductor can be changed based on the electronics of the system in question. Again, changing one component can have ripple effects on the rest of the DSC system requirements, but in principle the semiconductor identity may be changed as long as the dye can still photoinject an excited electron. As an additional practical consideration, the semiconductor should not compete appreciably with the dye for visible light absorption (otherwise, the dye would not be necessary). This is a non-issue for wide-bandgap semiconductors like TiO_2 that primarily absorb in the UV. However, if visible photons can be absorbed by the semiconductor, then the dye should be engineered to complement that profile rather than overlap it. Selection of the semiconductor and dye can therefore be a conjoined process.

As the maximum open-circuit voltage (V_{OC}) allowed is determined in part by the Fermi energy of the semiconductor (and therefore by the conduction band edge), it is tempting to replace TiO_2 with a semiconductor possessing a higher energy conduction band. To elaborate this point, consider the energetics of the classic Grätzel system in Fig. 1.5. If a semiconductor were chosen with a conduction band 300 mV higher than TiO_2 , then the electron would be unable to inject from the dye excited state. Assuming a dye could be designed such that the HOMO remained the same as N3 but the LUMO shifted 300 mV higher and all else remained the same, then the V_{OC} could be substantially increased. However, this would also blue-shift the absorption profile of the dye significantly and lead to lower currents due to a lower fraction of solar photons being absorbed. All of this is to say that although the semiconductor can be changed, it is most certainly a non-trivial matter and judicious planning of the dye and mediator components is also necessary.

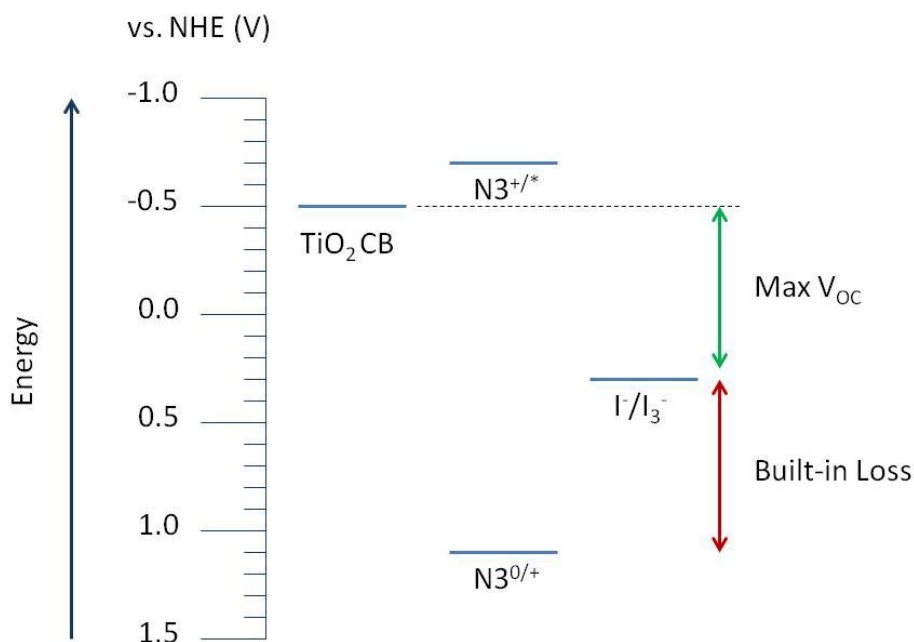


Figure 1.5. Energy diagram of archetype N3 system coupled with I^-/I_3^- .

Replacing the I^-/I_3^- Mediator

The most commonly altered components of a DSC are the dye and the mediator. Although new dyes are sometimes designed in systems employing alternative mediators^{6,18–20}, frequently they are present in the literature coupled with the I^-/I_3^- mediator.^{4,5,8,21,22} Although the investigation of novel sensitizers is a primary concern in the work described here, the specific background pertaining to those dyes will be discussed in subsequent chapters. However, it is relevant to discuss the selection of alternate mediator species (i.e., other than I^-/I_3^-) at this time since Chapters 2–5 focus on their usage.

Considering the generally good performance and widespread usage of I^-/I_3^- in the literature, the substitution of this mediator may seem an unnecessary pursuit. However, I^-/I_3^- has a number of shortcomings. It is toxic, corrosive to many metals, and has a fixed redox couple. In the case of N3-type dyes, the fixed redox couple corresponds to a ca. 500 mV loss in

theoretical maximum photovoltage (see Fig. 1.5). Its corrosiveness and electrochemistry also necessitate the use of platinum cathodes, an obvious cost escalator, though the advent of solution-processable platinized cathodes mitigates this to some extent. Because I_2 is an intermediary in the rather complicated I^-/I_3^- formation process, cells must also be sealed to avoid evaporative losses. Generally this means that the anode and cathode are essentially one-time use, which is acceptable from a commercialization standpoint if the cell is to stand for 20 years but potentially a large headache from a laboratory research standpoint.

Despite all of the downsides to I^-/I_3^- , it tends to function exceedingly well for the evaluation of N3-type dyes. Although complicated, the electron transfer processes at both the photoanode (regeneration of the dye ground state) and the cathode (catalyzed reduction of I_3^- by Pt) are quite fast.^{11,23} In addition, recombination with photoinjected e_{CB} 's is quite slow. These properties lead to improvements in photocurrent and fill factor over alternative mediators that generally outweigh the loss of photovoltage to result in higher overall cell efficiencies.

Several mediator species have been investigated as alternatives to I^-/I_3^- including ferrocene/ferrocenium (and derivatives), Ni(III/IV) bis(dicarbollide), Cu(I) bis(phenanthroline), and hole-conducting organic polymers.^{11,24} Over the past decade or so, $[Co(LL)_3]^{2+}$ -type complexes (LL = 2,2'-bipyridyl or 1,10-phenanthroline) have emerged as potential mediator alternatives to I^-/I_3^- .^{6,25-30} These complexes are non-volatile and non-corrosive to metals, making them attractive practical options. They also absorb light poorly ($\epsilon \approx 100 \text{ M}^{-1} \text{ cm}^{-1}$) so as to not compete with dye absorption. In addition, and quite possibly the most important feature from a device performance standpoint, the $E_{1/2}$ of the $2+/3+$ couple can be shifted substantially by ligand variation which could lead to a higher cell V_{OC} when the $E_{1/2}$ is shifted to a more positive potential than that of I^-/I_3^- .

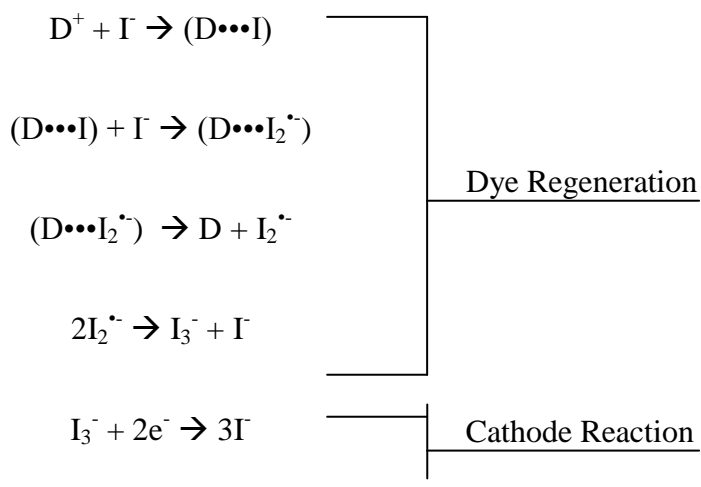
Strictly speaking, the thermodynamic requirement of the mediator is that its redox potential lies sufficiently negative of the dye ground state to support facile regeneration of the dye. However, this requirement is simply satisfied by a large number of compounds if that were the only consideration. Given that this requirement is fulfilled, more complicated kinetic conditions must also be met: 1) fast electron transfer from the reduced form of the mediator to the oxidized dye and 2) fast reduction of the oxidized mediator at the cathode (see Figure 1.2 above). While $[\text{Co}(\text{LL})_3]^{2+}$ -type complexes satisfy the first condition without much trouble, the second condition depends strongly on other factors.

First, Pt is inappropriate as a cathode material for these cells. While Pt is a fantastic catalyst for the I^-/I_3^- couple, the generally poor electronic coupling between the Pt cathode and $[\text{Co}(\text{LL})_3]^{3+}$ -type complexes results in slow electron-transfer kinetics at the electrode's surface.²⁷ Glassy carbon is a better catalyst option for these complexes, but gold tends to exhibit the fastest, most reversible electron transfer kinetics (subject to cathode history and complex identity – see Chapter 4).²⁷ Platinizing a suitable glass or FTO substrate by thermally decomposing chloroplatinic acid on the surface yields relatively cheap cathodes for use with I^-/I_3^- .^{31,32} In contrast, gold cathodes are manufactured by thermally evaporating high purity gold onto the substrate surface. This actually results in a more expensive cathode due to the processing method *at this scale*. However, if care is taken in fabrication and preservation of the surface between measurements, then this cost can largely be considered negligible over the life of the cathode regardless of the catalytic material used and provided that the cell is not sealed (i.e., if the cathode is not one-time use).

Second, the electrochemistry of I^-/I_3^- is rather complicated due to it being a multi-electron/multi-atom process (Scheme 1.1). On the other hand, the cobalt complexes in question

undergo one-electron reductions and oxidations. While at first glance this might seem to be advantageous as far as the reduction of oxidized dye (also a one-electron process), the kinetics of reduction for either mediator are quite fast.³⁰ In other words, the simplified oxidative process from Co^{2+} to Co^{3+} does not lead to any substantial improvement in dye regeneration. Unfortunately, the simplified reduction of Co^{3+} to Co^{2+} does have a noticeable detrimental effect due to increased scavenging of conduction band electrons. Several years ago Gregg et al.

Scheme 1.1. Electrochemical Mechanism of I^-/I_3^- Mediator



showed that one-electron mediators such as ferrocene/ferrocenium (Fc/Fc^+) could perform competently if a recombination barrier was placed between the TiO_2 and the mediator.³³ In 2011 Spiccia et al. further validated this approach by demonstrating a 7.5% overall efficient cell using Fc/Fc^+ in conjunction with a sterically demanding organic dye and an anti-aggregate.³⁴ Although both of these approaches utilized a barrier extending out from the TiO_2 surface, the barrier could also be incorporated into the mediator design. For instance, replacing $\text{LL} = \text{bpy}$ in $[\text{Co}(\text{LL})_3]^{2+}$ with $\text{LL} = \text{DMB}$ or DTB ($\text{DMB} = 4,4'$ -di-methyl-2,2'-bipyridyl and $\text{DTB} = 4,4'$ -di-*t*-butyl-2,2'-bipyridyl) results in progressively slower electron recombination versus the bpy complex when

paired with N3 as shown in Figure 1.6. This allows $[\text{Co}(\text{LL})_3]^{2+/3+}$ -type mediators to reach up to 80% of the efficiency attained by cells mediated by I^-/I_3^- .²⁷

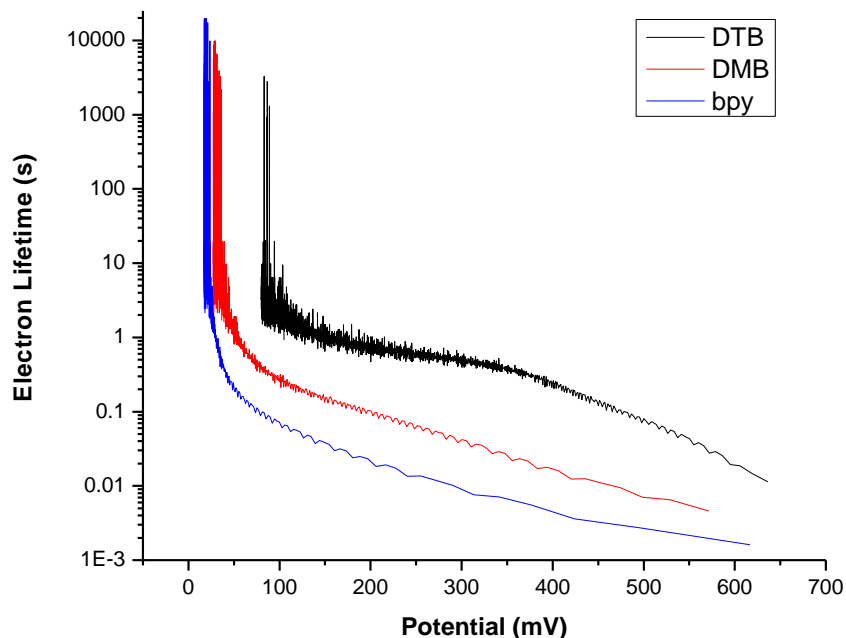


Figure 1.6. Sample recombination kinetics of commonly used $[\text{Co}(\text{LL})_3]^{2+/3+}$ -type mediators coupled with N3.

Note that the barrier is not necessary for a working cell – $[\text{Co}(\text{bpy})_3]^{2+}$ complexes have no such barrier and can still function competently, but the recombination rate to the 3+ complex from TiO_2/FTO is greater than with I_3^- .³⁰ The fact these complexes can function without a barrier (unlike ferrocene) is due to their relatively slow recombination kinetics: the 2+ form is high-spin d^7 , while the 3+ form is low-spin d^6 .³⁰ This results in a large reorganizational energy and therefore a slower rate of electron transfer per Marcus theory.

Applied Techniques in Solar Cell Evaluation

Since data presented throughout subsequent chapters regarding cell performance is all obtained on the same equipment, the experimental setup is described here. As shown in Figure

1.7, a 100 mW cm^{-2} Oriel xenon arc lamp beam passes through an Oriel 1/8M Cornerstone monochromator. For the results presented in Chapters 2 and 3, the beam then passes through a UV filter to avoid direct excitation of the TiO_2 , some focusing optics, and then onto the cell holder which has a 0.385 cm^2 aperture masking the active area of the cell.

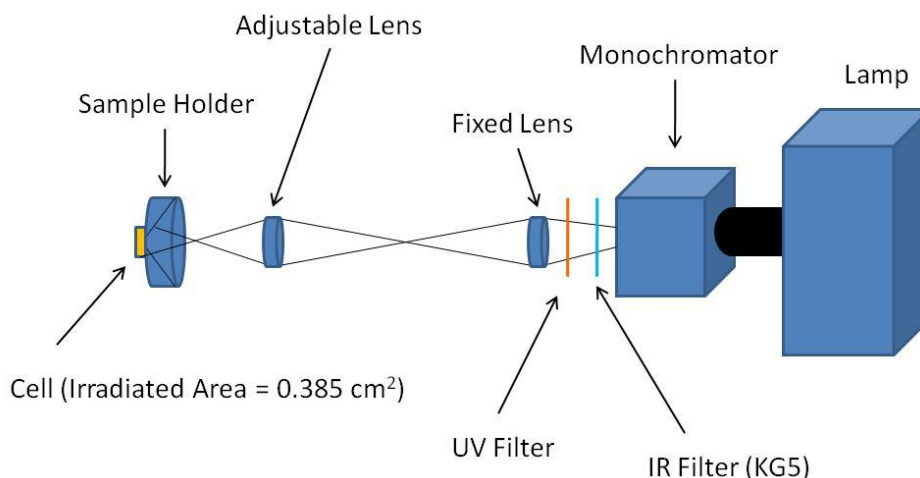


Figure 1.7. Experimental setup for solar cell testing.

For the results presented in Chapters 4 and 5, the beam also passes through a KG5 IR filter. Calibration of the lamp is controlled by focusing the beam through the aperture and then adjusting the focusing lens until the lamp power incident on the sample is 100 mW cm^{-2} . This produces a reasonable approximation of the solar spectrum. This power is measured using a thermopile. It was discovered during the course of this research that, although the arc lamp closely matches the solar spectrum, it does so *only in the visible region*. The arc lamp emits substantially more infrared (approximately 50% of the total light power) and therefore the calibration effectively set the incident light power at ca. 0.5 sun across the visible region where the dyes in question absorb. Calibration with the IR filter corrects this issue. Once the light power is adjusted appropriately, the IR filter is then removed. For IPCE calibration (*vide infra*),

the thermopile is replaced by a photodiode which detects the light power at individual wavelengths controlled by the monochromator.

The DSC cell is connected to a Keithley 2400 SourceMeter which allows for the control of an applied potential while measuring current. In the case of voltage transients, the potential is allowed to change while the current is held at 0 A. The monochromator and sourcemeter are both controlled by a custom Labview program written by Dr. Jeremy Nelson. Data are collected using the same program.

Several experiments are central to the performance evaluation of solar cells in general. The most prevalent of these experiments is the J-V curve (Figure 1.8). This technique consists of scanning the applied potential and monitoring the resultant current density while the cell is under illumination. Like a cyclic voltammogram, the J-V curve is a quick method to obtain information about the system investigated. Several other figures of merit can be extracted from this data: 1) the maximum open-circuit voltage (V_{OC}), which is the voltage at zero current density; 2) the maximum short-circuit current density (J_{SC}), which is the current density at zero voltage; 3) the fill factor (FF), which is an ideality factor relating the actual maximum power density to the theoretical maximum power density (Eq. 1.1). All of these values enter into the calculation of the most sought-after figure of merit in the literature, the overall efficiency, η (Eq. 1.2, shown with incident light power as 100 mW cm^{-2}). The overall efficiency is the least interesting quantity from a scientific point of view because it does not highlight individual processes governing performance, but a high η is the ultimate practical goal of all research in this field. Note that, for all J-V curves presented in this dissertation, the potential sweep is conducted from high negative voltage (generally -850 mV) to low positive voltage (generally +100 mV) but is reported with a sign flip introduced. This is a common convention in the field.

A J-V curve can also be obtained in the dark by blocking the light source and will be referred to as a “dark current” plot. Since there is no illumination, the dye cannot excite and inject electrons into the TiO₂ conduction band. Also, since the dye never leaves the ground state,

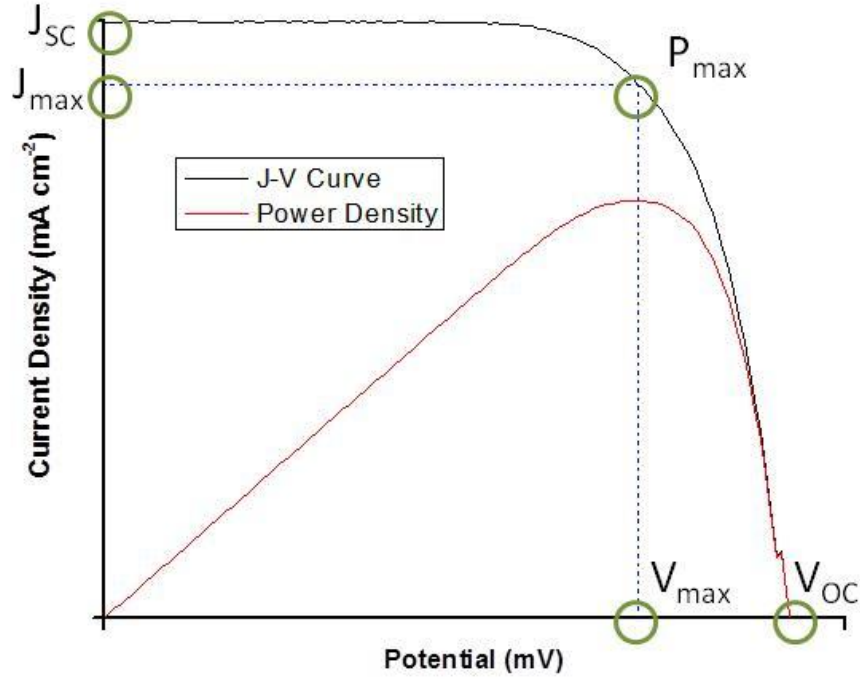


Figure 1.9. Figures of merit obtained from a J-V curve. The power density is calculated as a product of the current density and the voltage. J_{\max} and V_{\max} refer to the current density and voltage, respectively, at the maximum power density.

$$FF = \frac{V_{\max} \times J_{\max}}{V_{OC} \times J_{SC}} \quad \text{Equation 1.1}$$

$$\eta = \frac{FF \times V_{OC} \times J_{SC}}{100 \text{ mW cm}^{-2}} \quad \text{Equation 1.2}$$

the mediator never transfers an electron to regenerate that ground state. The dark current therefore measures the amount of current flowing in the *opposite* direction; that is, the reverse current resulting from electrons flowing from the TiO₂ or FTO to the oxidized form of the mediator at a given potential. (It should be noted here for clarity that mediator solutions are

typically composed of 10-20% oxidized form since electrons still need to flow from the cathode in order to complete the circuit. Therefore, the potential for back electron transfer to oxidized mediator exists even before any dye regeneration occurs.) As the potential of the photoanode is made more negative (i.e., shifted to higher energy), the driving force for reduction of oxidized mediator increases and the current becomes more and more negative as electrons flow to the mediator. The shape of this plot has ramifications on both V_{OC} and J_{SC} . This measurement frequently provides more qualitative than quantitative information, but nevertheless provides a powerful method for comparing similar systems.

Transient measurements may also be conducted by introducing a controllable shutter into the path of the beam. Voltage transient measurements (Fig. 1.9A) consist of exposing the cell to light at open circuit (i.e., with no current flowing) until the equilibrium V_{OC} is reached, and then abruptly blocking the light and observing the voltage decay. Since no current is allowed to flow in these measurements, the decay represents the rate at which TiO_2 electrons recombine with oxidized mediator. This is similar to the dark current measurement but different in that quantitative rate information at a particular voltage can be determined using Eq. 1.3 as originally developed by Bisquert et. al.^{35,36} (see Chapters 2 and 5).

In current transient measurements (Fig. 1.9B), the potential is held at 0 V (i.e., short circuit). The light is then abruptly pulsed on for a set amount of time while current is allowed to flow freely. For I/I_3^- this experiment does not provide any useful information beyond the J-V curve because the current reaches a steady state value of J_{SC} near-instantaneously with light exposure and completely terminates near-instantaneously in the dark. This can be interpreted as the mass transport of the mediator not limiting the current. Because the $[Co(LL)_3]^{3+}$ complexes are much larger than I_3^- , the current becomes limited by mass transport of the $[Co(LL)_3]^{3+}$ to the

cathode. This process can be observed in the current transient measurement. The initial spike in current is due to the concentration of $[\text{Co}(\text{LL})_3]^{2+}$ at the photoanode's surface which can immediately reduce oxidized dye. After this initial population of $[\text{Co}(\text{LL})_3]^{2+}$ is converted to the

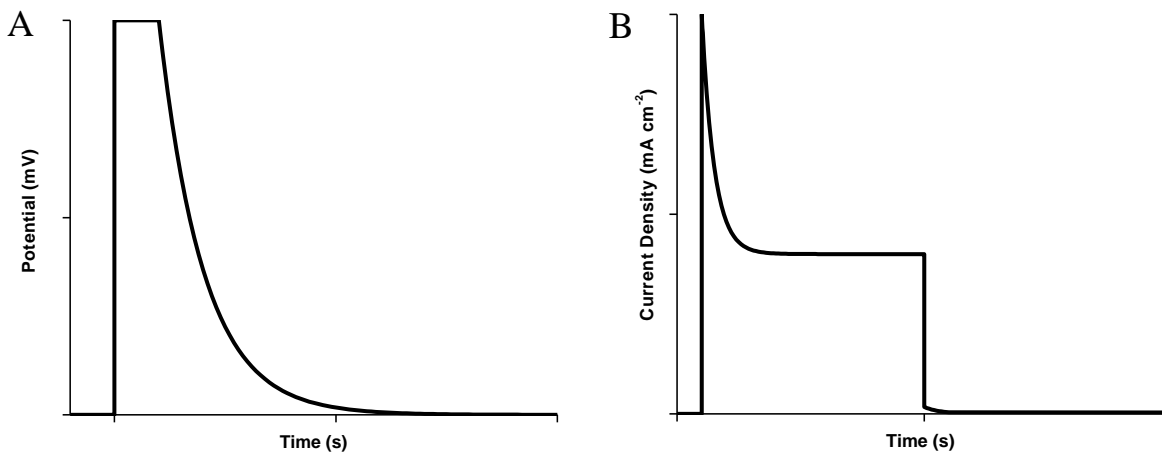


Figure 1.9. Sample voltage and current transient plots. The shapes of these plots will vary significantly depending on dye and mediator selection.

$$\tau_n = -\frac{k_B T}{e} \left(\frac{dV_{OC}}{dt} \right)^{-1} \quad \text{Equation 1.3}$$

oxidized form, the now oxidized $[\text{Co}(\text{LL})_3]^{3+}$ must move out of the film and $[\text{Co}(\text{LL})_3]^{2+}$ must take its place in order to continue regenerating dye. Since $[\text{Co}(\text{LL})_3]^{3+}$ diffuses more slowly than $[\text{Co}(\text{LL})_3]^{2+}$, it takes time for these rates to equilibrate (indicated by the decay curve immediately following the spike). The mass transport limited current is reached at this point, which is shown in Fig. 1.9B as a steady state (SS) current some time after light exposure. All of the aforementioned measurements generally require less than a minute to perform and can easily be incorporated into the evaluation of a cell.

Frequently an incident photon conversion efficiency, or IPCE, measurement is also conducted. This experiment measures the current produced from the cell at a particular wavelength of light and compares it to the background current measured by the photodiode. It is

calculated using Eq. 1.4, where the short-circuit current density and incident power density are measured as functions of the incident light's wavelength. This value is also known as the external quantum efficiency of the cell. The most efficient DSCs produce IPCEs around 80-90% near λ_{\max} (the loss being attributed to glass absorption and scattering).⁴⁻⁶ These data can also be transformed into absorbed photon conversion efficiencies (APCEs), or internal quantum efficiencies, by correcting for the actual absorption of the cell at a particular wavelength (see Eq. 1.5). Measured currents vary from cell-to-cell ostensibly due to differences in absorbed light from variations in photoanode thickness. Since thicker films have more dye in the light path, these differences are also observed in the absorption spectra. Therefore, APCEs should be fairly reproducible between cells fabricated with the same dye/mediator combination regardless of film thickness.

$$IPCE(\%) = \frac{1240}{\lambda(nm)} \frac{J_{SC}(A\ cm^{-2})}{P_{INC}(W\ cm^{-2})} \times 100 \quad \text{Equation 1.4}$$

$$APCE(\%) = \frac{IPCE(\%)}{1 - 10^{-A}} \quad \text{Equation 1.5}$$

The last technique to be addressed is transient absorption spectroscopy (TAS). In the form used throughout this research it is also known as laser flash photolysis and is shown in Fig. 1.10. A pump laser pulse (triggered by the chopper wheel) excites the dye and a chopped xenon arc lamp beam probes the species after excitation. The lifetime of such transient species can then be measured by observing the absorption spectrum decay back to that of the ground state. In solution experiments, these beams are oriented at 90° to each other and the active volume being probed is the cross section of solution where the pump and probe beams overlap. To achieve higher signal, the concentration of the solution can simply be increased. In the solid state measurements conducted herein, the analog of increasing the concentration is to use thicker

films. When constructing a DSC, 1 “Scotch” thick films are used, which are made by doctor-blading TiO_2 paste into a trench formed between two parallel pieces of standard Scotch tape applied to an FTO substrate. While the thickness of the tape is substantially larger (ca. $50\text{ }\mu\text{m}$), the dried film is ca. $3.5\text{ }\mu\text{m}$ thick. In TAS experiments, 2 or 3 Scotch films are doctor-bladed onto a glass microscope slide by doubling or tripling the tape layers, respectively. These slides are then oriented at a 45° angle as shown in Fig. 1.10 such that the two beams overlap in a ca. 1 cm area.

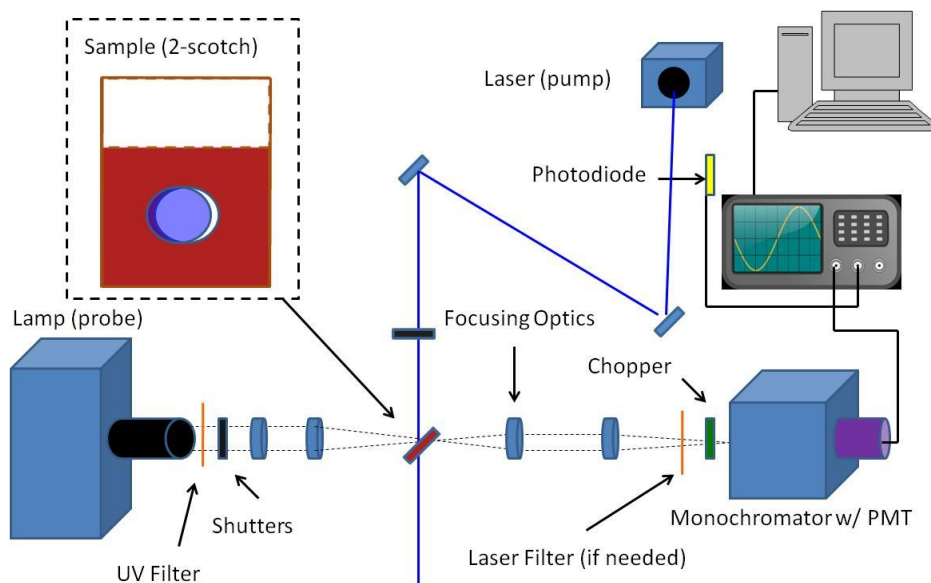


Figure 1.10. Experimental setup for a typical TAS measurement.

The probe beam is oriented on-axis with the monochromator, where the signal is monitored as a function of wavelength and amplified by a Hamamatsu photomultiplier tube. The output is displayed on a Tektronix TDS 620B oscilloscope. For each wavelength, four measurements are taken: pump and probe (both), probe only, pump only, and neither pump nor probe (none). These measurements are recorded using another custom Labview program written

by Dr. Jeremy Nelson which essentially copies the readout of the oscilloscope. The difference absorption is then calculated by Eq. 1.6.

$$\Delta A = -\log \left[\frac{\text{Both-Pump}}{\text{Probe-None}} \right] \quad \text{Equation 1.6}$$

TAS measurements are useful in elucidating many relevant rates in a DSC. The current experimental setup incorporates an Opotek Opolette OPO laser with a < 10 ns FWHM beam (30 mW @ 20 or 15 Hz); therefore, very fast rates such as electron injection into TiO_2 cannot be measured. However, slower rates like dye regeneration, which occur on the microsecond timescale, *can* be measured. After excitation, electrons are injected into the TiO_2 within the timescale of the laser pulse. In the absence of mediator solution and since the microscope slide is non-conductive, the electrons have nowhere to go but back to the dye and regenerate the ground state. This rate can then be determined. Alternatively, a mediator can be introduced to the system by trapping a drop of solution against the pseudo-photoanode with a cover slide. The ability of the mediator to regenerate the dye can then be evaluated.

A point not addressed above is the signal gain required with thin film measurements. Although the surface concentration of dye can be increased with thicker TiO_2 layers, the scattering is also increased. This applies to both the incoming probe beam as well as exiting measured beam and translates to a degradation of the signal-to-noise ratio. The PMT signal (current) is converted to a voltage signal by the input impedance of the oscilloscope. By Ohm's law, a larger resistance should therefore yield a larger voltage signal. However, the time response (f_c) of the oscilloscope is also *inversely* dependent on the impedance (R_L) as shown in Eq. 1.7, with better time resolution obtained at smaller impedance. C_S in this equation is the combination of the capacitance of the PMT and additional stray capacitance due to electrical connections and wiring.

$$f_c = \frac{1}{2\pi C_S R_L} \quad \text{Equation 1.7}$$

The standard options for input impedance on the oscilloscope are 50 Ω and 1 M Ω . Unfortunately both of these options yield little to no signal: not enough gain in the case of the former and a response time too slow in case of the latter. To this end, a series of custom resistive BNC connectors are employed in parallel to the oscilloscope (set to 1 M Ω input impedance) using a T-junction. The input impedance can thus be adjusted to balance signal gain with instrument time response. Generally, these measurements are performed with a 5 k Ω resistor (ca. 4975 Ω resultant input impedance).

Other experimental techniques are useful as complementary methods. For instance, UV-VIS spectroscopy can be used to determine absorption coefficients as well as dye LUMO levels. Cyclic voltammetry can be used to find standard reduction potentials of mediators and dye HOMO levels. All of these methods are used conjunctively in the following chapters to probe various DSC systems.

The remainder of this dissertation will describe studies primarily focused on novel sensitizer synthesis and evaluation in working solar cell devices. Chapter 2 and 5 will discuss copper and ruthenium dyes, respectively, which incorporate electron donor species into their designs in order to increase the electron-hole separation distance. Durrant and co-workers have shown that increasing this distance leads to substantially lower rates of recombination between injected electrons and oxidized dye species.³⁷ Chapter 3 presents a brief study on the addition of Li⁺ to mediator solutions, which appears to have consequences on [Co(LL)₃]^{2+/3+} electrochemistry at bare FTO surfaces. Chapter 4 discusses the modification of gold cathodes for use with [Co(LL)₃]^{2+/3+} complexes. These cathodes generally exhibit more reversible electrochemistry than platinum, but with largely irreproducible results. A relatively simple

modification is proposed which appears to significantly improve reproducibility between cathodes.

Chapter 1 References

- (1) Green, M. A.; Emery, K.; Hishikawa, Y.; Warta, W.; Dunlop, E. D. *Prog. Photovolt. Res. Appl.* **2013**, *21*, 827–837.
- (2) Grätzel, M. *Nature* **2001**, *414*, 338–344.
- (3) West, W. *Photogr. Sci. Eng.* **1974**, *18*, 35–48.
- (4) O'Regan, B.; Grätzel, M. *Nature* **1991**, *353*, 737–740.
- (5) Nazeeruddin, M. K.; Kay, A.; Rodicio, I.; Humphry-Baker, R.; Mueller, E.; Liska, P.; Vlachopoulos, N.; Grätzel, M. *J. Am. Chem. Soc.* **1993**, *115*, 6382–6390.
- (6) Yella, A.; Lee, H.-W.; Tsao, H. N.; Yi, C.; Chandiran, A. K.; Nazeeruddin, M. K.; Diau, E. W.-G.; Yeh, C.-Y.; Zakeeruddin, S. M.; Grätzel, M. *Science* **2011**, *334*, 629–634.
- (7) Kalyanasundaram, K. *Photochemistry of Polypyridine and Porphyrin Complexes*; Academic Press: London, 1992.
- (8) Nazeeruddin, M. K.; Zakeeruddin, S. M.; Humphry-Baker, R.; Jirousek, M.; Liska, P.; Vlachopoulos, N.; Shklover, V.; Fischer, C.-H.; Grätzel, M. *Inorg. Chem.* **1999**, *38*, 6298–6305.
- (9) Wang, P.; Zakeeruddin, S. M.; Moser, J. E.; Nazeeruddin, M. K.; Sekiguchi, T.; Grätzel, M. *Nat. Mater.* **2003**, *2*, 402–407.
- (10) Chiba, Y.; Islam, A.; Watanabe, Y.; Komiya, R.; Koide, N.; Han, L. *Jpn. J. Appl. Phys.* **2006**, *45*, L638–L640.
- (11) Hagfeldt, A.; Boschloo, G.; Sun, L.; Kloo, L.; Pettersson, H. *Chem. Rev.* **2010**, *110*, 6595–6663.

- (12) Hagberg, D. P.; Edvinsson, T.; Marinado, T.; Boschloo, G.; Hagfeldt, A.; Sun, L. *Chem. Commun.* **2006**, 2245.
- (13) Liang, M.; Chen, J. *Chem. Soc. Rev.* **2013**, 42, 3453.
- (14) Kojima, A.; Teshima, K.; Shirai, Y.; Miyasaka, T. *J. Am. Chem. Soc.* **2009**, 131, 6050–6051.
- (15) Burschka, J.; Pellet, N.; Moon, S.-J.; Humphry-Baker, R.; Gao, P.; Nazeeruddin, M. K.; Grätzel, M. *Nature* **2013**, 499, 316–319.
- (16) Liu, M.; Johnston, M. B.; Snaith, H. J. *Nature* **2013**, 501, 395–398.
- (17) Zhou, H.; Chen, Q.; Li, G.; Luo, S.; Song, T. -b.; Duan, H.-S.; Hong, Z.; You, J.; Liu, Y.; Yang, Y. *Science* **2014**, 345, 542–546.
- (18) Feldt, S. M.; Gibson, E. A.; Gabrielsson, E.; Sun, L.; Boschloo, G.; Hagfeldt, A. *J. Am. Chem. Soc.* **2010**, 132, 16714–16724.
- (19) Bai, Y.; Zhang, J.; Zhou, D.; Wang, Y.; Zhang, M.; Wang, P. *J. Am. Chem. Soc.* **2011**, 133, 11442–11445.
- (20) Cai, N.; Li, R.; Wang, Y.; Zhang, M.; Wang, P. *Energy Environ. Sci.* **2013**, 6, 139.
- (21) Wang, P.; Klein, C.; Humphry-Baker, R.; Zakeeruddin, S. M.; Grätzel, M. *J. Am. Chem. Soc.* **2005**, 127, 808–809.
- (22) Jang, S.-R.; Yum, J.-H.; Klein, C.; Kim, K.-J.; Wagner, P.; Officer, D.; Grätzel, M.; Nazeeruddin, M. K. *J. Phys. Chem. C* **2009**, 113, 1998–2003.
- (23) Boschloo, G.; Hagfeldt, A. *Acc. Chem. Res.* **2009**, 42, 1819–1826.
- (24) Hamann, T. W.; Ondersma, J. W. *Energy Environ. Sci.* **2011**, 4, 370.
- (25) Nusbaumer, H.; Moser, J.-E.; Zakeeruddin, S. M.; Nazeeruddin, M. K.; Grätzel, M. *J. Phys. Chem. B* **2001**, 105, 10461–10464.

- (26) Nelson, J. J.; Amick, T. J.; Elliott, C. M. *J. Phys. Chem. C* **2008**, *112*, 18255–18263.
- (27) Sapp, S. A.; Elliott, C. M.; Contado, C.; Caramori, S.; Bignozzi, C. A. *J. Am. Chem. Soc.* **2002**, *124*, 11215–11222.
- (28) Feldt, S. M.; Wang, G.; Boschloo, G.; Hagfeldt, A. *J. Phys. Chem. C* **2011**, *115*, 21500–21507.
- (29) Feldt, S. M.; Lohse, P. W.; Kessler, F.; Nazeeruddin, M. K.; Grätzel, M.; Boschloo, G.; Hagfeldt, A. *Phys. Chem. Chem. Phys.* **2013**, *15*, 7087.
- (30) Hamann, T. W. *Dalton Trans.* **2012**, *41*, 3111.
- (31) Papageorgiou, N. *J. Electrochem. Soc.* **1997**, *144*, 876.
- (32) Katsanaki, A. V.; Tsoukleris, D. S.; Falaras, P.; Karayianni, H. S.; Bernard, M.-C. *J. Sol. Energy Eng.* **2008**, *130*, 041008.
- (33) Gregg, B. A.; Pichot, F.; Ferrere, S.; Fields, C. L. *J. Phys. Chem. B* **2001**, *105*, 1422–1429.
- (34) Daeneke, T.; Kwon, T.-H.; Holmes, A. B.; Duffy, N. W.; Bach, U.; Spiccia, L. *Nat. Chem.* **2011**, *3*, 213–217.
- (35) Bisquert, J.; Zaban, A.; Greenshtein, M.; Mora-Seró, I. *J. Am. Chem. Soc.* **2004**, *126*, 13550–13559.
- (36) Zaban, A.; Greenshtein, M.; Bisquert, J. *Chem. Phys. Chem.* **2003**, *4*, 859–864.
- (37) Clifford, J. N.; Palomares, E.; Nazeeruddin, M. K.; Grätzel, M.; Nelson, J.; Li, X.; Long, N. J.; Durrant, J. R. *J. Am. Chem. Soc.* **2004**, *126*, 5225–5233.

Chapter 2: Dye-Sensitized Solar Cell Studies of a Donor-Appended Bis(2,9-dimethyl-1,10-phenanthroline) Cu(I) Dye Paired with a Cobalt-Based Mediator^A

Introduction

As mentioned in Chapter 1, appropriate sensitizers for DSCs must have high molar extinction coefficients in the visible light region. To this end, Ru(II) polypyridyl-based complexes have worked remarkably well.¹⁻⁸ In addition, the MLCT excitation facilitates electron injection into the semiconductor, thus helping to physically separate the electron and hole produced. Proper engineering of these sensitizers has also shown impressive long-term stability, which shows great promise for commercial application of the technology.³

As with many things, these advantages come with a price – a rather large price, in fact. As of April 2014, the price of ruthenium metal was ca. \$1200/lb. A logical place to improve a DSC from a commercialization point of view, then, would be to develop sensitizers with a cheaper metal center or eliminate the metal entirely. While the second option has significant appeal due to a significant processing cost savings, a generally higher degree of counterproductive electron-hole recombination within the dye remains a significant hurdle. In contrast, swapping the metal center with another can be a potentially straightforward method of preserving some of the advantages inherent to the Ru(II) complexes while significantly reducing the price tag.

An intriguing prospect along these lines of thought is the use of copper. In comparison with ruthenium, copper is far more abundant and, as a result, about 400× cheaper. Cu(I)

^A With the exception of the introduction, previously unpublished experiments, and some minor wording changes, the remainder of this chapter was: Reproduced with permission from *J. Phys. Chem. C* **2013**, *117* (8), 3853-3864. DOI: 10.1021/jp3123693. Copyright 2013, American Chemical Society. Link: pubs.acs.org/doi/abs/10.1021/jp3123693

bipyridine and phenanthroline complexes, abbreviated as $[\text{Cu}(\text{LL})_2]^+$ from here on (where each LL = a 2,2'-bipyridine or 1,10-phenanthroline species), have also been extensively studied by McMillin and coworkers⁹⁻¹¹ in various solvents and states (both solution and solid). These studies have revealed several interesting points that both liken and differentiate them from their Ru(II) counterparts. Both types of complexes have high molar extinction coefficients in the visible region which can be tuned depending on the ligand substitution.¹² Ru(II) complexes tend to have more variability than the $[\text{Cu}(\text{LL})_2]^+$ complexes in this regard due to the fact that they form octahedral six-coordinate complexes rather than tetrahedral four-coordinate complexes. By substituting one bipyridyl group for two SCN^- ligands, for instance, the absorption maximum can be red-shifted ca. 100 nm to better overlap with the sun's spectral output.²

Protection of the Metal Center. One might ask why the same sort of scenario cannot simply be repeated for $[\text{Cu}(\text{LL})_2]^+$ complexes. Replacing ligands is trickier in these situations due to 1) a lower number of coordination sites and therefore fewer options for ligand swapping and 2) far more complicated excited state kinetics. The first issue is compounded further by the fact that at least one ligand must possess binding groups (carboxylic acids, for example) to efficiently couple to the TiO_2 surface, eliminating to some degree the alternative ligand options available. Given that bipyridines and phenanthrolines are both bidentate ligands (and ignoring the more complicated cases of higher order polypyridyl ligands), that leaves one ligand or two coordination sites available for swapping.

The second issue is related to structural changes in the complex. $[\text{Cu}(\text{LL})_2]^+$ complexes, unlike their Ru(II) counterparts, can potentially coordinate an additional ligand depending on the chemical conditions. This can occur either in the excited state or after electron injection. Because the excited state is a MLCT state, the metal center after excitation is formally Cu(II). In

the case of $[\text{Ru}(\text{LL})_3]^{2+}$ complexes, the oxidation of Ru(II) to Ru(III) has no bearing on the structure of the complex. In either case it remains locked in a six-coordinate octahedral-like geometry. This is not true with copper complexes. $[\text{Cu}(\text{LL})_2]^+$ complexes adopt the D_{2d} flattened tetrahedral geometry, whereas Cu(II) complexes tend to undergo Jahn-Teller distortion that furthers the flattening of the geometry to D_2 (Fig. 2.1).¹³ In practical terms, this can be visualized as a transition from a tetrahedral-like shape to a square planar shape.

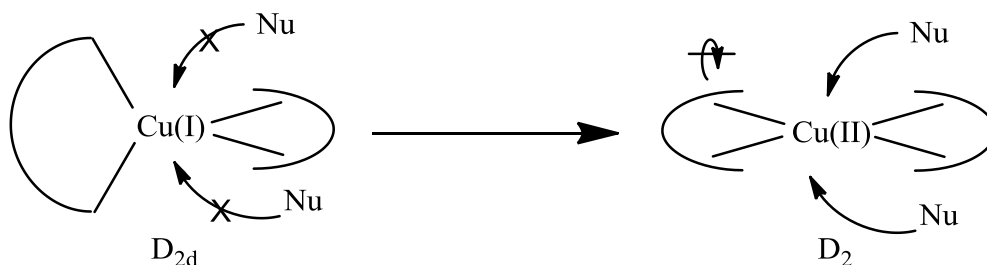


Figure 2.1. Distortion of complex geometry upon oxidation from Cu(I) to Cu(II). When in a flattened D_2 geometry, the metal center is then susceptible to nucleophilic attack (*vide infra*).

Cu(II) complexes tend to be five or six coordinate, and the flattening of the geometry to square planar-like opens up additional coordinate sites around the copper center. Strong evidence has been shown to support the theory that the presence of nucleophiles (solvent or ions in solution) can then coordinate to Cu(II) via these newly available sites as shown in Fig. 2.1.¹⁰ If this occurs in the excited state (i.e., when the electron is located on the ligand and the coordination center is quasi-Cu(II)), then the complex is referred to as an “exciplex.” These complexes tend to be short-lived and only occur in the excited state. Exciplexes undergo non-radiative decay back to the ground state, which effectively truncates the excited state lifetime.¹⁴

Exciplexes are generally undesirable in applications where maintaining the excited state for a relatively long period of time is important. In a DSC the excited state must persist long enough for electron injection to occur (generally under a picosecond).⁸ The simplest method to prevent exciplex formation is to expose the $[\text{Cu}(\text{LL})_2]^+$ complex to an environment without

potential coordinating nucleophiles. In the context of DSCs, however, this method is problematic since nucleophilic solvents and/or additives are frequently employed. The second, more prevalent method, is to control the coordination sphere by careful ligand selection. In the case of $[\text{Cu}(\text{LL})_2]^+$ complexes, this is readily achieved by substitution at the 6,6' positions on bipyridine or 2,9 positions on phenanthroline (Fig. 2.2). This has the effect of physically preventing the complex from extensive flattening due to steric interactions.¹² Generally speaking, the degree to which D_{2d} geometry is preserved (and therefore the excited state lifetime is extended) increases with bulkier substituents, though even substitution with methyl groups has a profound difference compared to no substitution at all. For example, the excited state lifetime of $[\text{Cu}(\text{dmp})_2]^+$ (where dmp = 2,9-dimethyl-1,10-phenanthroline) is ca. 90 ns, whereas for $[\text{Cu}(\text{phen})_2]^+$ it is ca. 2 ns.^{12,13}

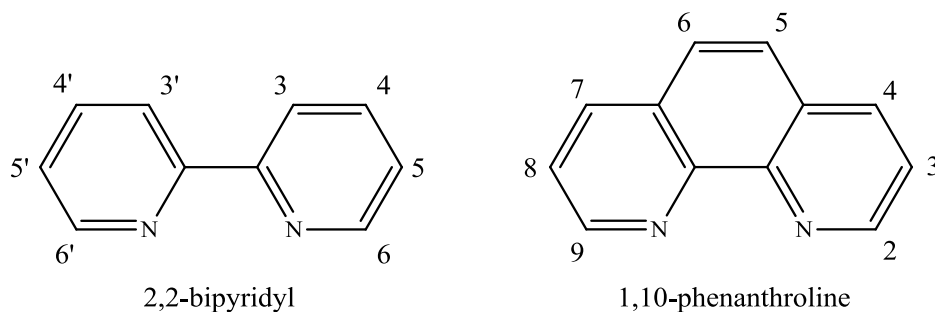


Figure 2.2. Structures of bpy and phen with ring substitution positions labeled. This is also Fig. 1.3 but is reproduced here due to its relevance to the current discussion.

It should also be mentioned that, although up to this point bipyridines have been given equal consideration with phenanthrolines as coordinating ligands, they are somewhat inappropriate when long excited state lifetimes are desired. This is due to the fact that bipyridines have increased torsional freedom about the 2,2'-bond, which can potentially allow nucleophilic attack even with substituents at the 6,6' positions. In contrast, the additional ring structure in phenanthrolines gives rise to a more rigid backbone, ensuring they are planar and

therefore that they rotate as a full unit. For this reason, bulky substitution at the 2,9 positions effectively crowds the coordination sphere.

For DSC applications, long-lived excited states are not overly necessary because the electron injects into the TiO₂ very shortly after excitation (generally within a few hundred femtoseconds for N3-type Ru(II) complexes).⁸ Therefore, as long as the relaxation from the excited state to the ground state is sufficiently slow, the excited state should live long enough for the electron to inject. (In commonly employed Ru dyes the excited state lifetime is on the order of 20-60 ns.⁸) For [Cu(LL)₂]⁺ complexes this decay can happen either through radiative means from the D_{2d} complex, or non-radiative means from the exciplex. Post-excitation, flattening occurs in less than a picosecond followed by intersystem crossing to the ³MLCT state within ca. 20 ps.^{15,16} If no care is taken to protect the copper center, then exciplex formation will occur and the excited state will be quenched.¹⁰ On the other hand, if the coordination sphere is protected against nucleophilic attack, then an appreciable emission can be observed up to hundreds of nanoseconds long. Assuming the rate of electron injection in [Cu(LL)₂]⁺ complexes is approximately the same as observed with the Ru(II) complexes, injection should proceed despite issues regarding the coordination sphere since relaxation should be significantly slower regardless of what state it occurs from. Thus, ligands with non-optimal rigidity like 2,2'-bipyridines or 2,2'-biquinolines can be employed in [Cu(LL)₂]⁺ sensitizers.¹⁷⁻²²

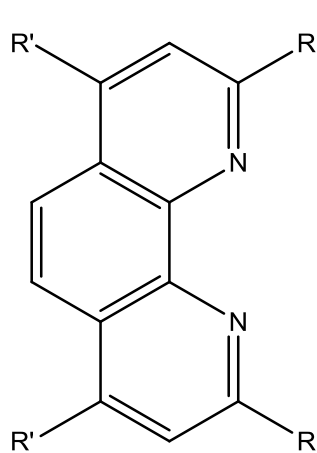
Still, without protecting the metal center, issues may arise regarding stability of the complex due to the spontaneity of Cu(I) oxidation. A modest driving force exists for this reaction:



Therefore, although the requirement of copper center protection is somewhat relaxed due to excited state kinetics, care must still be taken to avoid accidental oxidation. This fact is evident in the storage of $[\text{Cu}(\text{ACN})_4](\text{BF}_4)$ under inert atmosphere since appreciable exposure to air (i.e., oxygen) will change the color from white to blue within a few minutes.

Tuning of Spectroscopic Properties. In reference to the earlier argument regarding ligand swapping to alter λ_{max} , it can plainly be seen that doing so in $[\text{Cu}(\text{LL})_2]^+$ complexes is more complicated due to the added requirement of sterically hindering the coordination sphere from nucleophilic attack. Related Ru(II) complexes do not have this restriction. This is not to say that there can be no control over the absorption properties in $[\text{Cu}(\text{LL})_2]^+$ complexes, however. In fact, the λ_{max} for Cu(I) bis-2,2'-biquinoline is red-shifted ca. 100 nm (to 545 nm) compared to Cu(I) bis-1,10-phenanthroline, but at a cost of a reduced molar extinction coefficient ($7000 \text{ M}^{-1}\text{cm}^{-1}$ for bis-phenanthroline and $5900 \text{ M}^{-1}\text{cm}^{-1}$ for bis-biquinoline).¹² 2,2'-biquinoline also can “twist” along the 2,2'-bond as with 2,2'-bipyridine (though probably to a lesser degree given the additional ring structure), again making it an inappropriate ligand choice for complexes with long-lived excited states.

Table 2.1. Effect of substitution on phenanthroline backbone in homoleptic Cu(I) complexes. Data from Ref. 11.

	R	R'	λ_{max} (nm)	ϵ ($\text{M}^{-1}\text{cm}^{-1}$)
	-H	-H	435	7000
	-CH ₃	-H	455	7950
	-Phenyl	-H	441	3620
	-Phenyl	-Phenyl	450	6400
	-CH ₃	-Phenyl	479	14200

Limiting the discussion to 1,10-phenanthroline based $[\text{Cu}(\text{LL})_2]^+$ complexes, i.e. $[\text{Cu}(\text{phen})_2]^+$ -type complexes, one can still attain a wide variety of spectroscopic properties as shown in Table 2.1.¹¹ Substitution at different positions around the phenanthroline backbone can have additional effects on λ_{max} , the absorption cross-section, extinction coefficient, and excited state lifetime.

Lability. In addition to the preservation of the Cu(I) metal center and unlike Ru(II) complexes, $[\text{Cu}(\text{LL})_2]^+$ complexes are labile. For several years many of the results from McMillin and others were based on homoleptic Cu(I) complexes, where both coordinating phenanthroline ligands were the same.⁹⁻¹⁵ Therefore, any ligands that were removed from the complex and free in solution would be the same ligands that coordinated again provided that the solvent was a poor nucleophile like dichloromethane. The lability of $[\text{Cu}(\text{LL})_2]^+$ complexes is particularly problematic in the case of DSCs because it hinders one-pot dyeing of substrates unless both ligands are equivalent. Although this scheme might have some appeal from the perspective of potentially faster dye uptake since both ligands would include binding groups to electronically couple to the TiO_2 , it drastically limits coordination options.

A wealth of research on $[\text{Ru}(\text{bpy})_3]^{2+}$ -type complexes^{12,23} led to their initial selection as sensitizers for Grätzel and coworkers.^{2,24} Likewise, there is a similar background of work for $[\text{Cu}(\text{LL})_2]^+$ complexes, but surprisingly few examples of their use in DSCs. To date, most examples of $[\text{Cu}(\text{LL})_2]^+$ dyes have consisted of 1-pot solutions where both LLs are the same due to the lability problem.^{17,18,20,25} Odobel and coworkers recently published a method for isolation of stable $[\text{Cu}(\text{LL})_2]^+$ heteroleptic complexes (i.e., where the two LLs are not equivalent, see Fig. 2.3).²⁰ Briefly, this method is based on the concept of creating sufficient steric bulk around the coordination sphere with one ligand such that the coordination sphere is too crowded to support a

second ligand of the same type. The introduction of another less bulky ligand then allows for the formation of the heteroleptic complex. Keep in mind that “bulk” here is again referring only to the coordination sphere; there is technically no restriction on the size of the ligands beyond this, though maintaining a small footprint on the surface of the TiO_2 is usually beneficial so as to increase the amount of surface-bound dye. There are exceptions of course, such as in the case of porphyrin-type sensitizers²⁶, where a drastically increased molar extinction coefficient compensates for fewer dye molecules on the surface.

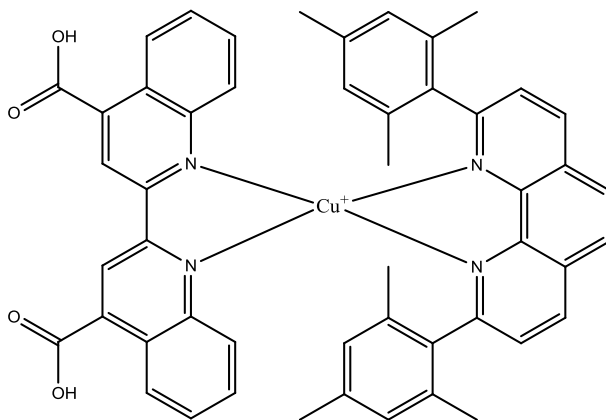


Figure 2.3. Example of a Cu(I) dye constructed by Odobel et al. using the HETPHEN strategy.

Constable and coworkers introduced an alternate, elegant approach for sensitization of TiO_2 with heteroleptic $[\text{Cu}(\text{LL})_2]^+$ complexes with arbitrary polypyridyl ligands.¹⁸ Treating the lability of Cu(I) as a boon rather than a hurdle, they suggested that treating a bare TiO_2 surface first with a solution of the binding ligand by itself would ensure complete coverage of the dye. After the film was rinsed and dried, it could be placed in a solution of bis- $[\text{Cu}(\text{LL})_2]^+$, where LL was the second desired ligand lacking anchoring groups. As one LL ligand exchanges with a surface bound anchoring ligand, the heteroleptic complex self-assembles on the film's surface.

The Constable group subsequently published several studies showing the efficacy of this approach.^{19,21,22}

Mediator Compatibility. The most common solution-based mediator in the DSC field is the I/I_3^- redox couple as discussed in Chapter 1. One of the major disadvantages of this couple is the loss in maximum attainable V_{OC} due to the mismatch between its $E_{1/2}$ (ca. 0.06 V vs. SCE) and that of the ground state of the dye (ca. 0.85 V vs. SCE for N3).⁸ $[\text{Cu}(\text{LL})_2]^+$ complexes typically have a higher energy ground state which ranges from 0.6 to 0.9 V vs. SCE depending on solvent choice.²⁷ Therefore, I/I_3^- should still be an effective mediator based entirely on thermodynamic considerations.

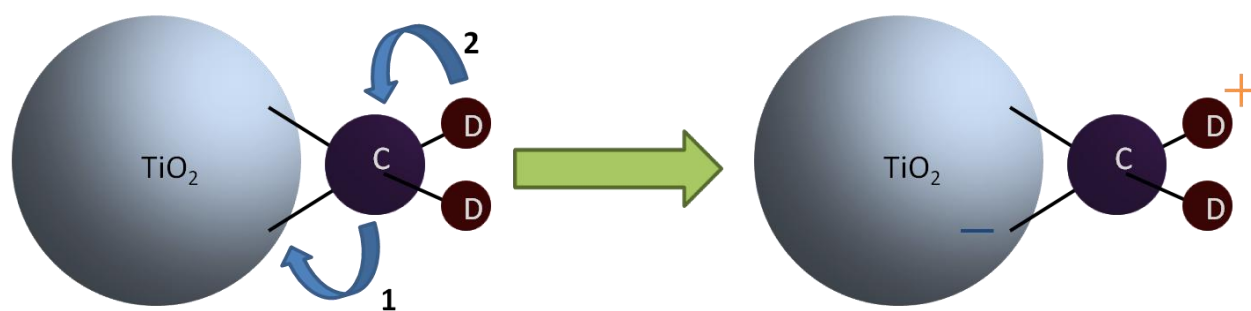
Indeed, current examples of $[\text{Cu}(\text{LL})_2]^+$ sensitizers employ I/I_3^- with great success on short timescales.^{17–19,22} These systems are not stable long-term, however, due to the formation of $\text{CuI}(\text{s})$.¹⁸ The low solubility of $\text{CuI}(\text{s})$ ($K_{\text{sp}} \approx 10^{-12}$ in H_2O at 25 °C) ensures that the equilibrium under prolonged exposure to I^- will result in the eventual loss of dye from the surface. Therefore, a traditional mediator solution based on this redox couple would not be appropriate for use with $[\text{Cu}(\text{LL})_2]^+$ sensitizers.

As has already been established in Chapter 1, $[\text{Co}(\text{LL})_3]^{2+/3+}$ complexes can be respectable substitutes for the I/I_3^- couple. In addition, long-term stability issues akin to what is observed with I^- should not exist. Although the bulkiness of these complexes could potentially still be problematic in terms of mass transport limited current, the added tunability of the redox potential with ligand selection can result in V_{OC} increases that can at least partially offset lower J_{SC} in the overall power conversion efficiency.

Incorporation of Electron Donating Species. The impetus for attaching an electron-donating species covalently within the dye molecule is to regenerate the metal center rapidly and

transport the hole from the metal center to the ligand exposed to solution as shown in Scheme 2.1. Suitable options for such species depend on the redox potential of the dye ground state. Phenothiazines (PTZs, Fig. 2.4) are one such appropriate species. The original report involving the use of covalently-bound PTZ donors in DSC sensitizers found that coordinating a PTZ-functionalized bipyridine to Ru(II) resulted in a long-lived charge-separated system akin to what was observed in Ru(II) donor-chromophore-acceptor (D-C-A) complexes.^{28,29} After excitation,

Scheme 2.1. Schematic representation of envisioned charge separation. Upon chromophore (“C”) excitation, the excited electron is injected into the TiO₂ on an ultrafast timescale. The formally oxidized metal center then is reduced by an appended donor (“D”).



the electron was injected into the TiO₂ followed by rapid reduction of Ru(III) by phenothiazine (< 20 ns).²⁸ [Ru(bpy)₃]^{2+/3+} possesses a ground-state redox potential of 1.3 V vs. SCE (ACN solvent, 25 °C), far positive of the PTZ redox couple (ca. 0.6 V vs. SCE under the same conditions). However, PTZ moieties are typically appended via nitrogen linkage, which has the effect of positively shifting the redox potential by ca. 100 mV and potentially further depending on the linkage length.³⁰ Still, a substantial driving force approaching 0.6 V results in swift reduction of the Ru(III) center. The direct application of this principle in N3-type dyes, which have ground state redox potentials significantly higher in energy than [Ru(bpy)₃]^{2+/3+}, will be addressed in Chapter 5.

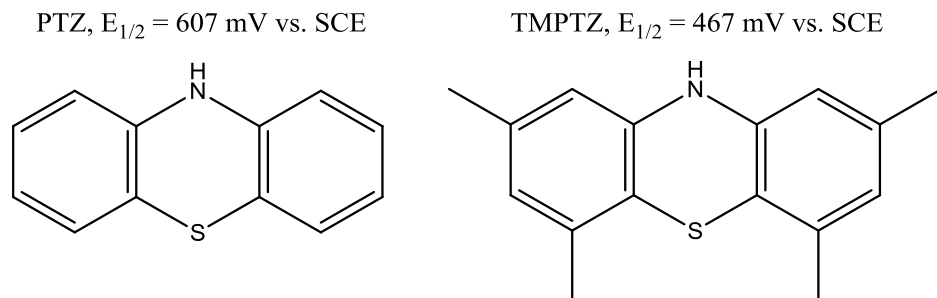


Figure 2.4. Phenothiazine (PTZ) and 2,4,6,8-tetramethyl phenothiazine (TMPTZ).

Unfortunately, the redox potential of an appended PTZ fits in the middle of the possible range for $[\text{Cu}(\text{LL})_2]^+$ complexes (*vide supra*), most likely making it an inappropriate donor choice. In order to use a PTZ species, the redox potential must be negatively adjusted by altering the molecular structure. One method to accomplish this is to substitute the PTZ with alkyl groups around the rings, such as with a 2,4,6,8-tetramethyl phenothiazine (TMPTZ) covalently bound to the dye ligand by the nitrogen. The negative shift in redox potential between free PTZ and TMPTZ is ca. 150 mV. However, the difference between N-methyl PTZ and N-methyl TMPTZ is only ca. 50 mV, indicating that the redox potentials when covalently bound may not be so dissimilar. Nevertheless, the more negative redox potential of TMPTZ would result in a somewhat larger driving force for Cu(II) reduction.

Project Rationale. Building on the body of work above, the studies presented here focus on the installation of $[\text{Cu}(\text{phen})_2]^+$ -based complexes as DSC sensitizers based on their potential to be less expensive alternatives to Ru(II) polypyridyl dyes. Ligands **2** and **3**, shown in Fig. 2.5, are prepared and evaluated in heteroleptic Cu(I) complexes bound to TiO_2 by ligand **4**, also shown in Fig 2.5. Another ligand, 2,9-dimethyl-1,10-phenanthroline, is shown and will be referred to as ligand **1** throughout the rest of the chapter. The most interesting of these complexes, $[\text{Cu}(\mathbf{3})(\mathbf{4})]^+$ incorporates a TMPTZ donor extending from the ether linkages of the phenanthroline backbone.

Ligands **2-4** were chosen as targets due to their apparent ease of synthesis from the parent diol (*vide infra*) via well-known amine chemistry.^{29,31} Methyl groups at the 2,9-positions on both ligands in all cases were employed to preserve the Cu(I) geometry in both the ground and excited states. The butyl chain linking the TMPTZ and the phenanthroline backbone in **3** was chosen based on past work in the Elliott group involving Ru(II) D-C-A assemblies which found that a

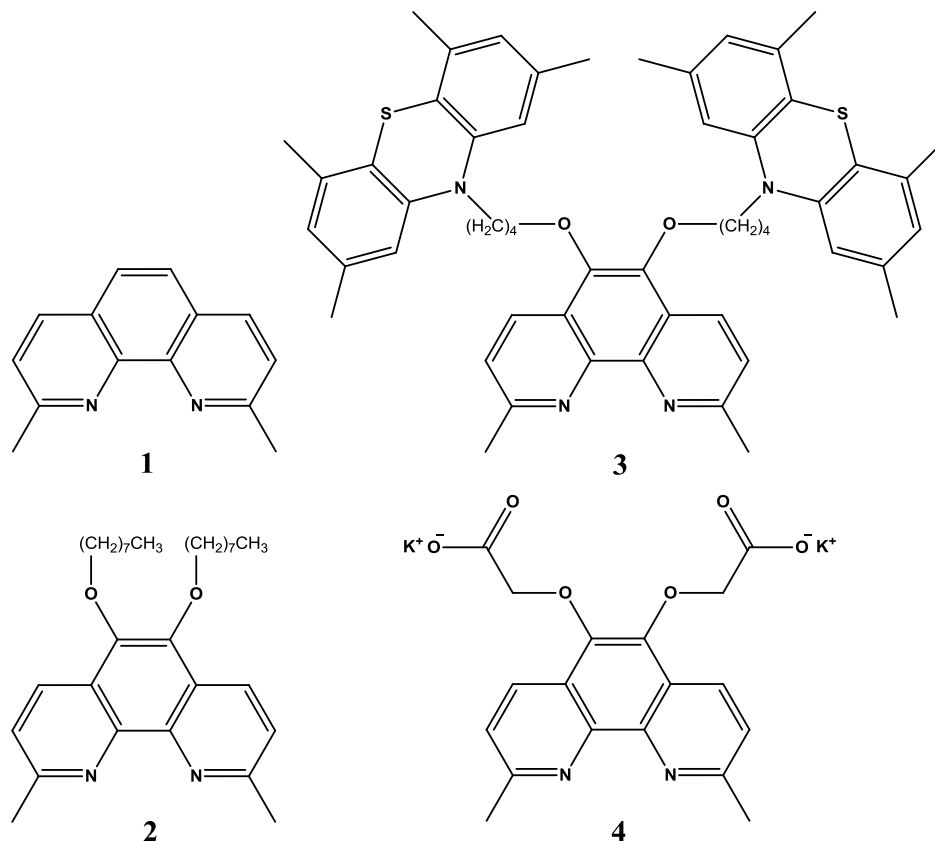


Figure 2.5. Ligands considered for heteroleptic Cu(I) dye formation. Complexes are prepared from one ligand of the type **1-3** and one ligand of **4**.

donor-chromophore pre-association existed in the ground state and was strongest with a butyl linkage as evidenced by the charge-separated state quantum yield.³¹ TMPTZ was chosen as the electron donor over PTZ due to its more reductive redox potential (*vide supra*). Carboxylate groups on **2** provide anchoring groups for effective binding to TiO_2 .

Ligand **1** and **2**, and more specifically the sensitizers constructed from them, were designed as controls to the performance of $[\text{Cu}(\mathbf{3})(\mathbf{4})]^+$. $[\text{Cu}(\mathbf{1})(\mathbf{4})]^+$ provides the case with no electron donor while still preserving the core $\text{Cu}(\text{phen})_2$ environment. $[\text{Cu}(\mathbf{2})(\mathbf{4})]^+$, on the other hand, allows de-convolution of possible steric effects since the alkyl chains extending from the back end of the molecule are roughly the same length as the butyl-appended PTZ (though without the steric bulk of the PTZ groups at the terminus).

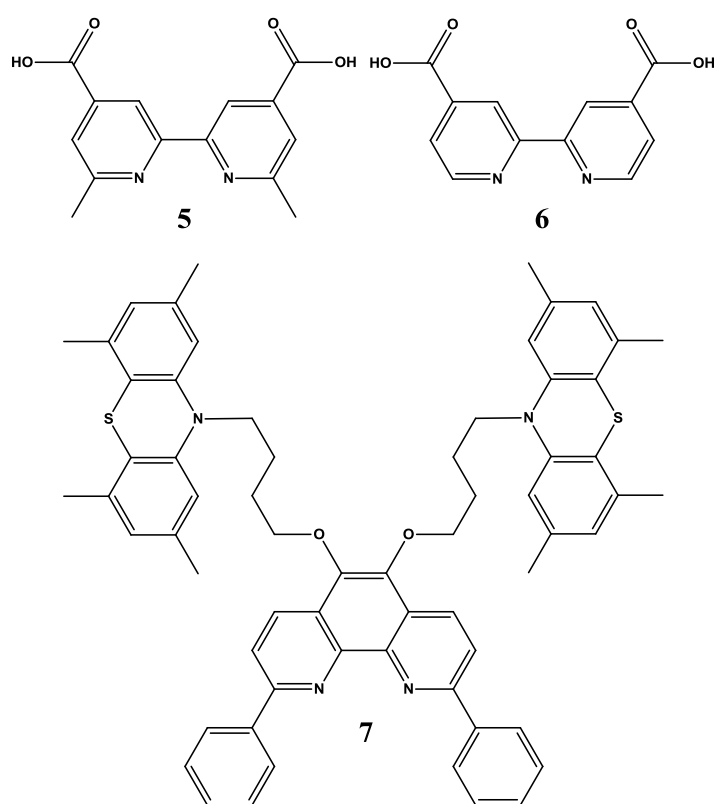


Figure 2.6. Additional ligands employed to investigate the importance of avoiding the flattened D_2 coordination geometry.

The previously published work presented here involves dyes all bound to the surface by the same ligand (**4**). Compound II in Scheme 2.1 (see Experimental) as well as the ethyl ester of **4** were also briefly evaluated as possible binding ligands on their own, but were found to perform rather poorly in this regard as evidenced by bare or weakly dyed films. Subsequent preliminary

experiments that are not part of the *J. Phys. Chem. C* publication involving ligands **5-7** in Fig. 2.6 are presented as well. These studies were conducted in order to further explore the importance of limiting the $D_{2d} \rightarrow D_2$ symmetry transition. Ligand **7** was synthesized independently by Ammon Lehnig.

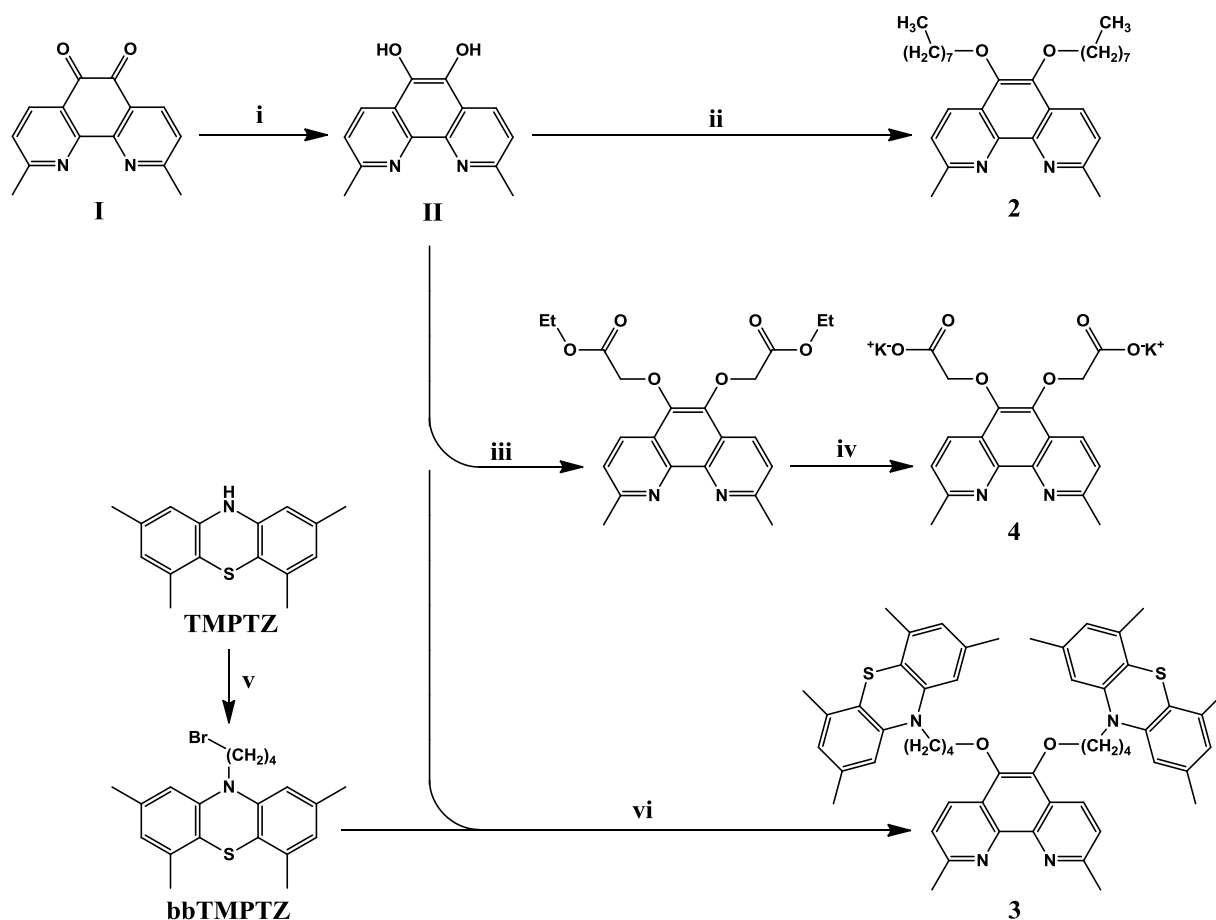
Experimental

Dry THF was obtained from an MBraun MB-SPS solvent purification system. All other chemicals were obtained from Aldrich or EMD Chemicals and used without further purification unless otherwise specified. Ligand **6** was synthesized previously.³² Absorption measurements were taken on an Agilent 8453 UV/VIS spectrometer. Infrared spectra were obtained using a Thermo Electron Corporation Nicolet 380 FT-IR Spectrometer. Nuclear magnetic resonance measurements were taken on a Varian Inova 300 MHz instrument. Electrochemical measurements were conducted using a CHI 750D potentiostat with 0.1 M TBAPF₆ as the supporting electrolyte and using a saturated sodium calomel electrode (SSCE) for the reference electrode, platinum wire as the auxiliary electrode, and glassy carbon as the working electrode.

2,9-dimethyl-1,10-phenanthroline-5,6-dione (I) was synthesized by Megan Lazorski using a similar method to that reported in the literature for forming 1,10-phenanthroline-5,6-dione.³² This dione was subsequently converted to 2,9-dimethyl-1,10-phenanthroline-5,6-diol (II) following a previously reported method³³ (step 1 in Scheme 2.2) except that, prior to filtering the product, the pH of the mixture was adjusted to 5-6 with a saturated aqueous Na₂CO₃ solution. All other syntheses began with II as depicted in Scheme 2.2.

Synthesis of 2,9-dimethyl-5,6-bis(octyloxy)-1,10-phenanthroline (2). Diol, II, (0.1003 g, 0.42 mmol) and Cs₂CO₃ (0.4108 g, 1.26 mmol) were combined in a 50 mL round-bottomed flask under N₂(g). 10 mL DMF were added and the reaction mixture was allowed to stir for 10 mins. 1-bromooctane (170 μ L, 1.0 mmol), which had previously been filtered through basic alumina, was then injected into the reaction mixture. The reaction was allowed to proceed for 21 hours, after which 40 mL of de-ionized water was added to quench the reaction. Chloroform (2 x 70 mL) was used to extract the product, and the solvent was removed by rotary evaporation. The

Scheme 2.2. Synthetic routes to desired ligands. i) H₂O, N₂H₄ • H₂SO₄, N₂(g), 100 °C, 2 mins.; ii) DMF, Cs₂CO₃, 1-bromooctane, N₂(g), room temp, 21 hrs.; iii) DMF, Cs₂CO₃, ethyl 2-bromoacetate, Ar(g), 0 °C, 4 hrs.; iv) KOH, 1:1 H₂O/MeOH; v) THF, KN[Si(CH₃)₃]₂, 1,4-dibromobutane, N₂(g), room temp, 2.5 hrs.; vi) DMF, Cs₂CO₃, N₂(g), room temp, 23 hours. Full details are described in Experimental section.



resulting residue was re-dissolved in dichloromethane (DCM) and purified by column chromatography on 200-400 mesh silica gel with 10% ethyl acetate in DCM as the eluent. ^1H NMR in CDCl_3 , δ in ppm: 8.44 (2H, d), 7.49 (2H, d), 4.22 (4H, t), 2.92 (6H, s), 1.90 (4H, m), 1.55 (4H, m), 1.37 (12H, m), 0.90 (6H, t).

Synthesis of 10,10'-(((2,9-dimethyl-1,10-phenanthroline-5,6-diyl)bis(oxy))bis(butane-4,1-diyl))bis(2,4,6,8-tetramethyl-10H-phenothiazine (3). 2,4,6,8-tetramethyl-10H-phenothiazine (TMPTZ) was prepared as previously reported from di(3,5-dimethylphenyl)amine.³⁴ A sample of TMPTZ (0.1048 g, 0.41 mmol) was placed in a 6 dram vial, capped with a rubber septum, and purged with $\text{N}_2(\text{g})$. Separately, $\text{KN}[\text{Si}(\text{CH}_3)_3]_2$ (0.0714 g, 0.36 mmol) was dissolved in 10 mL THF under $\text{N}_2(\text{g})$, and then injected into the vial containing the TMPTZ. The solution was allowed to stir for 10 mins, followed by addition of 1,4-dibromobutane (0.5 mL, 4.1 mmol). The solution was allowed to stir in the dark for 2.5 hours, after which THF was removed by rotary evaporation and excess 1,4-dibromobutane was removed overnight in a vacuum oven. Most of the unreacted TMPTZ was removed by extracting the solid residue after drying with hexanes (in which TMPTZ is only sparingly soluble), filtering the solids, and then removing the hexanes by rotary evaporation.

The intermediate product, 10-(4-bromobutyl)-2,4,6,8-tetramethyl-10H-phenothiazine (bbTMPTZ), was used without further purification. Diol, II, (0.0326 g, 0.14 mmol) and Cs_2CO_3 (0.1430 g, 0.44 mmol) were combined in a 25 mL round bottom flask under $\text{N}_2(\text{g})$, dissolved in 5 mL dry DMF, and sonicated for 10 mins. During this time, the solution turned from a clear yellow to a clear dark brown color. Separately, bbTMPTZ (0.1131 g, 0.29 mmol) was dissolved in 3 mL dry DMF under $\text{N}_2(\text{g})$ and then injected into the reaction solution. The reaction was allowed to proceed for 23 hours, after which the DMF was removed by rotary evaporation. The

crude product was re-dissolved in DCM and purified by column chromatography on 200-400 mesh silica gel, eluting first with neat DCM to elute unreacted starting material, followed by elution with a 1:1 solution of DCM and NH₃-saturated DCM. The desired product was isolated as a tan solid after solvent removal. ¹H NMR in CDCl₃, δ in ppm: 8.21 (2H, d), 7.40 (2H, d), 6.65 (4H, s), 6.56 (4H, s), 4.14 (4H, t), 3.92 (4H, t), 2.91 (6H, s), 2.33 (12H, s), 2.26 (12H, s), 1.97 (8H, m).

Synthesis of diethyl 2,2'-((2,9-dimethyl-1,10-phenanthroline-5,6-diyl)bis(oxy))diacetic acid, potassium salt (4). Diol, II, (0.5010 g, 2.1 mmol) and Cs₂CO₃ (1.6225 g, 5.0 mmol) were combined in a 50 mL round bottomed flask under Ar(g). The flask was cooled to 0 °C and 8 mL DMF added. The reaction was allowed to stir for 75 mins. Ethyl 2-bromoacetate (0.69 mL, 6.2 mmol), which had been previously filtered through basic alumina, was added to the reaction, and allowed to stir for 4 hours. DMF and most of the excess ethyl 2-bromoacetate were then removed by rotary evaporation. The crude di-ester product was re-dissolved in DCM and purified by column chromatography on 200-400 mesh silica gel, eluting first with neat DCM to remove excess ethyl 2-bromoacetate and then 20% ethyl acetate in DCM to isolate the product. ¹H NMR in CDCl₃, δ in ppm: 8.63 (2H, d), 7.53 (2H, d), 4.89 (4H, s), 4.27 (4H, q), 2.93 (6H, s), 1.29 (6H, t).

The di-ester compound was converted to the potassium salt using 3× equiv. KOH in a 1:1 H₂O:methanol solution. After hydrolysis, the ethyl peaks in the NMR spectrum disappeared and IR stretches at 1611 and 1406 cm⁻¹ were observed, corresponding to the ionized COO⁻ stretching modes.

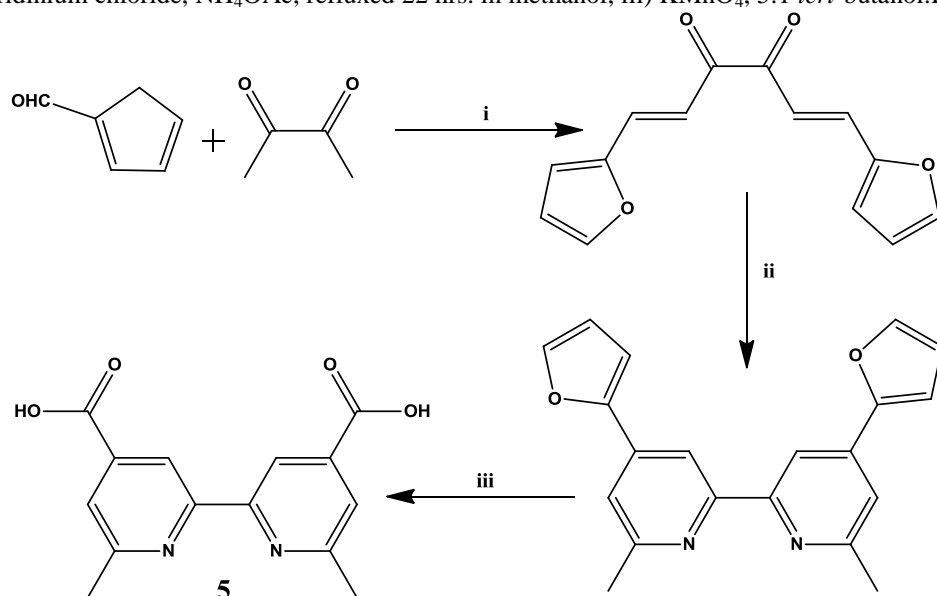
Synthesis of 6,6'-dimethyl-[2,2'-bipyridine]-4,4'-dicarboxylic acid (5). Synthesis of **5** was accomplished by following a detailed literature procedure from Constable and coworkers.¹⁸ and

as shown in Scheme 2.3. The first step (i) was modified slightly following Sørensen's procedure using the in-situ formation of a piperidinium acetate catalyst.³⁵ The cinnamil was isolated as a bright orange solid and recrystallized from ethanol. Column chromatography was also investigated as an alternative purification avenue, and a column separation was briefly attempted noting the good separation on TLC (10% ethyl acetate in CHCl₃), but the compound decomposed on a test mini-column. MP: 155-156.5 °C. ¹H NMR in CDCl₃, δ in ppm: 7.68 (1H, s), 7.63 (1H, s), 7.61 (2H, d), 7.39 (1H, s), 7.34 (1H, s), 6.85 (1H, s), 6.84 (1H, s), 6.58 (2H, m).

The difuryl substituted dimethyl bipyridine was filtered as a white solid after the second reaction step (ii) and was used without further purification. ¹H NMR in CDCl₃, δ in ppm: 8.47 (2H, s), 7.55 (2H, s), 7.44 (2H, s), 7.00 (2H, s), 6.53 (2H, m), 2.69 (6H, s). The oxidation with KMnO₄ in the third step (iii) was accomplished by three separate equivalent additions approximately one hour apart. MnO₂ was then filtered from solution and the volume reduced before acidic workup. The desired product **5** was then filtered as a white solid. ¹H NMR in DMSO, δ in ppm: 13.76 (2H, s), 8.67 (2H, d), 7.81 (2H, d), 2.70 (6H, s).

Synthesis of 10,10'-(((2,9-diphenyl-1,10-phenanthroline-5,6-diyl)bis(oxy))bis(butane-4,1-diyl))bis(2,4,6,8-tetramethyl-10H-phenothiazine) (7). The primary difference between the preparation of this compound and that of **3** is the synthesis of the 2,9-diphenyl dione. This reaction is challenging due to the formation of a complex mixture of undesired oxidation products.³⁶ In addition, the reduction to the diol is not as easily accomplished with acidic hydrazine as with **3**. Thus, Ammon Lehnig synthesized the reduced dione by a different method as detailed elsewhere.³⁶ This compound was then converted to **7** by reaction with bbTMPTZ.

Scheme 2.3. Synthetic route to **5**. i) 2% piperidine and 2% glacial acetic acid in ethanol, room temp., 4days; ii) 1-acetonylpyridinium chloride, NH_4OAc , refluxed 22 hrs. in methanol; iii) KMnO_4 , 5:1 *tert*-butanol: H_2O



DSC Testing. Cells were evaluated employing the experimental setup and protocol that follows: A Keithley 2400 SourceMeter controlled by a Labview virtual instrument was connected to the cell in a two-electrode configuration. The cell was illuminated by a 100 W Oriel xenon arc lamp calibrated to 100 mW cm^{-2} . Light was passed through an Oriel 1/8M Cornerstone monochromator and subsequently through a 400 nm high-pass cutoff filter before illuminating the cell through an aperture of 0.4 cm^2 . The monochromator, and therefore wavelength selection, was controlled during incident photon conversion efficiency (IPCE) measurements by the Labview virtual instrument. Potentials were applied from 700 mV to -100 mV when evaluating IV performance.

Cells were constructed in a classic sandwich cell arrangement.³⁷ The photoanode consisted of a compact TiO_2 underlayer beneath a mesoporous TiO_2 layer, and the cathode was thermally evaporated gold-on-chromium-on-FTO. Compact TiO_2 underlayers were spin-coated as described below onto pre-scored fluorine-doped tin oxide coated glass (FTO, TEC 15, Hartford Glass). The sides of the glass were masked by tape (Scotch™) and a TiO_2 paste (T-37

nanoxide, Solaronix) was doctor-bladed into the gap, resulting in ca. 2.5 μm (“1-scotch”) films. After drying in air for ca. 15 mins, the glass plates were annealed in air following literature procedure³⁸: 180 °C for 10 mins, 320 °C for 10 mins, 390 °C for 10 mins, 500 °C for 60 mins. The plates were then allowed to cool slowly before breaking. If not placed into solution immediately following annealing, the individual photoanodes were re-heated to 150 °C for 30 mins and placed in solution while still hot.

The TiO_2 sol for depositing the compact underlayer was prepared similarly to a prior method.³⁹ 250 μL of de-ionized water was pH-adjusted to 1-2 with HNO_3 . The diluted acid was added to 10 mL ethanol at 0 °C and allowed to stir for 5 mins. 750 μL of distilled titanium isopropoxide was then added slowly with constant stirring. The sol was allowed to stir at 0 °C for one hour, and rested for at least 12 hours but no longer than 72 hours at 2 °C. Prior to spin-coating, the sol was allowed to warm to room temperature with constant stirring. Tape was used to mask the edges of an FTO substrate in order to keep a bare contact surface when the cell was fully assembled. 1.5 mL of sol was applied in a steady stream via syringe over 10-15 seconds to each substrate spinning at 1600 rpm. Following application, the substrate was allowed to spin for one minute to dry. This procedure resulted in < 150 nm compact TiO_2 underlayers.

Photoanodes dyed with N3 (see Chapter 1, Fig. 1.4 for structure) were placed into a 0.5 mM ethanol solution of the dye while hot. Cu(I) polypyridyl dyes constructed from **1-4** were fabricated on the surface of the photoanode in stepwise fashion as suggested by Constable et. al.¹⁸ The hot photoanode was first placed in a 1.5 mM solution of **4** in methanol for 3 hours followed by rinsing with methanol and drying by compressed air or $\text{N}_2(\text{g})$. The photoanode was then placed in a 1.5 mM solution of $[\text{Cu}(\mathbf{3})_2]\text{BF}_4$, $[\text{Cu}(\mathbf{2})_2]\text{BF}_4$, or $[\text{Cu}(\mathbf{1})_2]\text{BF}_4$ in acetonitrile for 18-60 hours. Each complex solution was prepared by adding appropriate stoichiometric amounts

of the respective ligand (2 equivalents) and $[\text{Cu}(\text{ACN})_4]\text{BF}_4$ (1 equivalent) into acetonitrile solvent. Lability of the Cu(I) allowed one existing ligand on the dissolved complex to exchange with a binder ligand, **4**, previously bound to the surface of the TiO_2 , resulting in a stepwise fabrication of the heteroleptic dye on the surface. Dyes made from **3** and **5-7** were constructed differently and will be addressed near the end of the chapter (*vide infra*).

Cells were assembled with 25 μm Kapton spacers between photoanode and cathode and left unsealed. The assembled cell was mounted in a cell holder equipped with a screw clamp to hold the halves of the cell together. The mediator complex salts, $[\text{Co}(\text{DTB})_3](\text{ClO}_4)_2$ and $[\text{Co}(\text{DTB})_3](\text{ClO}_4)_3$ (DTB = 4,4'-di-*tert*-butyl-2,2'-bipyridine), were prepared as described previously.³⁹ Mediator solution, consisting of 0.135 M $[\text{Co}(\text{DTB})_3](\text{ClO}_4)_2$, 0.015 M $[\text{Co}(\text{DTB})_3](\text{ClO}_4)_3$, 0.2 M lithium trifluoromethanesulfonate ("triflate"), and 0.2 M 4-*tert*-butylpyridine (TBP) in γ -butyrolactone, was introduced at the interface between the photoanode and cathode and drawn into the cell by capillary action. Cells were allowed to equilibrate with the mediator solution for 10 mins followed by removal of the solution from the cell by wicking it into the corner of a Kimwipe. The cells were filled and emptied of mediator solution via this approach at least twice prior to final filling with mediator solution and solar testing.

Transient Absorption Measurements. Transient absorption (TA) spectra were obtained using a dyed "3-scotch" TiO_2 -on-glass film oriented at 45° to a 475 or 500 nm 15 Hz pulsed pump beam (ca. 4 ns FWHM) generated by an Opolette OPO laser (Opotek) and defocused to a diameter of ca. 1 cm. The laser power was ca. 35 mW. The probe beam was from a 100 W xenon arc lamp oriented at approximately 90° to the laser and defocused to match the area of laser excitation. The probe beam was passed through a 400 nm high-pass cutoff filter to remove UV light. The response was monitored using a Hamamatsu photomultiplier tube connected to an

oscilloscope. A two-slit chopper wheel operating at 15 Hz acted as the trigger for the laser and defined the window for data collection. A 5 k Ω measuring resistor was connected in parallel with the oscilloscope to modify the input impedance, which resulted in signal gain but also a lower signal-to-noise ratio.

Results and Discussion

Although DSCs are frequently constructed without spacers and with photoanode and cathode in direct contact, this arrangement resulted in large variability in cell performance. The use of spacers afforded better reproducibility at a cost of lower currents due to the increased mediator diffusion distance.

Typical J-V curves for the three heteroleptic Cu(I) complexes adsorbed to TiO₂ by **4** are depicted in Fig. 2.7. [Cu(**3**)(**4**)]⁺ exhibits the best performance ($J_{SC} = 0.54 \text{ mA cm}^{-2}$, $V_{OC} = 570 \text{ mV}$, FF = 0.69) among these complexes, but with significantly inferior photocurrent compared to a similar N3 cell ($J_{SC} = 1.74 \text{ mA cm}^{-2}$, $V_{OC} = 610 \text{ mV}$, FF = 0.72). The J-V curves obtained for the [Cu(**3**)(**4**)]⁺ dye are rather conventionally shaped; however, those of [Cu(**1**)(**4**)]⁺ and [Cu(**2**)(**4**)]⁺ reach a maximum current during the voltage scan between ca. 300 and 400 mV which slowly diminishes as the applied voltage approaches 0 mV (rendering a determination of FF inappropriate). The curves in Fig. 2.7 were obtained by scanning the potential from positive to negative (i.e., right to left in the figure). When the scan direction is reversed, the qualitative shapes of the curves for photoanodes dyed with [Cu(**1**)(**4**)]⁺ and [Cu(**2**)(**4**)]⁺ change. There is no longer a maximum in the current at positive potential and the current slopes in the opposite direction. This observation suggested a time dependence for the photocurrent and prompted

transient current measurements (Fig. 2.8) which reveal slow current decays (over 10-100s of seconds) for both $[\text{Cu}(\text{1})(\text{4})]^+$ and $[\text{Cu}(\text{2})(\text{4})]^+$.

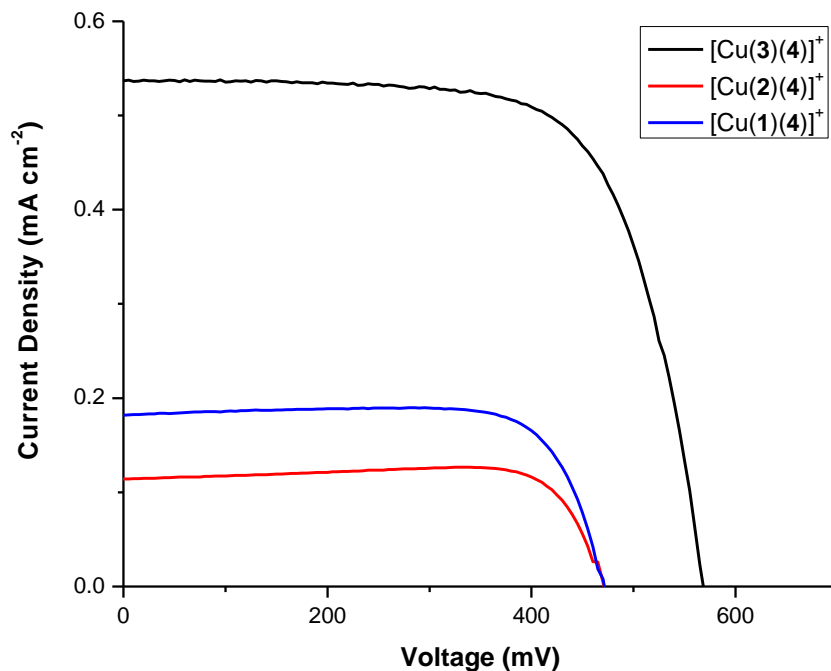


Figure 2.7 J-V curves for the three heteroleptic Cu(I) complexes anchored by **4**. The cell dyed with $[\text{Cu}(\text{3})(\text{4})]^+$ exhibited ca. 15% greater dye uptake based on the MLCT absorbance of the dyed photoanode.

Fig. 2.8 shows the time course of the normalized J_{SC} after pulsing on the illumination. Normalization was accomplished by dividing all the currents by the maximum instantaneous current for the 100 mW cm^{-2} illumination. All measurements were made using the $[\text{Co}(\text{DTB})_3]^{2+/3+}$ mediator as described in the Experimental section. Fig. 2.8A shows results for a N3-dyed photoanode, which are qualitatively identical to results reported previously.³⁹ The current peaks upon initial illumination and then rapidly decays to a steady state value. The explanation for this behavior involves mass transport of the 3+ form of the mediator and will be considered in detail below. Fig. 2.8B shows analogous results for a photoanode dyed with $[\text{Cu}(\text{3})(\text{4})]^+$. In contrast to the results in Fig. 2.8A, there is no spike in the current. The current

rapidly reaches a steady state which scales directly with the light intensity. The absence of a spike for this cell is not unexpected and easily explained by noting that the maximum absolute J_{SC} values (i.e, not normalized) for the $[\text{Cu}(\mathbf{3})(\mathbf{4})]^+$ dye are smaller than the steady-state current obtained for the N3-dyed photoanode (*vide supra*); therefore, the mass-transport limitation is never reached. Figs. 2.8C and 2.8D show results for $[\text{Cu}(\mathbf{1})(\mathbf{4})]^+$ and $[\text{Cu}(\mathbf{2})(\mathbf{4})]^+$. For both of these complexes, current spikes but then slowly decays until a pseudo-steady state is reached *only after several minutes*.

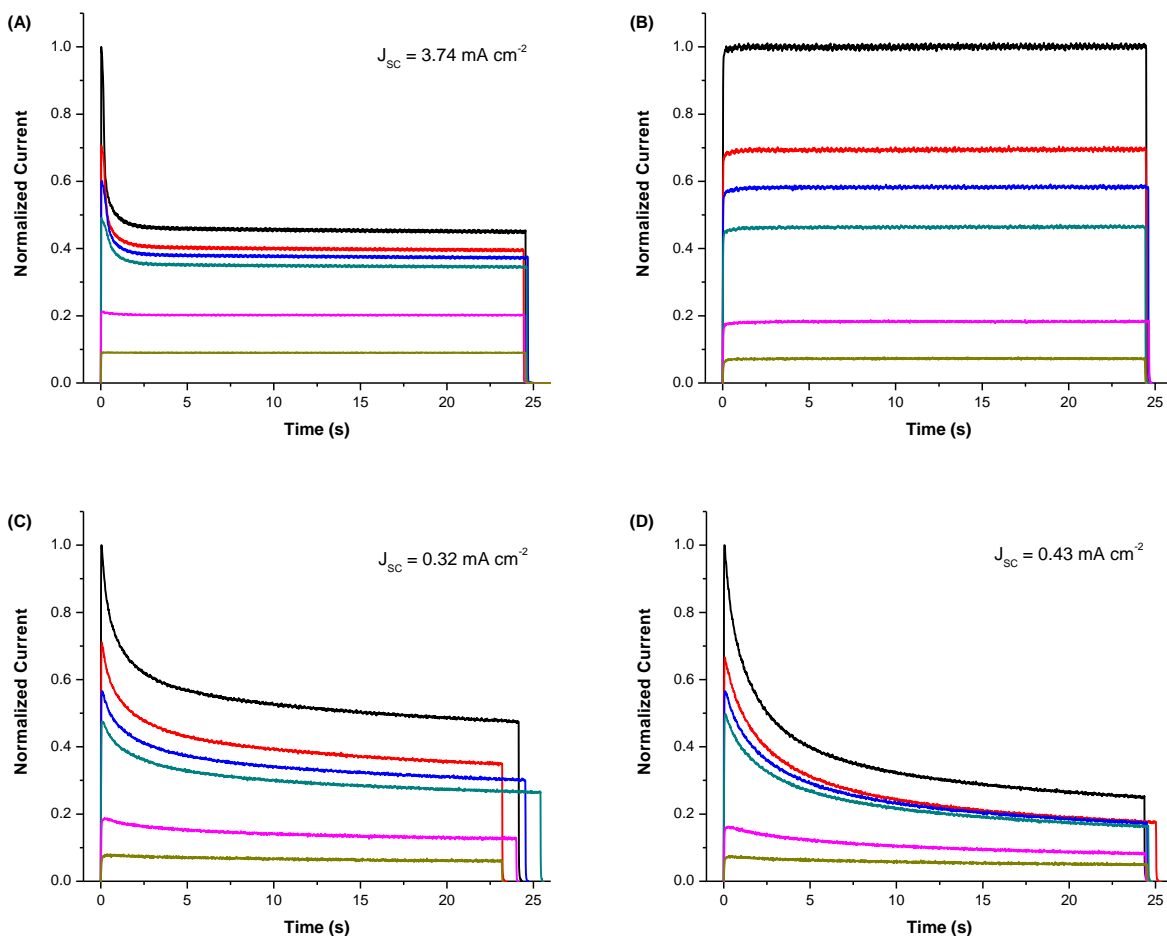


Figure 2.8. Normalized (see text) current transients for cells dyed with N3 (A), $[\text{Cu}(\mathbf{3})(\mathbf{4})]^+$ (B), $[\text{Cu}(\mathbf{1})(\mathbf{4})]^+$ (C), and $[\text{Cu}(\mathbf{2})(\mathbf{4})]^+$ (D). Light intensity was varied as a fraction of one sun: 100% (black), 71% (red), 57% (blue), 41% (cyan), 26% (pink), 12% (gold). In the cases of C and D, the cell was allowed to sit in the dark for 10 mins. between measurements. Photoanodes are different from those in Fig. 2.7. Peak currents at one sun illumination are provided for cases A, C, and D.

Fig. 2.9, shows the incident photon to current efficiencies (IPCEs). The IPCE responses for the copper-based dyes investigated here are substantially lower and are red-shifted to different degrees compared to their TiO₂-adsorbed absorption spectra centered around 450 nm. Of note is the broad shoulder present in [Cu(1)(4)]⁺ extending out over 50 nm further into the red than the other two complexes, which is attributed to the absence of substitution at the 5,6 positions on the phenanthroline backbone.

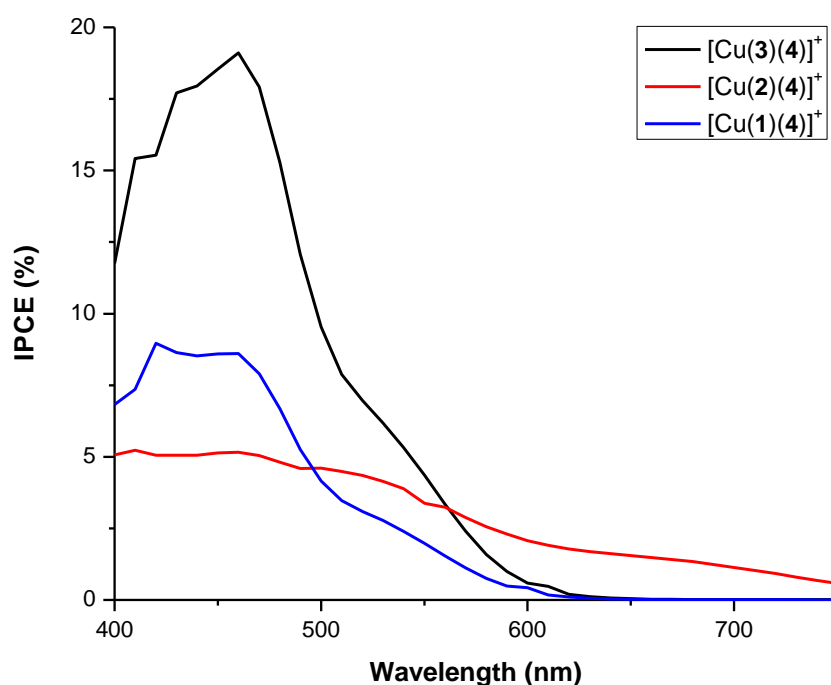
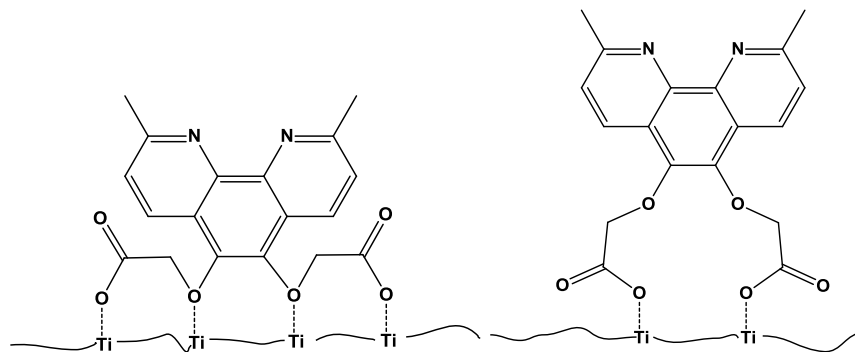


Figure 2.9. IPCE curves of heteroleptic Cu(I) complexes anchored to TiO₂ by **4**.

IPCE values for analogous cells having photoanodes dyed with N3 are considerably larger due to greater dye absorption and a larger molar absorptivity at the λ_{max} for the dye. Typically, identical photoanodes dyed with N3 have absorbances that are ca. 2.5-3 \times greater than that of [Cu(3)(4)]⁺. This is in part due to the inherently smaller molar extinction coefficient for the MLCT transition of the copper dyes (ca. 8000 M⁻¹ cm⁻¹ for [Cu(1)₂]⁺)¹¹ but also results from a lower surface loading (*vide infra*).⁴⁰ However, comparisons of absorbed photon to current

efficiency (APCE) curves for N3 and $[\text{Cu}(\mathbf{3})(\mathbf{4})]^+$ are more similar (data not shown). At λ_{max} the APCE for $[\text{Cu}(\mathbf{3})(\mathbf{4})]^+$ is 35-40%, which is considerably lower than for N3, but indicates that the photoinjection process is still reasonably efficient despite the longer linking moiety between the TiO_2 surface and the dye.

Scheme 2.4. Possible binding modes for dyes bound by **4**.



Because the core chromophore of each dye is essentially a $[\text{Cu}(\mathbf{1})_2]^+$ differing only in the total number of ether functions at the 5,6-positions of the ligands, the MLCT state of each dye should exhibit similar optical and photophysical properties. Indeed, photoanodes dyed with $[\text{Cu}(\mathbf{1})(\mathbf{4})]^+$, $[\text{Cu}(\mathbf{2})(\mathbf{4})]^+$, and $[\text{Cu}(\mathbf{3})(\mathbf{4})]^+$ exhibit very similar absorption spectra centered around 450 nm. Comparable photoanodes dyed with these copper complexes, however, absorb only ca. 30%-40% as much light at λ_{max} as ones dyed with N3. Assuming that N3 adsorbs in a complete monolayer and that it has a $\epsilon(\lambda_{\text{max}})$ ca. 1.8x larger than $[\text{Cu}(\mathbf{1})_2]^+$,^{2,11} one can conclude either that the surface coverage of copper dyes is only 50-70% of a monolayer or that they have 1.5-2.0x larger effective footprints. Because of the *in situ* fabrication of the dye, it is possible that not all of the surface bound **4** is sterically capable of binding a $\text{Cu}(\mathbf{1})$ moiety which could account for the lower dye loading. On the other hand, the binding groups on **4** extend out further than the COOH functions on the N3. Moreover, once one or more carboxylates bind, it is possible that

the ether functions might also participate in surface binding (because of the favorable entropy, Scheme 2.4). If so, the effective dye footprint could be considerably larger than otherwise.

The alkyl linkages connecting TMPTZ to the phenanthroline backbone in **3** were selected for two reasons. The first arises from past work with Ru(bpy)₃-based (D-C-A) triads.⁴¹ In these systems a ground-state association occurs between the bipyridine ligands and the π -system of the donor which is instrumental in affording efficient photoinduced charge-separated state formation.⁴¹ Although there is no experimental evidence of a similar interaction with these dyes, the butyl ether linkage would certainly allow for such in [Cu(**3**)(**4**)]⁺. The second arises from advantages obtained from amphiphilic ruthenium-based dyes such as Z-907 relative to N3 or N-719 (see Chapter 1, Fig. 1.4 for structures). Having the lipophilic ligand oriented away from the surface of the TiO₂ results in greater long-term stability for cells utilizing Z-907, supposedly due to inhibited access of water to the surface.³ Cu(I)-based dyes are anticipated to have inherently lower stability towards competitive coordination at the metal center, as well as competition for adsorption to surface sites on the TiO₂; thus, the incorporation of such a lipophilic component could have advantages from several angles related to dye stability.

Because the TMPTZ appendages likely impact the dye behavior in multiple ways, deconvoluting purely lipophilic effects from effects due to the electron donor is important. To that end, [Cu(**2**)(**4**)]⁺ was synthesized. It is clear from data in Figs. 2.7-2.9 that incorporating a lipophilic appendage alone does not improve cell performance; in fact, the IPCE, J_{SC} and V_{OC} are all lowest for [Cu(**2**)(**4**)]⁺. Particularly with respect to the J_{SC} this is not entirely surprising given that the octyl substituents likely restrict access by the large cobalt mediator to the copper center.⁴²

The result for the pulsed-light current transients given in Figs. 2.8A and 2.8B are typical of what is expected. As discussed above, N3-dyed photoanodes mediated with $[\text{Co}(\text{DTB})_3]^{2+/3+}$ exhibit mass-transport limited currents at high light intensities which is manifested in these experiments as an initial spike in J_{SC} that rapidly decays to a steady state.^{39,43} At lower light intensities the spike becomes less prominent until it disappears at the point where mass transport no longer is rate determining.³⁹ The current transients in Fig. 2.8B for $[\text{Cu}(\mathbf{3})(\mathbf{4})]^+$ lack the same spike only because the absolute currents at 1-sun are below the threshold where mass-transport limitations of $[\text{Co}(\text{DTB})_3]^{3+}$ are encountered. Consequently, the currents rise rapidly to their steady state values.

While the current-time transients in Figs. 2.8C and 2.8D for $[\text{Cu}(\mathbf{1})(\mathbf{4})]^+$ and $[\text{Cu}(\mathbf{2})(\mathbf{4})]^+$, respectively, bear some qualitative resemblance to the behavior of the N3 cell, the observed behavior is clearly not due to mediator mass transport limitation issues. First, the maximum current densities in both cases are well below the diffusion-limited current density as observed by evaluation of N3 (ca. $850 \mu\text{A cm}^{-2}$). Second, the decays are much slower than those observed for the N3 case. Finally, reduced light intensity does not result in elimination of the current peak.

Initially, it was hypothesized that the observed behavior could be the result of some undetermined thermal process affecting one of the various kinetic processes in an undesirable way. As the cell is illuminated it does heat up moderately. Moreover, it requires several minutes in the dark to recover to its initial current, *but it does eventually recover*. To probe this possible explanation, the cell was heated gently in the dark (with a heat gun) prior to pulsing on the illumination. The result is shown in Fig. 2.10. External heating actually resulted in a moderately

higher current density and no significant change in the rate of the current decay. Tentatively this thermally-induced current increase is assigned to reduced γ -butyrolactone viscosity.

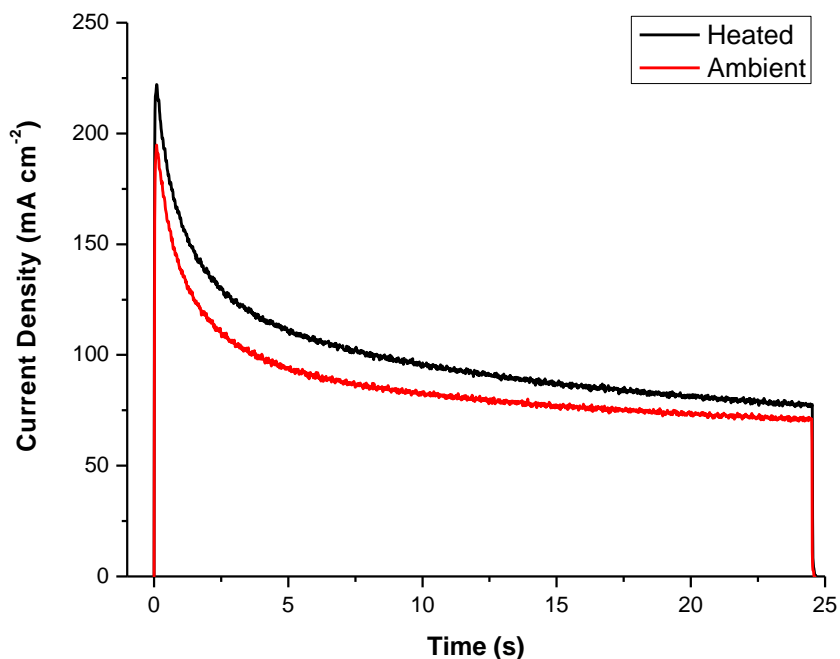


Figure 2.10. Effect of heating on the current transient of a cell dyed with $[\text{Cu}(2)(4)]^+$. Heating was applied via heat gun from the back of the cell for 10 seconds.

In an effort to gain some understanding of the origin of the time dependent current for cells dyed with $[\text{Cu}(1)(4)]^+$ and $[\text{Cu}(2)(4)]^+$, other constituents in the mediator solution were considered. In high-performance cells based on ruthenium polypyridyl dyes, the mediator (both I^-/I_3^- and cobalt complexes) solutions typically contain "additives": Li^+ (usually as the triflate salt) to increase photocurrent and TBP to increase the photovoltage.^{8,37} The exact mechanisms whereby Li^+ and TBP affect the cell performance is still a matter of some discussion and in fact may be different depending which mediator system is being employed.³⁷ Nonetheless, with either type mediator, TBP decreases the dark current which increases the V_{OC} . The TBP ostensibly adsorbs to free sites on the TiO_2 and thus physically hinders electron-transfer between

oxidized mediator and the semiconductor surface.⁴⁴ Additionally, TBP has a supposed small negative impact on the photo-injection efficiency.^{44,45} Together these effects generally result in enhancements in both photovoltage and fill factor at the expense of a nominal diminution of photocurrent. Generally, the simultaneous presence of both Li^+ and TBP in the mediator solution results in a substantial improvement in both photocurrent and photovoltage.^{8,37} As such, it was initially assumed the same would hold true in the copper-dye cells investigated here. However, it was determined that TBP impacts the performance of cells employing these copper-based dyes very differently.

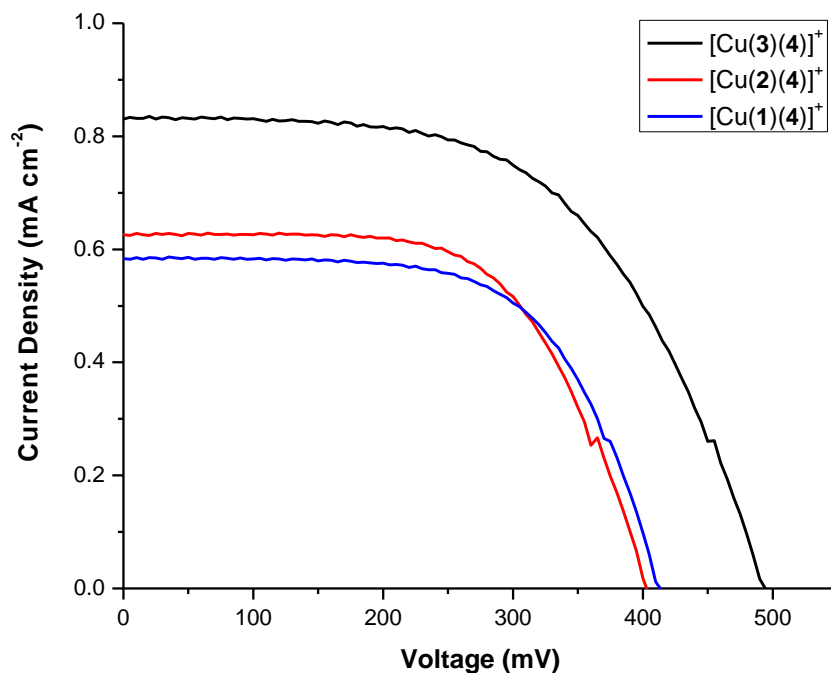


Figure 2.11. J-V curves of heteroleptic Cu(I) dyes bound by **4**. Mediator consisted of 0.2 M lithium triflate, 0.135 M $[\text{Co}(\text{DTB})_3](\text{ClO}_4)_2$, and 0.015 M $[\text{Co}(\text{DTB})_3](\text{ClO}_4)_3$ in γ -butyrolactone. The cell dyed with $[\text{Cu}(3)(4)]^+$ exhibited ca. 10% greater dye uptake relative to the other two photoanodes based on the MLCT absorbance of the dyed photoanode.

Comparing the data in Fig. 2.11 with that in Fig. 2.7, the decrease in V_{OC} was expected and is reflected in the difference in dark current irrespective of the dye. What was not expected

was that the J_{SC} *significantly increased* for all three dyes examined. Moreover, the shapes of the J-V curves for the $[\text{Cu}(2)(4)]^+$ and $[\text{Cu}(1)(4)]^+$ cells in Fig. 2.11 are relatively flat which prompted re-examination of the pulsed-light transients in the absence of TBP for all three copper dyes. First, in the case of $[\text{Cu}(3)(4)]^+$, the increase in J_{SC} is sufficient for it to exceed the threshold for mediator mass-transport limitation at 1-sun; consequently, at this high light intensity a rapidly decaying initial current spike is present just as is for N3 but otherwise the behavior is the same as in Fig. 2.8B. For the cases of $[\text{Cu}(2)(4)]^+$ and $[\text{Cu}(1)(4)]^+$ the changes are qualitatively and quantitatively quite different (*vide infra*). However, before considering these data in more detail it is useful to first consider cyclic voltammetry results for $[\text{Cu}(2)_2]^+$.

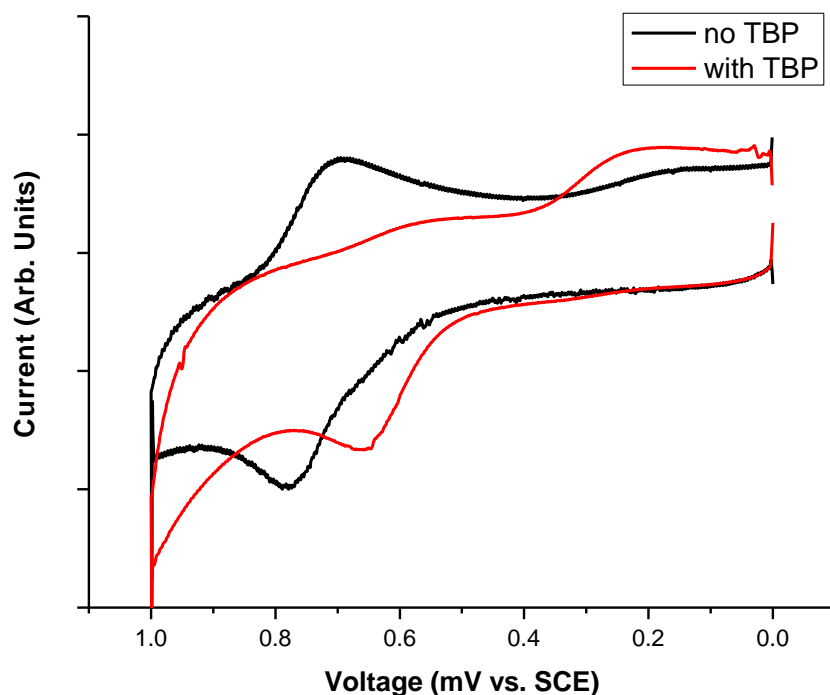
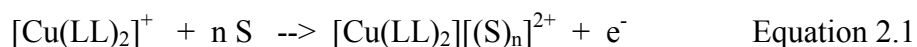


Figure 2.12. Cyclic voltammogram of $[\text{Cu}(2)_2]^+$ in γ -butyrolactone. Scans were run at 100 mV/s with and without TBP added. The addition of TBP was at an equivalent concentration (0.2 M) as that in a working DSC.

Fig. 2.12 shows cyclic voltammograms at a glassy carbon electrode in γ -butyrolactone of $[\text{Cu}(\mathbf{2})_2]^+$ with and without TBP present. In the absence of TBP the Cu(I/II) couple appears fairly reversible. However, as discussed briefly above, there are dramatic solvent dependencies of the $E_{1/2}$ for the Cu(I/II) couple for phenanthroline complexes.²⁷ For example, the $E_{1/2}$ for the $[\text{Cu}(\mathbf{1})_2]^{+/2+}$ couple shifts 290 mV negative in DMSO relative to its position in DCM.²⁷ This solvent dependence is interpreted in terms of a rapid, concerted EC mechanism (Eq. 2.1) wherein Cu(II) picks up a solvent molecule(s) to become five (or six) coordinate concomitantly with the electron transfer²⁷:



Consequently, the measured $E_{1/2}$ in a non-coordinating solvent such as DCM should more nearly reflect the instantaneous driving force for an electron transfer (e.g., after photoinjection of an electron by the copper dye) whereas the $E_{1/2}$ measured in γ -butyrolactone (which is a moderately good donor solvent) should reflect the equilibrium driving force for the thermally relaxed species. These results shall be revisited shortly.

Transient absorption (TA) measurements were conducted on mesoporous TiO_2 (Solaronix Nanoxide HT, 3-scotch thickness) films on glass substrates (“pseudo photoanodes”) dyed with $[\text{Cu}(\mathbf{3})(\mathbf{4})]^+$ to measure recombination rates and rates of dye regeneration by the mediator. Fig. 2.13 depicts the TA transients at 550 nm near the maximum absorption of the oxidized TMPTZ donor.⁴⁶ For the red curve, the pseudo photoanode was contacted with γ -butyrolactone containing 0.2 M lithium triflate and 0.2 M TBP. The blue curve was for the same pseudo photoanode in contact with an identical solution but containing 0.135 M $[\text{Co}(\text{DTB})_3](\text{ClO}_4)_2$ as well. It is clear from these two curves that, first, the recombination with

the conduction band electrons with the TMPTZ^+ is slow (on the order of 80-100 μs) and, second, the reduction of the TMPTZ^+ by the $[\text{Co}(\text{DTB})_3]^{2+}$ is considerably faster than recombination.

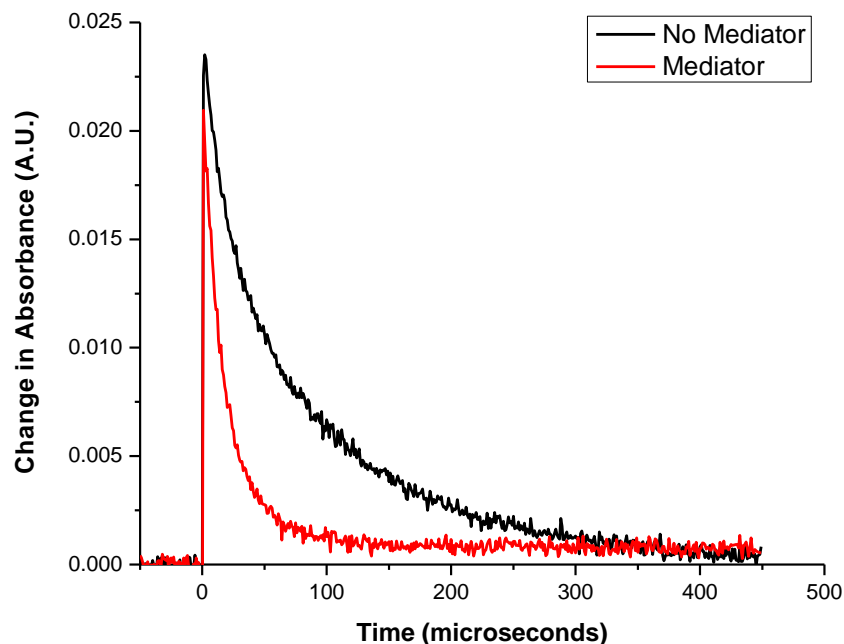


Figure 2.13. TA measurement at 550 nm of $[\text{Cu}(\mathbf{3})(\mathbf{4})]^+$ on TiO_2 . Excitation was accomplished at 475 nm. The black curve was obtained when the sample was contacted with a solution containing 0.2 M lithium triflate and 0.2 M TBP in γ -butyrolactone. The red curve is for the same TiO_2 sample in contact with an identical solution except also containing 0.135 M $[\text{Co}(\text{DTB})_3](\text{ClO}_4)_2$.

The spectrum obtained from these measurements shows the clear spectral feature of TMPTZ^+ with its λ_{max} at ca. 550 nm.⁴⁶ The appearance of the TMPTZ^+ absorption is multi-exponential but with ca. 80% of the signal appearing within the laser pulse (ca. 7 ns) and complete oxidation being realized by ca. 100 ns. Fig. 2.13 gives the time evolution of the TMPTZ^+ signal decay after excitation. The MLCT state of the dye is a very weak oxidizing agent, too weak to directly oxidize the donor.^{27,46} Therefore, there is no ambiguity about the order of electron transfer events: the photo-excited dye first injects an electron into the semiconductor and then the resulting $\text{Cu}(\text{II})$ oxidizes the TMPTZ . Without greater time resolution than is possible with the current laser system, the quantitative rates of charge injection,

recombination, or donor oxidation cannot be commented on. Suffice it to say, the very fact that a signal for TMPTZ^+ is observed indicates that TMPTZ oxidation by the Cu(II) is at least competitive with charge recombination and possibly much faster. Interestingly, cyclic voltammetry measurements of $[\text{Cu(2)}_2]^{+/2+}$ in γ -butyrolactone (vide infra) place the Cu(I/II) redox potential only ca. 130 mV positive of the $\text{TMPTZ}^{0/+}$ couple; therefore, either the oxidation of TMPTZ by the Cu(II) is very rapid despite a small driving force (indicating a small reorganizational energy) or the solution electrochemistry does not reflect the appropriate redox potential for the surface-bound, photo-generated $[\text{Cu(3)(4)}]^+{}^{2+}$. The latter is a distinct possibility given the strong solvent dependence of the $E_{1/2}$ observed for $[\text{Cu(1)}_2]^{+/2+}$ -type complexes. This point will be considered in more detail below. Irrespective of the molecular details, the appearance of TMPTZ^+ is almost complete after 10 ns indicating very rapid regeneration of Cu(I) . The time course of the decay of the TMPTZ^+ signal (both with and without $[\text{Co(DTB)}_3]^{2+}$ present) occurs on the μs timescale. In the absence of $[\text{Co(DTB)}_3]^{2+}$ the decay requires at least two exponentials to be reasonably fit with lifetimes of ca. 20 and 80-100 μs . In the presence of 0.135 M $[\text{Co(DTB)}_3]^{2+}$ the decay can be fit with a single exponential with a lifetime of ca. 20 μs .

Matters are more complicated for the other two dye systems because they lack the strongly absorbing TMPTZ^+ chromophore; consequently, it was necessary to monitor the dye bleach between 400-500 nm (data not shown). The data is of much poorer quality due to much weaker signal, making quantitative inference difficult. Nonetheless, for both $[\text{Cu(2)(4)}]^+$ and $[\text{Cu(1)(4)}]^+$, the addition of mediator results in faster regeneration of the bleach. However, the effect does not seem to be as pronounced as in the case of $[\text{Cu(3)(4)}]^+{}^{2+}$. One factor of note which will be addressed in more detail below is that, with or without mediator, there is a small but

significant very slow component to the bleach recovery that has a lifetime > 2.5 ms (the maximum window of the current experimental setup).

Electrochemical, TA, and cell testing results provide a basis to explain a number of observations for the cells comprising these copper based dyes including: (1) the surprisingly rapid oxidation of the TMPTZ by the photogenerated Cu(II) in $[\text{Cu}(\mathbf{3})(\mathbf{4})]^+$; (2) the likely origin of the current decay in Figs. 2.8C and 2.8D and (3) the increased J_{SC} in Fig. 2.11 (relative to that in Fig. 2.7) for $[\text{Cu}(\mathbf{2})(\mathbf{4})]^+$ and $[\text{Cu}(\mathbf{1})(\mathbf{4})]^+$.

First, in the case of $[\text{Cu}(\mathbf{3})(\mathbf{4})]^+$, after photoinjection of the electron, if the closely packed dye molecules restrict access of the metal center to solvent (and/or other potential ligands), then the unsolvated Cu(II) should be a considerably stronger oxidant than the thermally equilibrated $[\text{Cu}(\mathbf{2})_2]^{2+}$ reflected by the voltammetry (by as much as ca. 300 mV).²⁷ This would make the apparent rapid oxidation of attached TMPTZ in $[\text{Cu}(\mathbf{3})(\mathbf{4})]^+$ less surprising (*vide supra*).

Second, the changes in the CV of $[\text{Cu}(\mathbf{2})_2]^+$ upon addition of TBP (at the same concentration used in the mediator solution) are fairly dramatic. The voltammogram becomes irreversible with the oxidation peak shifting modestly negatively (ca. 100 mV) and the reduction peak shifting over 500 mV negatively and becoming very broad. This dramatic change suggests several things: (1) that TBP is a significantly better ligand for Cu(II) than γ -butyrolactone and (2) that the kinetics for the association/dissociation of TBP are much slower. Because of the irreversible nature of the latter CV (even at a scan rate of 50 mV/s) an $E_{1/2}$ calculated from the voltammetric peaks does not reflect the true equilibrium potential for the equivalent process in Eq. 2.1 where $S = \text{TBP}$. However, when photoanodes dyed with any one of the three copper complexes are contacted with full mediator solution (i.e., containing $[\text{Co}(\text{DTB})_3]^{2+}$,

$[\text{Co}(\text{DTB})_3]^{3+}$ lithium triflate, and TBP) they are stable indefinitely *in the dark*. Therefore, whatever the equilibrium potential for the Cu(I/II) couple is under these solution conditions, it is positive of the potential for the $[\text{Co}(\text{DTB})_3]^{2+/3+}$ couple ($E^0 \approx 0.120$ V vs. SSCE); otherwise the dyes would be oxidized in the dark by the mediator solution. However, once the copper center is oxidized, it can coordinate TBP. Based on the CV results of Fig. 2.12, the reduction of that species by the $[\text{Co}(\text{DTB})_3]^{2+}$ could be quite slow.

At this point speculation on the origins of the time dependence of the currents in Figs. 2.8C and 2.8D is appropriate. Recall for $[\text{Cu}(\mathbf{2})(\mathbf{4})]^+$ and $[\text{Cu}(\mathbf{1})(\mathbf{4})]^+$ in contact with the full mediator solution (i.e., with TBP present), after the current reaches its pseudo-steady state, the initial current fully recovers in the dark after several minutes. Thus, the process responsible for the current decrease is reversible in the dark but only slowly. Under illumination there must exist a steady-state concentration of oxidized dye. If the dye is regenerated by the mediator rapidly enough, it will recycle in the photo-injection; however, if TBP coordinates to the Cu(II) before it can be regenerated, the driving force for regeneration is much reduced. Furthermore that process, based on the CV results, should be quite slow. Also, in a closely packed monolayer of dye on the TiO_2 surface, it is likely that some dye molecules will be more accessible to coordination by TBP than others. Thus the hypothesis is that the decay of the current in Figs. 2.8B and 2.8C results from Cu(II) being intercepted by coordination of TBP which temporarily removes it from participation in photo-injection. Under illumination a steady state is reached wherein a significant fraction of the dye is inactive for this reason. In the dark, all of the copper is eventually returned to the active Cu(I) form. When it is again irradiated, the process starts anew. Furthermore, this model would be consistent with the presence of the long-lived bleach of the MLCT noted above in the TA experiments with $[\text{Cu}(\mathbf{2})(\mathbf{4})]^+$ and $[\text{Cu}(\mathbf{1})(\mathbf{4})]^+$.

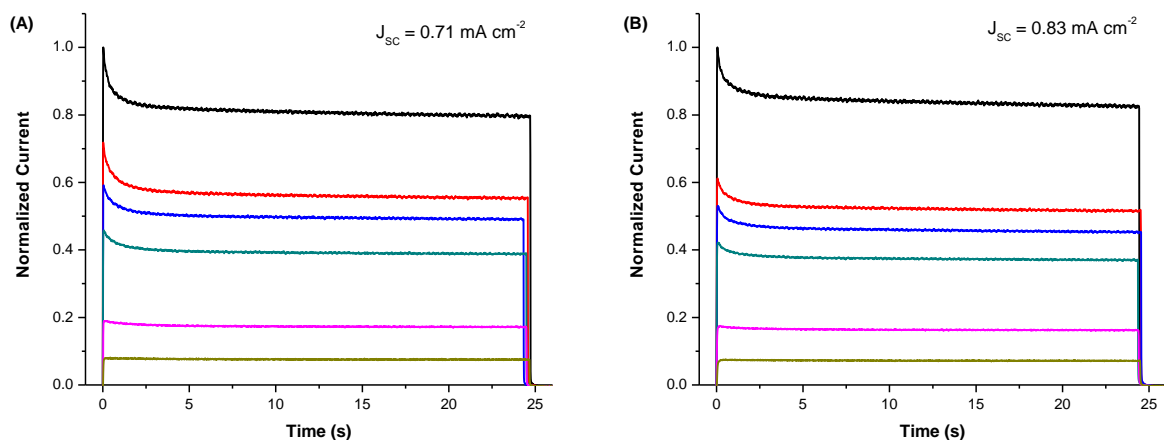


Figure 2.14. Normalized current transients of $[\text{Cu}(\mathbf{2})(\mathbf{4})]^+$ (A) and $[\text{Cu}(\mathbf{1})(\mathbf{4})]^+$ (B) in the absence of TBP. Mediator consisted of 0.135 M $[\text{Co}(\text{DTB})_3](\text{ClO}_4)_2$, 0.015 M $[\text{Co}(\text{DTB})_3](\text{ClO}_4)_3$, and 0.2 M Li triflate in γ -butyrolactone. Colored traces correspond to 100% sun (black), 71% sun (red), 57% sun (blue), 41% sun (cyan), 26% sun (pink), 12% sun (gold). Peak current values at one sun illumination are larger here than in Fig. 2.8 due to the lack of TBP and an increased amount of dye adsorbed to the surface.

The pulsed-light experiments for $[\text{Cu}(\mathbf{2})(\mathbf{4})]^+$ and $[\text{Cu}(\mathbf{1})(\mathbf{4})]^+$ in the absence of TBP (Fig. 2.14) still show initial spikes but steady state is reached within a few seconds and the steady state currents are ca. 85% of the maximum at the spike more or less independent of the light intensity. This result is consistent with the same general mechanism proposed above for solutions containing TBP. The fact that the $E_{1/2}$ for $[\text{Cu}(\mathbf{2})_2]^{+/2+}$ in γ -butyrolactone is shifted ca. 100 mV negative of the value in DCM indicates that γ -butyrolactone also binds to Cu(II) but less strongly than TBP (see Figs. 2.12 and 2.15). Also, based on the CV results (i.e., the more nearly diffusion controlled shape), the on- and off-binding rates for γ -butyrolactone are likely faster than with TBP. Thus, the rates of regeneration of the Cu(II) by the mediator at steady state should be faster. Since the steady state concentration of Cu(II) in the absence of TBP is smaller and the steady-state current is attained more quickly under illumination, it is consistent with this model that the J_{SC} should be larger and that there should be no time dependence to the plateau current. Comparing Figs. 2.7 and 2.11 this is precisely what is observed for $[\text{Cu}(\mathbf{2})(\mathbf{4})]^+$ and $[\text{Cu}(\mathbf{1})(\mathbf{4})]^+$.

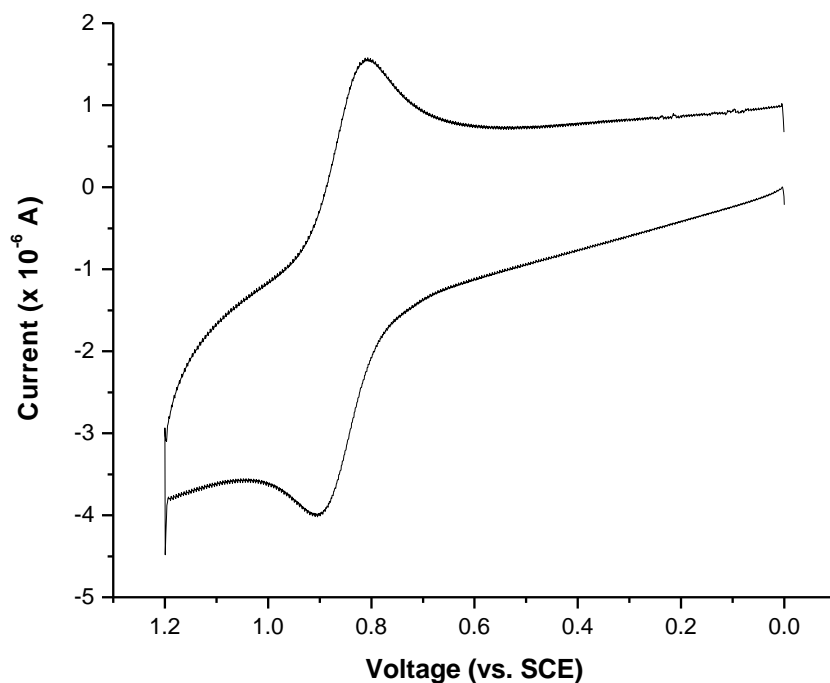


Figure 2.15. Cyclic voltammogram of $[\text{Cu}(\mathbf{2})_2]^{+/2+}$ in dichloromethane/0.1 M TBAPF₆.

Interestingly, Constable et al.^{17,18} did not report observations suggesting similar issues with TBP in combination with their bipyridine based dyes mediated with I^-/I_3^- . The COOH functions on their dyes are essentially the same as for typical ruthenium-based dyes; therefore, the dye packing densities may be greater which would be expected to restrict access of TBP to the Cu(II) center. Also, the reduction rate of Cu(II) by I^- could be inherently faster than with $[\text{Co}(\text{DTB})_3]^{2+}$. Either could account for the apparent differences in behavior of their dyes relative to those presented here.

In contrast to the donor-free dyes, the effect of TBP on cells dyed with $[\text{Cu}(\mathbf{3})(\mathbf{4})]^+$ is qualitatively and quantitatively different. First, there is no slow decay of the current with time irrespective of the presence of TBP and the J_{SC} is substantially smaller when TBP is present (ca. 50 % although the relative cell efficiency is essentially the same due to the higher V_{OC} and FF). The lack of a decay in current with time, however, is straightforwardly rationalized using the

same basic argument applied to the two other dyes. First, because the Cu(II) formed upon photoinjection is essentially instantly reduced by a TMPTZ (in less than 100 ns), the steady state concentration of Cu(II) under illumination should be vanishingly small. Moreover, the external surface of the dyed TiO₂ presented to the solution should be highly sterically congested because of the bulk of the two appended TMPTZ moieties. These two factors combined make it much less likely that Cu(II) would become kinetically trapped by coordination with TBP than is the case for the other two dyes.

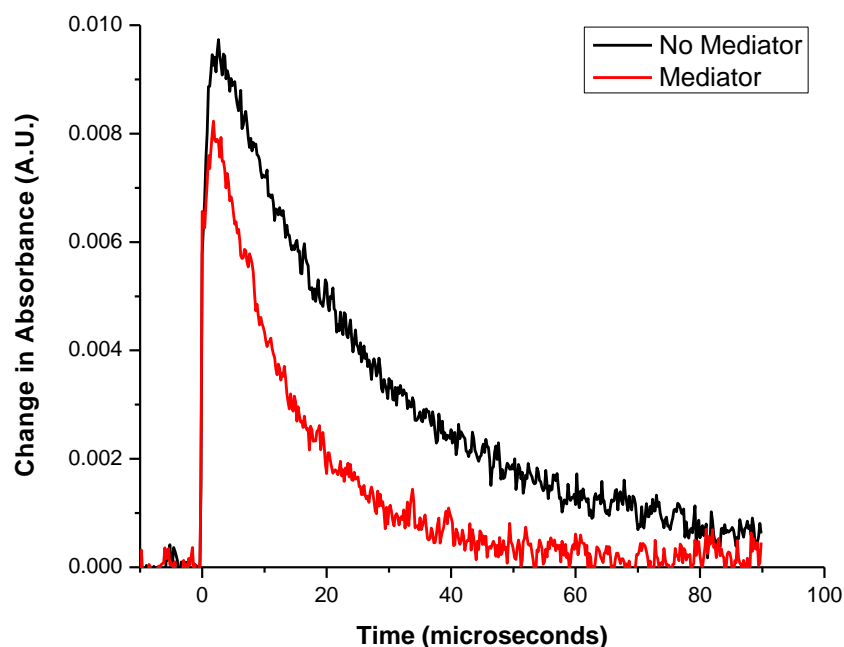


Figure 2.16. TA spectrum of [Cu(3)(4)]⁺ at 550 nm in the absence of TBP. Pseudoanode was contacted with 0.2 M Li triflate in γ -butyrolactone (“No Mediator”) followed by contacting with 0.2 M Li triflate and 0.135 M [Co(DTB)₃](ClO₄)₂ in γ -butyrolactone (“Mediator”).

Rationalizing the large relative decrease in J_{SC} caused by TBP for [Cu(3)(4)]⁺ presents more of a challenge. The IPCE is diminished roughly proportionally to the decrease in J_{SC} , and any nominal loss of dye from the TiO₂ surface in the presence of TBP is consistent across all three Cu(I) dyes. Comparison of TA data obtained at 550 nm (λ_{max} for TMPTZ⁺) without

$[\text{Co}(\text{DTB})_3](\text{ClO}_4)_2$ shows that recombination of the conduction band electrons with TMPTZ^+ is significantly faster in the absence of TBP (see Figs. 2.13 and 2.16). Therefore, TBP-induced changes in the rate of recombination of conduction-band electrons with TMPTZ^+ cannot be used to explain the differences in current.

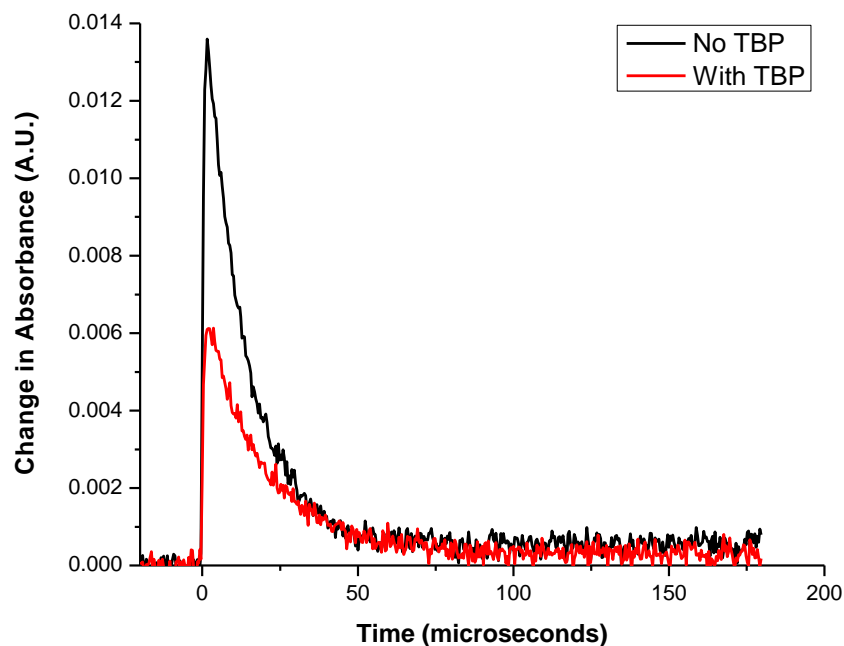


Figure 2.17. TA at 550 nm of $[\text{Cu}(\mathbf{3})(\mathbf{4})]^+$ on TiO_2 contacting 0.135 M $[\text{Co}(\text{DTB})_3]^{2+}$ and 0.2 M lithium triflate in γ -butyrolactone with (red) and without (black) TBP. See text for experimental detail.

Given the proportional decrease in J_{SC} and IPCE, it is reasonable then to argue that TBP might be affecting the injection efficiency of the dye. However, the relative decrease in J_{SC} caused by TBP is much larger for $[\text{Cu}(\mathbf{3})(\mathbf{4})]^+$ than typically observed for ruthenium-based dyes, so there is likely more going on than just a TBP-induced shift in the conduction band energy as is usually invoked for N3-type dyes.^{8,44} Fig. 2.17 shows TA data obtained from a single TiO_2 on glass film dyed with $[\text{Cu}(\mathbf{3})(\mathbf{4})]^+$. These data were first taken with the film in contact with mediator solution containing only $[\text{Co}(\text{DTB})_3](\text{ClO}_4)_2$ and lithium triflate. Then the solution was replaced with one also containing $[\text{Co}(\text{DTB})_3](\text{ClO}_4)_2$, lithium triflate, and TBP. Finally, the

TBP-containing solution was washed from the film with ethanol and the original solution (i.e., without TBP) reintroduced. First, the initial intensity of the TMPTZ⁺ signal for the TBP containing solution is only about half that of the TBP-free solution. Second, the lifetime of the TMPTZ⁺ is minimally affected by the presence of TBP. Finally, when the original solution is reintroduced to the film, the initial signal intensity significantly recovers (data not shown). Given the two proposed modes of interaction for **4** with the TiO₂ surface suggested in Scheme 2.4, it is possible that TBP could compete with the weaker ether-oxygen interactions without disrupting the COO⁻ interactions. This could allow for a decrease in efficiency of photoinjection without any concomitant loss of dye from the surface. While this notion has some appeal, TBP is a large molecule and, just from a steric standpoint, it is somewhat difficult to imagine how it could displace the Ti-O ether interactions without disrupting the COO-Ti interactions as well. Two alternate hypotheses are that either the TBP is slowing down the electron transfer rate between the Cu(II) and the TMPTZ relative to e⁻_{CB}/Cu(II) recombination or, instead, TBP is speeding up e⁻_{CB}/Cu(II) recombination relative to TMPTZ oxidation. While these latter two possibilities cannot be ruled out, they seem less likely. In order for TBP to affect the quantum yield of TMPTZ⁺ formation by one of these mechanisms the rates of e⁻_{CB}/Cu(II) recombination and Cu(II)/TMPTZ reaction would have to be similar in magnitude, which seems fortuitous but not impossible.

On the other hand, if the mechanism proposed for the TBP-induced decreasing of the injection efficiency were correct, it should manifest to some degree for all three dyes. Unfortunately, with [Cu(**2**)(**4**)]⁺ and [Cu(**1**)(**4**)]⁺ the situation is complicated by the slow current decay for both dyes in the presence of TBP. Nevertheless, if the initial current densities for Figs. 2.8C and 2.8D (i.e., t = 0) are compared with the J_{SC} values obtained in Fig. 2.11 the latter

currents are about 70% larger. This result is consistent with the argument that the injection efficiency is being negatively impacted by TBP in similar ways for all three dyes.

Lastly (for this set of dyes), electron lifetime profiles for typical cells incorporating each of the three dyes were evaluated from open-circuit voltage decay (OCVD) analysis originally developed by Bisquert and coworkers. (Fig. 2.18).^{47,48} This analysis assumes that all electron recombination is from the TiO_2 to the oxidized mediator, and not recombination with oxidized dye. Bisquert and coworkers⁴⁸ confirmed the presence of three separate regions of the curve on a log-linear plot of V_{OC} vs. time in cells dyed with N3 and mediated by I^-/I_3^- : (1) at higher potentials, recombination from the TiO_2 conduction band dominates (electron lifetime = constant); (2) at moderate potentials, recombination from the conduction band still dominates but is influenced by the presence of bulk trap states (electron lifetime = linear); (3) at low potentials, surface trap states dominate recombination (electron lifetime = parabolic). Although $[\text{Cu}(\mathbf{3})(\mathbf{4})]^+$ has three regions vaguely resembling those described by Bisquert, the system is quite different from N3 and I^-/I_3^- . Qualitatively, the shape of the curves for $[\text{Cu}(\mathbf{2})(\mathbf{4})]^+$ and $[\text{Cu}(\mathbf{1})(\mathbf{4})]^+$ differ significantly from that in $[\text{Cu}(\mathbf{3})(\mathbf{4})]^+$: both are roughly linear at lower potentials and tend to curve down towards shorter lifetimes at higher potentials. The primary difference between the data for the three dyes is the relatively constant electron lifetime for $[\text{Cu}(\mathbf{3})(\mathbf{4})]^+$ between ca. 430 and 550 mV which is longer than for either of the other two dyes over the same potential range. Since the $[\text{Cu}(\mathbf{3})(\mathbf{4})]^+$ is sterically more encumbered than either of the other two dyes, it is reasonable that recombination of e_{CB}^- with $[\text{Co}(\text{DTB})_3]^{3+}$ would be slower.

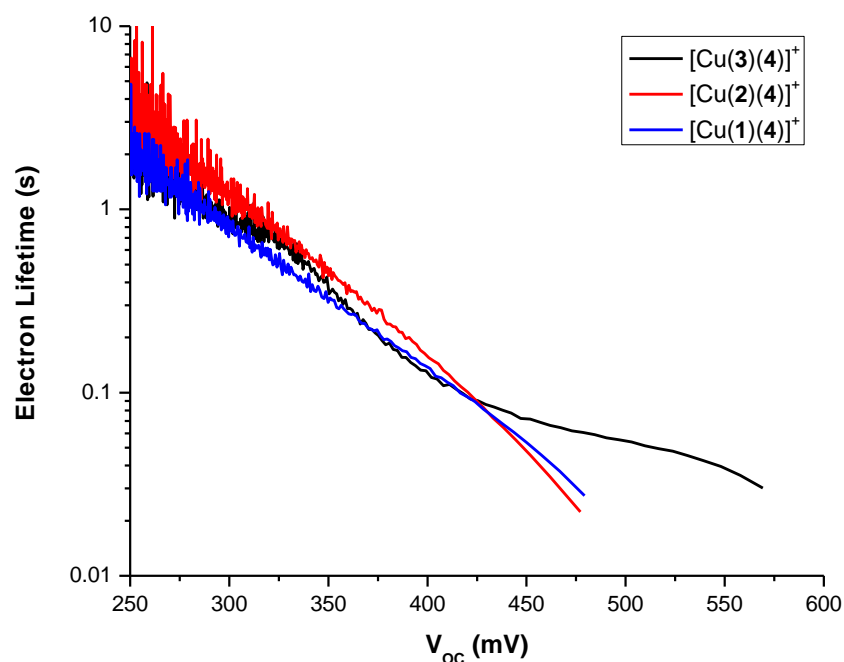


Figure 2.18. Electron lifetimes as a function of V_{OC} for cells dyed with $[Cu(3)(4)]^+$ (A), $[Cu(2)(4)]^+$ (B), and $[Cu(1)(4)]^+$ (C). Electron lifetimes were calculated from decays of the V_{OC} following Bisquert, et al.^{47,48} Cells were illuminated for several seconds prior to blocking the light and monitoring the V_{OC} decay. At V_{OC} values lower than 250 mV, changes in voltage become very small and create large variations in dV_{OC}/dt . Therefore, the plots are truncated at this potential.

The focus will now shift briefly to dyes made from ligands **5-7**. These ligands were designed to further probe the importance of 1) the electron donor and 2) the congestion of the coordination sphere preventing a full shift to D_2 geometry. Unlike **4**, both **5** and **6** have additional rotational freedom due to the fact they are bipyridines rather than phenanthrolines, with the only difference being that **5** has methyl groups at the 6,6' positions. Therefore, one might expect any effects promoting flattening to be enhanced in these complexes relative to **4**. Constable and coworkers have shown that **5** in particular is a competent binding ligand.¹⁸ Given the lackluster solar cell performance of $[Cu(1)(4)]^+$ and $[Cu(2)(4)]^+$, it is apparent that simple methyl groups are not sufficient to prevent TBP from coordinating to the oxidized Cu(II) center on the timescale of dye regeneration by Co(II) complexes. Phenyl groups are substantially larger

and should therefore inhibit flattening to a larger extent. Ligand **7** was thus designed to be essentially identical to **3** but with phenyl groups at the 2,9 positions rather than methyl groups. With enough steric hindrance around the coordination sphere, complexation even without the presence of a species capable of rapidly reducing the metal center (like a covalently bound electron donor or a mediator with a faster rate of regeneration) should be unfavorable.

For these experiments the stepwise method is abandoned in favor of single-pot dye solutions of $[\text{Cu}(\mathbf{3})(\mathbf{5})]^+$, $[\text{Cu}(\mathbf{7})(\mathbf{5})]^+$, $[\text{Cu}(\mathbf{3})(\mathbf{6})]^+$, and $[\text{Cu}(\mathbf{7})(\mathbf{6})]^+$ in a mixture of DMF and acetonitrile for solubility reasons. Although the in-situ identities of the complexes were not verified, a large excess (ca. 10 \times) of the donor ligand relative to the binding ligand was used to drive the equilibrium toward the heteroleptic complex and the bis donor complex. Since the bis donor complex has no functional groups to adsorb to the TiO_2 , complexes bound to the dyed surface should be nearly all heteroleptic.

To reiterate, these experiments were preliminary and therefore do not lend an abundance of data to draw conclusions from. Only a couple cells from each dye were tested with significant variation between them. However, qualitative comparisons can be made. Fig. 2.19 shows J-V curves from cells fabricated with the above dyes. (Note that $[\text{Cu}(\mathbf{7})(\mathbf{6})]^+$ performed very poorly with $J_{\text{SC}} < 50 \mu\text{A cm}^{-2}$ and is therefore left out of discussion.) $[\text{Cu}(\mathbf{3})(\mathbf{6})]^+$ also performed rather poorly, but was somewhat improved over $[\text{Cu}(\mathbf{7})(\mathbf{6})]^+$. This was a surprising result given the substantially smaller footprint at the 2,9 positions on **3** compared to **7**. Undoubtedly the lack of any sterically demanding groups at the 2,9-positions on **6** leads to a higher degree of geometric freedom and therefore a higher probability of additional complexation to the Cu(II) center. However, it is rather surprising that the rate of electron transfer from **3** or **7** (and specifically the TMPTZ groups) does not compensate for this. Given the apparent rate of reduction of the Cu(II)

center to Cu(I) in $[\text{Cu}(\mathbf{3})(\mathbf{4})]^+$ (< 10 ns, *vide supra*), one possibility is the electron donating character of the phenyl groups creates a larger barrier to the process by which an electron from the TMPTZ reduces the metal center (believed to be the pre-association mechanism as discussed above).

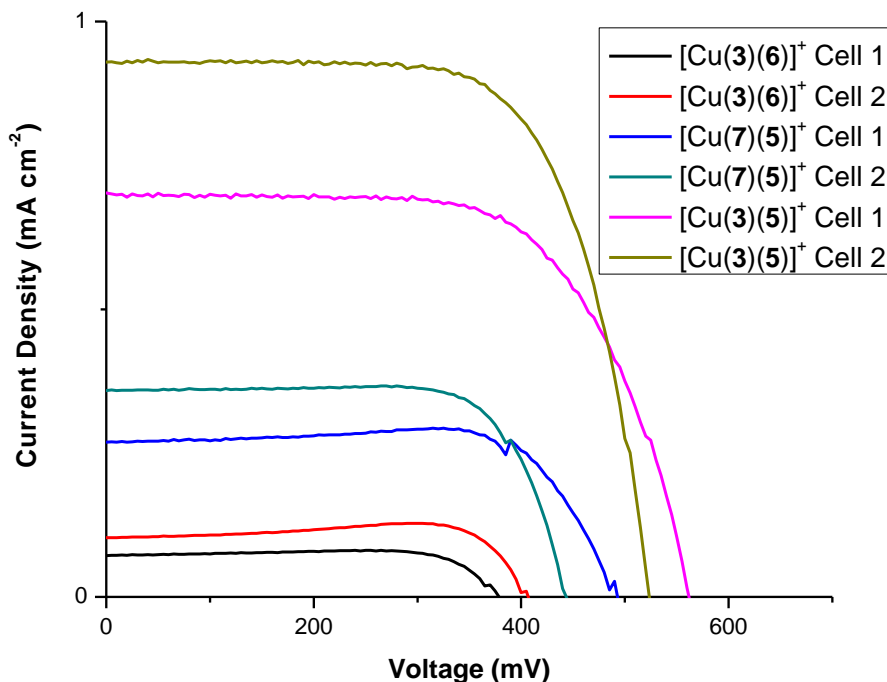


Figure 2.19. J-V curves of cells constructed from photoanodes dyed from single-pot solutions of $[\text{Cu}(\mathbf{3})(\mathbf{6})]^+$, $[\text{Cu}(\mathbf{7})(\mathbf{5})]^+$, and $[\text{Cu}(\mathbf{3})(\mathbf{5})]^+$. Mediator consisted of 0.135 M $[\text{Co}(\text{DTB})_3](\text{ClO}_4)_2$, 0.015 M $[\text{Co}(\text{DTB})_3](\text{ClO}_4)_3$, 0.2 M TBP and 0.2 M Li triflate in γ -butyrolactone. Cells were allowed to equilibrate in the light for 10-15 minutes.

A more likely explanation is that complexes constructed with **7** are simply unstable. Indeed, it was observed that rinsing the photoanodes after cell testing resulted in a noticeable dye loss from the surface, most likely due to **7** uncoordinating from the copper center. This behavior was observed in the case of the $[\text{Cu}(\mathbf{7})(\mathbf{5})]^+$ complex as well. However, $[\text{Cu}(\mathbf{7})(\mathbf{5})]^+$ performs moderately better in a DSC than $[\text{Cu}(\mathbf{7})(\mathbf{6})]^+$, indicating the methyl groups differentiating **5** and **6** clearly have a beneficial effect. The hypothesis at this point is that TBP most likely coordinates

to the Cu center and the additional steric bulk of the methyl groups in **5** is responsible for impeding this process to some degree.

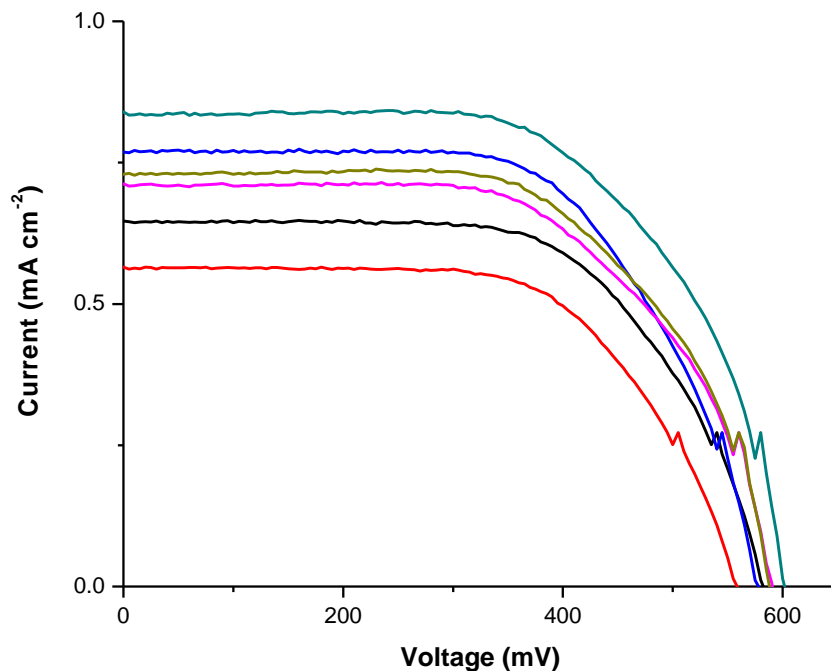


Figure 2.20. Variation in cell performance using photoanodes dyed stepwise with $[\text{Cu}(\mathbf{3})(\mathbf{5})]^+$. Mediator was the same as in Fig. 2.19. Cells were allowed to equilibrate in the light for 10-15 minutes.

Interestingly, $[\text{Cu}(\mathbf{3})(\mathbf{5})]^+$ outperformed the other dyes in these experiments, with substantially higher J_{SC} and V_{OC} values. Although the variation in J-V curves for $[\text{Cu}(\mathbf{3})(\mathbf{5})]^+$ in Fig. 2.19 is rather large, it appears that they exhibit higher J_{SC} values (but similar V_{OC} s) compared to $[\text{Cu}(\mathbf{3})(\mathbf{4})]^+$. In subsequent experiments where the stepwise dyeing method was employed to assemble $[\text{Cu}(\mathbf{3})(\mathbf{5})]^+$ on the surface, considerable variation in the current was still observed (Fig. 2.20). The improvement in J_{SC} is most likely due to the conjugated nature of **5**. By the same note, alkoxy linkages to the carboxylic acids in **4** most likely hinder electron transfer to some extent. Still, it seems reasonable to state that, overall, binders **4** and **5** both appear to be successful whereas **6** is not. Additionally, both $[\text{Cu}(\mathbf{3})(\mathbf{4})]^+$ and $[\text{Cu}(\mathbf{3})(\mathbf{5})]^+$ appear

to be very stable on the photoanode surface, as long illumination times and rinsing do not appear to appreciably alter the photoanode's appearance.

Conclusions

It has been demonstrated that bis(2,9-dimethyl-1,10-phenantroline) Cu(I)-based chromophores paired with $[\text{Co}(\text{DTB})_3]^{2+/3+}$ mediator can function competently as dyes in DSCs. By avoiding the traditional I^-/I_3^- mediator, a major stability problem noted previously for copper-based systems is avoided.¹⁸ In the current application 2,9-dimethyl-1,10-phenantroline-5,6-diol provides an excellent ligand platform in that: it has the rigidity afforded by the phenanthroline backbone, it has the desired substitution in the 2,9-positions to hinder J-T distortion and it is easily synthetically modified via standard Williamson ether chemistry at the 5,6-positions. Following the approach developed originally by Constable and coworkers, it is straightforward to synthesize stable heteroleptic Cu(I)-complex dyes directly on the TiO_2 surface for study.¹⁸

While these dyes are stable under operating cell conditions (at least on the time scale of the current studies), when oxidized to Cu(II) the metal center appears to interact with Lewis bases such as TBP and solvent. This is clearly the case in solution (as evidenced by the CV behavior) and likely also true in the surface-bound form. The behavior of the $[\text{Cu}(\mathbf{2})(\mathbf{4})]^+$ and $[\text{Cu}(\mathbf{1})(\mathbf{4})]^+$ dyes in the presence of TBP and under irradiation is consistent with formation of a Cu(II)-TBP adduct that is stable to reduction by the mediator on the time scale of minutes. In $[\text{Cu}(\mathbf{3})(\mathbf{4})]^+$ the appended TMPTZ very rapidly re-reduces the Cu(II) preventing it from becoming kinetically trapped by coordination with TBP. However, TBP does have a significant effect on the $[\text{Cu}(\mathbf{3})(\mathbf{4})]^+$ dye photoinjection efficiency. In that regard, the effect could arise because of competition for sites on the TiO_2 between TBP and weak interaction of the ether

oxygens of the **4** ligand; however, this is purely speculation and other possible explanations cannot be ruled out at this point.

Preliminary attempts at Cu(I) dyes incorporating 2,9-diphenyl-1,10-phenanthrolines did not prove successful. These complexes appear to be unstable on the photoanode surface during excitation. Reduction of the formally oxidized Cu(II) center by TMPTZ appears to be at least competitive with, if not slower than, the rate at which diphenyl ligands uncoordinate. It is believed that these ligands are replaced by TBP.

Chapter 2 References

- (1) Nazeeruddin, M. K.; Zakeeruddin, S. M.; Humphry-Baker, R.; Jirousek, M.; Liska, P.; Vlachopoulos, N.; Shklover, V.; Fischer, C.-H.; Grätzel, M. *Inorg. Chem.* **1999**, *38*, 6298–6305.
- (2) Nazeeruddin, M. K.; Kay, A.; Rodicio, I.; Humphry-Baker, R.; Mueller, E.; Liska, P.; Vlachopoulos, N.; Grätzel, M. *J. Am. Chem. Soc.* **1993**, *115*, 6382–6390.
- (3) Wang, P.; Zakeeruddin, S. M.; Moser, J. E.; Nazeeruddin, M. K.; Sekiguchi, T.; Grätzel, M. *Nat. Mater.* **2003**, *2*, 402–407.
- (4) Gao, F.; Cheng, Y.; Yu, Q.; Liu, S.; Shi, D.; Li, Y.; Wang, P. *Inorg. Chem.* **2009**, *48*, 2664–2669.
- (5) Grätzel, M.; Péchy, P.; Renouard, T.; Zakeeruddin, S. M.; Humphry-Baker, R.; Comte, P.; Liska, P.; Cevey, L.; Costa, E.; Shklover, V.; Spiccia, L.; Deacon, G. B.; Bignozzi, C. *J. Am. Chem. Soc.* **2001**, *123*, 1613–1624.
- (6) Jang, S.-R.; Yum, J.-H.; Klein, C.; Kim, K.-J.; Wagner, P.; Officer, D.; Grätzel, M.; Nazeeruddin, M. K. *J. Phys. Chem. C* **2009**, *113*, 1998–2003.
- (7) Yu, Q.-Y.; Lei, B.-X.; Liu, J.-M.; Shen, Y.; Xiao, L.-M.; Qiu, R.-L.; Kuang, D.-B.; Su, C.-Y. *Inorganica Chim. Acta* **2012**, *392*, 388–395.
- (8) Hagfeldt, A.; Boschloo, G.; Sun, L.; Kloo, L.; Pettersson, H. *Chem. Rev.* **2010**, *110*, 6595–6663.
- (9) Cunningham, C. T.; Cunningham, K. L. H.; Michalec, J. F.; McMillin, D. R. *Inorg. Chem.* **1999**, *38*, 4388–4392.

- (10) Palmer, C. E. A.; McMillin, D. R.; Kirmaier, C.; Holten, D. *Inorg. Chem.* **1987**, *26*, 3167–3170.
- (11) Phifer, C. C.; McMillin, D. R. *Inorg. Chem.* **1986**, *25*, 1329–1333.
- (12) Kalyanasundaram, K. *Photochemistry of Polypyridine and Porphyrin Complexes*; Academic Press: London, 1992.
- (13) Armaroli, N. *Chem. Soc. Rev.* **2001**, *30*, 113–124.
- (14) Crane, D. R.; DiBenedetto, J.; Palmer, C. E. A.; McMillin, D. R.; Ford, P. C. *Inorg. Chem.* **1988**, *27*, 3698–3700.
- (15) Shaw, G. B.; Grant, C. D.; Shirota, H.; Castner, E. W.; Meyer, G. J.; Chen, L. X. *J. Am. Chem. Soc.* **2007**, *129*, 2147–2160.
- (16) Iwamura, M.; Takeuchi, S.; Tahara, T. *J. Am. Chem. Soc.* **2007**, *129*, 5248–5256.
- (17) Bessho, T.; Constable, E. C.; Grätzel, M.; Redondo, A. H.; Housecroft, C. E.; Kylberg, W.; Nazeeruddin, M. K.; Neuburger, M.; Schaffner, S. *Chem. Commun.* **2008**, 3717–3719.
- (18) Redondo, A. H.; Constable, E. C.; Housecroft, C. E. *Chim. Int. J. Chem.* **2009**, *63*, 205–207.
- (19) Bozic-Weber, B.; Constable, E. C.; Housecroft, C. E.; Kopecky, P.; Neuburger, M.; Zampese, J. A. *Dalton Trans.* **2011**, *40*, 12584–12594.
- (20) Sandroni, M.; Kayanuma, M.; Planchat, A.; Szuwarski, N.; Blart, E.; Pellegrin, Y.; Daniel, C.; Boujtita, M.; Odobel, F. *Dalton Trans.* **2013**, *42*, 10818.
- (21) Bozic-Weber, B.; Constable, E. C.; Fürer, S. O.; Housecroft, C. E.; Troxler, L. J.; Zampese, J. A. *Chem. Commun.* **2013**, *49*, 7222.

- (22) Bozic-Weber, B.; Brauchli, S. Y.; Constable, E. C.; Furer, S. O.; Housecroft, C. E.; Malzner, F. J.; Wright, I. A.; Zampese, J. A. *Dalton Trans.* **2013**, 42, 12293.
- (23) Juris, A.; Balzani, V.; Barigelletti, F.; Campagna, S.; Belser, P.; von Zelewsky, A. *Coord. Chem. Rev.* **1988**, 84, 85–277.
- (24) O'Regan, B.; Grätzel, M. *Nature* **1991**, 353, 737–740.
- (25) Alonso-Vante, N.; Nierengarten, J.-F.; Sauvage, J.-P. *J. Chem. Soc. Dalton Trans.* **1994**, 1649.
- (26) Yella, A.; Lee, H.-W.; Tsao, H. N.; Yi, C.; Chandiran, A. K.; Nazeeruddin, M. K.; Diau, E. W.-G.; Yeh, C.-Y.; Zakeeruddin, S. M.; Grätzel, M. *Science* **2011**, 334, 629–634.
- (27) Scaltrito, D. V.; Thompson, D. W.; O'Callaghan, J. A.; Meyer, G. J. *Coord. Chem. Rev.* **2000**, 208, 243–266.
- (28) Argazzi, R.; Bignozzi, C. A.; Heimer, T. A.; Castellano, F. N.; Meyer, G. J. *J. Phys. Chem. B* **1997**, 101, 2591–2597.
- (29) Cooley, L. F.; Larson, S. L.; Elliott, C. M.; Kelley, D. F. *J. Phys. Chem.* **1991**, 95, 10694–10700.
- (30) Larson, S. L.; Elliott, C. M.; Kelley, D. F. *Inorg. Chem.* **1996**, 35, 2070–2076.
- (31) Larson, S. L.; Elliott, C. M.; Kelley, D. F. *J. Phys. Chem.* **1995**, 99, 6530–6539.
- (32) Sapp, S. A.; Elliott, C. M.; Contado, C.; Caramori, S.; Bignozzi, C. A. *J. Am. Chem. Soc.* **2002**, 124, 11215–11222.
- (33) Margiotta, N.; Bertolasi, V.; Capitelli, F.; Maresca, L.; Moliterni, A. G. G.; Vizza, F.; Natile, G. *Inorganica Chim. Acta* **2004**, 357, 149–158.
- (34) Wu, J.-Z.; Li, H.; Zhang, J.-G.; Xu, J.-H. *Inorg. Chem. Commun.* **2002**, 5, 71–75.

- (35) Hebký, J.; Kejha, J.; Karasek, M. *Collect. Czechoslov. Chem. Commun.* **1961**, *26*, 1559–1567.
- (36) Sörensen, N. A.; Samuelsen, E.; Oxaal, F. R.; Linnasalmi, A.; Laukkanen, P. *Acta Chem. Scand.* **1947**, *1*, 458–460.
- (37) Lehnig, A. P.; Lazorski, M. S.; Mingroni, M.; Pacheco, K. A. O.; Elliott, C. M. *J. Heterocycl. Chem.* **2014**, In print.
- (38) Feldt, S. M.; Wang, G.; Boschloo, G.; Hagfeldt, A. *J. Phys. Chem. C* **2011**, *115*, 21500–21507.
- (39) Nelson, J. J.; Amick, T. J.; Elliott, C. M. *J. Phys. Chem. C* **2008**, *112*, 18255–18263.
- (40) Grätzel, M. *Nature* **2001**, *414*, 338–344.
- (41) Weber, J. M.; Rawls, M. T.; MacKenzie, V. J.; Limoges, B. R.; Elliott, C. M. *J. Am. Chem. Soc.* **2007**, *129*, 313–320.
- (42) Mosconi, E.; Yum, J.-H.; Kessler, F.; García, C. J. G.; Zuccaccia, C.; Cinti, A.; Nazeeruddin, M. K.; Grätzel, M.; De Angelis, F. *J. Am. Chem. Soc.* **2012**, *134*, 19438–19453.
- (43) Klahr, B. M.; Hamann, T. W. *J. Phys. Chem. C* **2009**, *113*, 14040–14045.
- (44) Boschloo, G.; Häggman, L.; Hagfeldt, A. *J. Phys. Chem. B* **2006**, *110*, 13144–13150.
- (45) Katoh, R.; Fuke, N.; Furube, A.; Koide, N. *Chem. Phys. Lett.* **2010**, *489*, 202–206.
- (46) Lazorski, M. S.; Gest, R. H.; Elliott, C. M. *J. Am. Chem. Soc.* **2012**, *134*, 17466–17469.
- (47) Zaban, A.; Greenshtein, M.; Bisquert, J. *ChemPhysChem* **2003**, *4*, 859–864.
- (48) Bisquert, J.; Zaban, A.; Greenshtein, M.; Mora-Seró, I. *J. Am. Chem. Soc.* **2004**, *126*, 13550–13559.

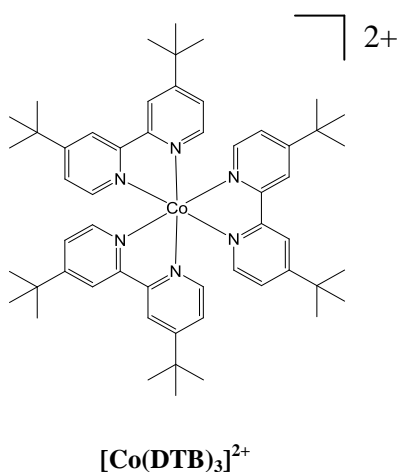
Chapter 3: Tris(4,4'-di-*t*-butyl-2,2'-bipyridine)cobalt: Cation Effects on the Voltammetry at ITO and on Mediator Performance in Dye-Sensitized Solar Cells^B

Introduction

For the first two decades following the introduction by O'Regan and Grätzel of mesoporous TiO₂ as a photoanode material for dye-sensitized solar cell (DSC) application, attention was almost exclusively focused on I⁻/I₃⁻ as the electron transfer mediator in these cells.¹ However, a decade ago two reports appeared (one from Grätzel's laboratory² and one from the Elliott laboratory³) which demonstrated that certain cobalt complexes could function well as electron-transport mediators in DSCs. These results were surprising because, unlike the I⁻/I₃⁻ couple, the relevant redox process (i.e., Co(II/III)) is a fully outer-sphere process. Because of the myriad of issues with I⁻/I₃⁻ when used as a DSC mediator, general interest in cobalt-based mediator systems (and, more specifically, cobalt polypyridine complexes) has grown almost exponentially since these early reports. Moreover, the record efficiency for a DSC of 12% is presently held from a cell mediated with a cobalt bipyridine complex.⁴

When used in conjunction with typical ruthenium-based dyes (e.g., so-called N3), sterically bulky substituents are required at the 4,4'-positions of the bipyridine ligand in order to prevent rapid recombination of the photoinjected electron with the oxidized form of the mediator. In that regard, 4,4'-di-*tert*-butyl-2,2'-bipyridine (DTB) is a particularly good ligand choice because it possesses sufficient steric bulk and is commercially available. The structure of [Co(DTB)₃]²⁺ is shown below.

^B With the exception of the introduction and some minor wording changes, the remainder of this chapter was: Reproduced with permission from *J. Electrochem. Soc.* **2013**, *160* (6), H355-H359. DOI: 10.1149/2.115306jes. Copyright 2013, The Electrochemical Society. Link: jes.ecsdl.org/content/160/6/H355



There are several features of this complex that make its redox chemistry unusual. First, the Co(III) form is low-spin d^6 and the Co(II) is predominantly high-spin d^7 , giving rise to a large inner-sphere contribution to the reorganizational energy for the Co(II/III) couple.^{5,6} Second, the insulating *t*-butyl substituents which project out along the apices of the octahedral coordination sphere prevent the π -systems of the bipyridine ligands from coming into intimate contact with electrode surfaces. As a result, the electron transfer process is significantly non-adiabatic; consequently, the electron transfer for the Co(II/III) couple does not follow simple Butler-Volmer type kinetics.⁷ Moreover, the combination of weak coupling and large reorganizational energy renders the kinetics of the Co(II/III) couple extremely electrode-surface and electrolyte dependent. For example, in $\text{TBA}^+\text{PF}_6^-/\text{acetonitrile}$ electrolyte on glassy carbon (GC) or Au, the voltammetry of the Co(II/III) couple looks quasireversible (i.e., $\Delta E_p < 100$ mV). In contrast, on ITO or fluorine-doped tin oxide (FTO) in $\text{Li}^+\text{ClO}_4^-/\text{acetonitrile}$, the overpotential required to observe any experimental Faradaic current for the oxidation of Co(II) is on the order of 1.0 V. Recently the Elliott group reported a study of the voltammetry of $[\text{Co}(\text{DTB})_3]^{2+}$ and the related bis-terpyridine complex $[\text{Co}(\text{TTT})_2]^{2+}$ on GC as a function of electrolyte.⁷ However, the

voltammetry on semiconductor oxides is likely of greater relevance to the behavior of the $[\text{Co}(\text{DTB})_3]^{2+/3+}$ as a mediator in DSCs, at least in so far as electron transfers at the photoanode are concerned.

Voltammetry studies of $[\text{Co}(\text{DTB})_3]^{2+/3+}$ on ITO as a function of electrolyte are reported in this chapter. These studies were performed by Dr. Di Xue several years ago in the Elliott group and are reproduced here due to their relevance to the work. The large dependence of the $[\text{Co}(\text{DTB})_3]^{2+/3+}$ electrochemistry on electrolyte composition that was observed justified further exploration. As an extension of her earlier work, these results are then correlated to the behavior of DSCs mediated by $[\text{Co}(\text{DTB})_3]^{2+/3+}$ solutions containing the same series of electrolytes. These studies were carried out by myself and undergraduate Ross Gaddie under my supervision. The Butterworth smoothing filter employed in the plots of electron lifetimes was developed solely by Ross Gaddie.

Experimental

Materials. The DTB ligand was either synthesized as previously reported³ or obtained from Aldrich. The $[\text{Co}(\text{DTB})_3](\text{ClO}_4)_2$ was prepared as previously reported.⁸ Solid $[\text{Co}(\text{DTB})_3](\text{ClO}_4)_3$ was prepared from $[\text{Co}(\text{DTB})_3](\text{ClO}_4)_2$ by oxidation with NOBF_4 .⁸

Electrochemistry. ITO on glass was obtained from Delta Technologies. Prior to use the electrodes were patterned and cleaned as previously described.⁹ The solvent was Optima grade acetonitrile (Fisher) and was used as received. Lithium perchlorate ($\text{Li}^+\text{ClO}_4^-$) (99.99%) was purchased from Aldrich and used as received after vacuum drying overnight. Tetra-n-alkylammonium perchlorate salts ($\text{TBA}^+\text{ClO}_4^-$; $\text{TEA}^+\text{ClO}_4^-$; $\text{TMA}^+\text{ClO}_4^-$) used in the voltammetry studies were obtained from various sources, recrystallized and vacuum-dried

overnight prior to use. Cyclic voltammograms were acquired using a BioAnalytical Systems BAS100A potentiostat. All reported voltages are vs. a sodium chloride saturated calomel reference electrode (SSCE).

DSC measurements. Dye cell construction and measurements were conducted in a manner similar to what has been reported previously in Chapter 2.¹⁰ The photoanodes were dyed as previously described by soaking for at least 18 hours in a 2 mM solution of *cis*-bis(isothiocyanato)-bis(2,2'-bipyridyl-4,4'-dicarboxylato)ruthenium(II) (N3) in ethanol. Mediator solution, consisting of 0.135 M [Co(DTB)₃](ClO₄)₂, 0.015 M [Co(DTB)₃](ClO₄)₃, 0.2 M 4-*tert*-butylpyridine (TBP) in γ -butyrolactone and 0.05 M electrolyte (either TBA⁺ClO₄⁻, TMA⁺ClO₄⁻ or Li⁺ClO₄⁻), was introduced at the interface between the photoanode and cathode and drawn into the cell by capillary action. Cells were allowed to equilibrate with the mediator solution for 10 minutes followed by removal of the solution from the cell by wicking it into the corner of a KimwipeTM. The cells were filled and emptied of mediator solution via this approach at least twice prior to final filling with mediator solution and solar testing.

Results and Discussion

Voltammetry. Fig. 3.1 shows a comparison of the voltammetry of [Co(DTB)₃](ClO₄)₂ on ITO and GC working electrodes, along with a blank scan of the electrolyte on ITO. The two CVs of the [Co(DTB)₃](ClO₄)₂-containing solution were obtained from the identical solution. The scan on the GC electrode was scaled to correct for differences in electrode area. In this electrolyte solution (0.10 M TMA⁺PF₆⁻/acetonitrile) the CV of the Co(II/III) couple on GC is quasireversible while the CV on ITO is barely discernible from the ITO background over this potential range. The lack of any observable redox process on ITO is indicative of extremely

slow electron transfer kinetics. By comparison, on GC the kinetics are clearly substantially faster.

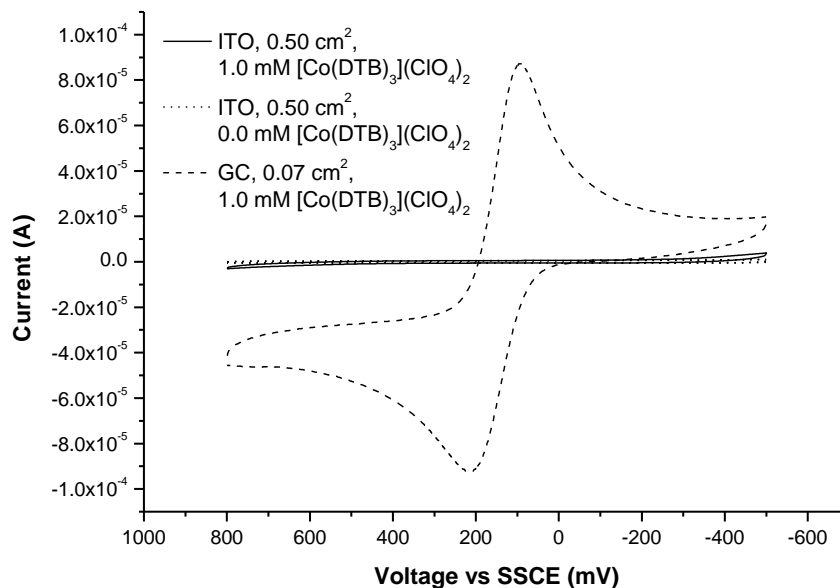


Figure 3.1. CVs of $[\text{Co}(\text{DTB})_3](\text{ClO}_4)_2$ on ITO (0.50 cm^2) and GC (0.07 cm^2) electrodes along with a background CV on ITO. The current for GC electrode was scaled by an area factor of $0.5/0.07$. The electrolyte is $100 \text{ mM TMA}^+\text{PF}_6^-/\text{acetonitrile}$ and the scan rate 100 mV/s .

While this result is perhaps not particularly intriguing on its own, the dependence of the ITO electrochemistry on electrolyte adds a new layer of interest. Fig. 3.2 compares the voltammetry of $[\text{Co}(\text{DTB})_3]^{2+}$ on ITO in acetonitrile solvent with four different electrolytes: $\text{Li}^+\text{ClO}_4^-$, $\text{TMA}^+\text{ClO}_4^-$, $\text{TEA}^+\text{ClO}_4^-$ and $\text{TBA}^+\text{ClO}_4^-$. All of the CVs are clearly non-Nernstian, but there is a trend in the overpotential with electrolyte cation size for both the oxidation and reduction. As the cation size decreases, the overpotential for both processes increases. The approximate $E^{0'}$ for the $[\text{Co}(\text{DTB})_3]^{2+/3+}$ couple is 0.12 V vs. SSCE , so in every case the overpotential to drive the oxidation is significantly larger than that to drive the reduction.⁷

Based on the results given in Fig. 3.2, in terms of the $[\text{Co}(\text{DTB})_3]^{2+/3+}$ voltammetry, it is of interest to address the question: Does TBA^+ "turn on" electron transfer for $[\text{Co}(\text{DTB})_3]^{2+/3+}$ or

does Li^+ "shut it off"? In order to address this question the experiment shown in Fig. 3.3 was performed. Fig. 3.3 again shows voltammograms for a 1 mM $[\text{Co}(\text{DTB})_3](\text{ClO}_4)_2$ solution. Curves 1 (black) and 3 (green) are for 0.1 M $\text{Li}^+\text{ClO}_4^-$ and $\text{TBA}^+\text{ClO}_4^-$ electrolytes, respectively. In order to evaluate if there is any dependence on the order to which the ITO surface is exposed to respective cations, curves 2 (red) and 4 (blue) were obtained by adding enough solid $\text{Li}^+\text{ClO}_4^-$ to solution 3 and $\text{TBA}^+\text{ClO}_4^-$ to solution 1 to make $[\text{TBA}^+] = [\text{Li}^+] = 0.10$ M in both solutions.

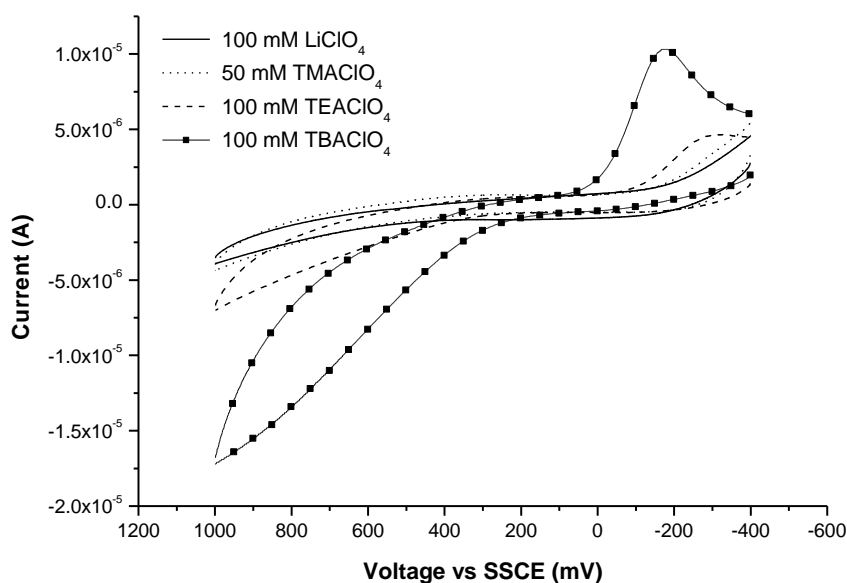


Figure 3.2. CVs of $[\text{Co}(\text{DTB})_3](\text{ClO}_4)_2$ (1 mM) in different electrolyte solutions. W.E., ITO (0.5 cm^2); R.E., SSCE; C.E., Pt; 100 mV/s. The concentration difference of $\text{TMA}^+\text{ClO}_4^-$ relative to other electrolytes is a consequence of its poor solubility in acetonitrile.

The voltammograms labeled 1 and 3 in Fig. 3.3 (black and green respectively) are for nominally identical solution conditions to those in Fig. 3.2 for 0.1 M $\text{Li}^+\text{ClO}_4^-$ and $\text{TBA}^+\text{ClO}_4^-$. First, voltammograms 2 and 4 are essentially identical; consequently there is no dependence of the $[\text{Co}(\text{DTB})_3]^{2+/3+}$ voltammetry on the order to which the ITO is exposed to the two different cations. Second, these voltammograms are very similar (albeit not identical) to voltammogram 1; consequently, it appears that the Li^+ serves to "shut off" the $[\text{Co}(\text{DTB})_3]^{2+/3+}$ electron transfer

more so than TBA^+ "turns it on." However, there is slightly more current for the oxidation of $[\text{Co}(\text{DTB})_3]^{2+}$ at the extreme positive overpotential in the mixed electrolyte than in the pure $\text{Li}^+\text{ClO}_4^-$. Therefore, there is some small residual effect of the TBA^+ , but it is quite modest.

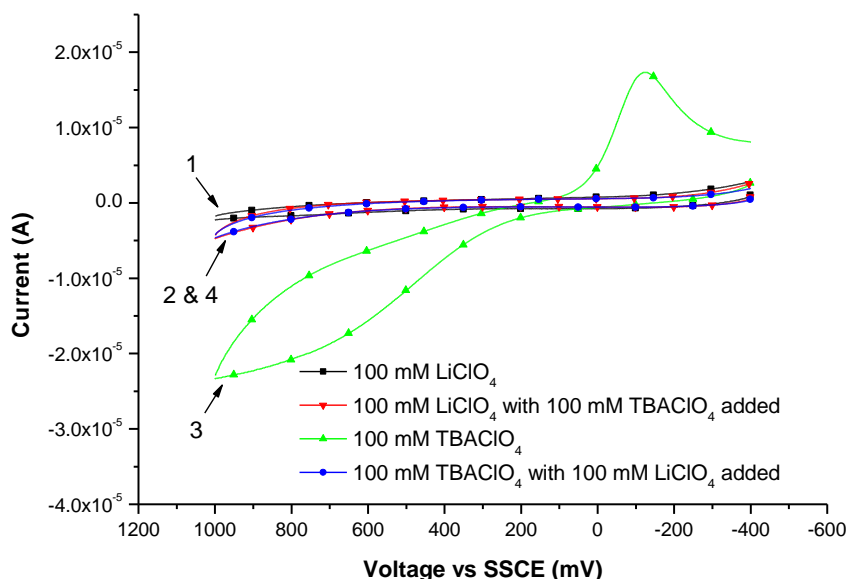


Figure 3.3. CVs of $[\text{Co}(\text{DTB})_3](\text{ClO}_4)_2$ (1 mM) in different electrolyte solutions. W.E., ITO (0.5 cm^2); R.E., SSCE; C.E., Pt; 100 mV/s. See text for details.

DSC Measurements. After observing the cation effects on the electrochemistry of the Co(II/III) redox couple (Fig. 3.2), the performance of DSCs in the presence of 50 mM TBA^+ , TMA^+ , or Li^+ was evaluated. Fig. 3.4 shows representative J-V curves of these cells. The same anode was used for each measurement. The cell was rinsed with ethanol and dried before introducing the next mediator solution. In addition, the anode remained mounted in the cell holder between each measurement such that the illuminated spot on the photoanode remained constant throughout testing. The order in which the different mediator solutions were examined was: $\text{TBA}^+\text{ClO}_4^-$ first, $\text{TMA}^+\text{ClO}_4^-$ second, and $\text{Li}^+\text{ClO}_4^-$ third. Although data in the literature implies TBA^+ does not adsorb to TiO_2 surfaces^{11,12}, the adsorption behavior of TMA^+ has not been examined to the best of my knowledge. Thus, this mediator-addition protocol was

established in order of increasing probability of cation adsorption. However, the $\text{Li}^+\text{ClO}_4^-$ J-V curve closely mirrors that of similar cells that have been tested previously using lithium triflate as a mediator-solution additive¹⁰, suggesting that effects from any potential residual adsorption of TMA^+ were minimal. All curves were conventionally shaped, with the $\text{Li}^+\text{ClO}_4^-$ curve exhibiting substantially greater current density than the other two electrolytes.

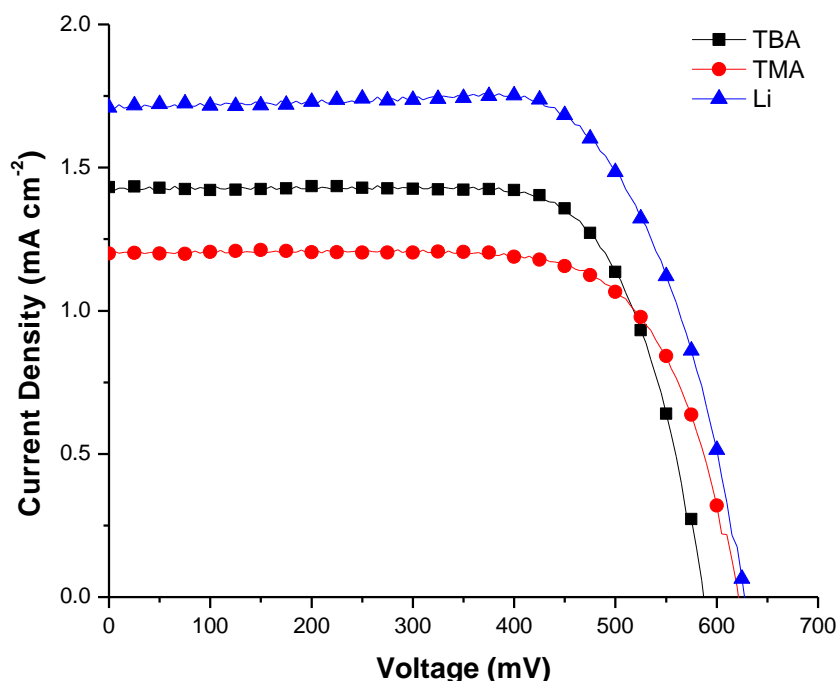


Figure 3.4. J-V curves of DSCs dyed with N3 and mediated by solutions of $[\text{Co}(\text{DTB})_3]^{2+/3+}$ containing supporting electrolytes of either 50 mM $\text{TBA}^+\text{ClO}_4^-$, $\text{TMA}^+\text{ClO}_4^-$, or $\text{Li}^+\text{ClO}_4^-$. See text for details.

There is a moderate degree of variability in J_{SC} between different photoanodes, so it is not possible to state with exact certainty what the trend in J_{SC} is among the three electrolyte cations. However, it is possible to say that the J_{SC} for the Li^+ electrolyte is significantly larger than for the other two, which are more nearly similar (based on data from several different photoanodes that were examined). The variability in the V_{OC} between photoanodes is smaller so it can therefore be said with some confidence that V_{OC} follows the trend that $\text{Li}^+ > \text{TMA}^+ > \text{TBA}^+$.

The differential effect of added Li^+ to otherwise identical DSCs mediated with either $[\text{Co}(\text{DTB})_3]^{2+/3+}$ or I^-/I_3^- has been previously examined in the Elliott group.³ In the case of I^-/I_3^- , addition of Li^+ decreases the open-circuit voltage (V_{OC}) ostensibly due to a decrease in the energy of the TiO_2 acceptor states upon lithium ion adsorption/intercalation.¹¹ In contrast, V_{OC} *increases* with the addition of Li^+ when $[\text{Co}(\text{DTB})_3]^{2+/3+}$ is the mediator. As has been noted in previous studies, it is highly unlikely that the presence of $[\text{Co}(\text{DTB})_3]^{2+/3+}$ would alter whatever effect Li^+ has on the band or surface-state energies of TiO_2 . Consequently, since Li^+ increases the V_{OC} in cells mediated with $[\text{Co}(\text{DTB})_3]^{2+/3+}$, some other process must be compensating for the lower band energy, most likely a decrease in recombination rate. In particular, the difference in V_{OC} between Li^+ and TBA^+ cells is typically on the order of 50 mV (with TMA^+ cells exhibiting V_{OC} values closer to Li^+ cells), which is consistent with the trend in dark currents presented in Fig. 3.5. At potentials near V_{oc} , where the TiO_2 is nominally conducting, dark currents should mirror the magnitude of electron recombination in the cell.

It has been the general observation in the Elliott group that, irrespective of the solvent or electrolyte, the heterogeneous electron transfer rate for the $[\text{Co}(\text{DTB})_3]^{2+/3+}$ couple is always much slower on oxide-containing surfaces than on nominally oxide-free surfaces. For example, even on Pt (which is generally considered to have a near monolayer of PtO on the surface), the $[\text{Co}(\text{DTB})_3]^{2+/3+}$ voltammetry is much less Nernstian than on either GC or Au.³ The relative electron-transfer behavior of $[\text{Co}(\text{DTB})_3]^{2+/3+}$ on ITO and FTO is semi-quantitatively the same and presents the extreme cases of slow heterogeneous electron transfer for this couple. Thus, it is reasonable to hypothesize that the electron transfer behavior on TiO_2 will at least qualitatively parallel that on the other semiconducting oxides (i.e., ITO and FTO). This seems to be borne out by a comparison of the CV data in Fig. 3.2 with the dark current data in Fig. 3.5. The

overpotentials required for reduction of $[\text{Co}(\text{DTB})_3]^{3+}$ in TMA^+ and Li^+ electrolytes are quite similar to each other and significantly larger than that for TBA^+ ; likewise, the onset of the dark current for the TBA^+ -containing mediator solution is at a considerably smaller potential than for mediator solutions containing TMA^+ and Li^+ .

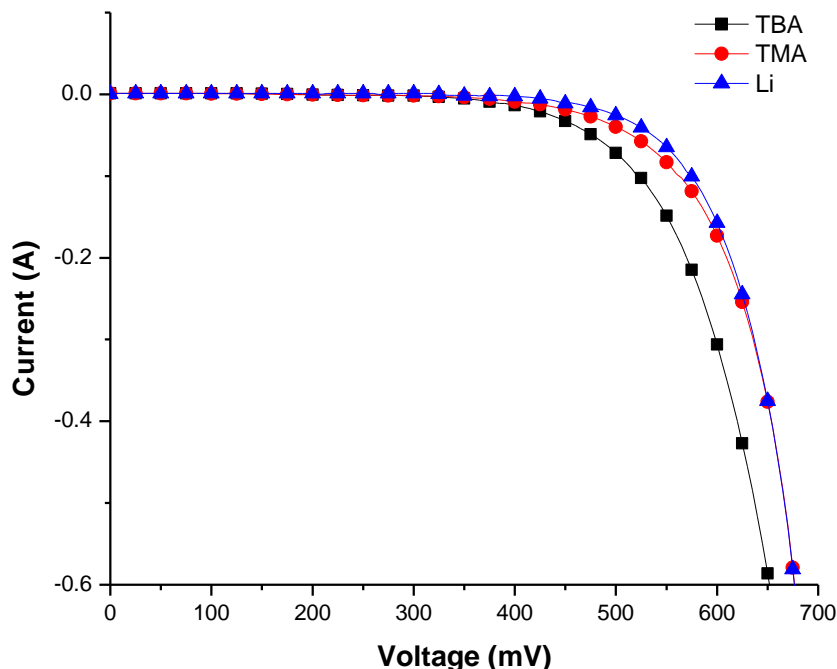


Figure 3.5. Dark currents for N3 DSCs mediated by solutions of $[\text{Co}(\text{DTB})_3]^{2+/3+}$ containing supporting electrolytes of 50 mM $\text{TBA}^+\text{ClO}_4^-$, $\text{TMA}^+\text{ClO}_4^-$, or $\text{Li}^+\text{ClO}_4^-$. Cells were the same as presented in Figure 3.4.

While the dark-currents provide some insight into the rates of recombination, a better strategy is to consider the V_{OC} decays for the various mediator solutions. Transient voltage decays shown in Fig. 3.6 were obtained by illuminating the cell at open circuit until a steady-state voltage was attained (i.e., a steady-state population of photo-injected conduction-band electrons in the TiO_2). The light was then blocked (using a camera shutter), and the voltage was recorded as a function of time. Assuming the near quantitative yield of electron injection by N3 into the TiO_2 conduction band¹³ and fast regeneration of the oxidized dye by the mediator

relative to recombination, any loss of voltage in the dark can be directly attributed to recombination of photo-injected electrons in the TiO_2 with the oxidized form of the mediator (i.e., $[\text{Co}(\text{DTB})_3]^{3+}$). Using the approach developed by Bisquert et al.^{14,15}, the $V_{\text{oc}}(t)$ decays in Fig. 3.6 can be transformed to give the electron lifetime in the TiO_2 as a function of voltage as shown in Fig. 3.7. The derivative of the voltage decay was approximated using a 5-point stencil, using the light-off event as one endpoint. This signal was then filtered through a first-order low pass Butterworth filter. For lifetimes less than 0.2 seconds, a cutoff frequency of 23 Hz was used, and for lifetimes greater than 0.2 seconds, a cutoff frequency of 5.4 Hz was used.

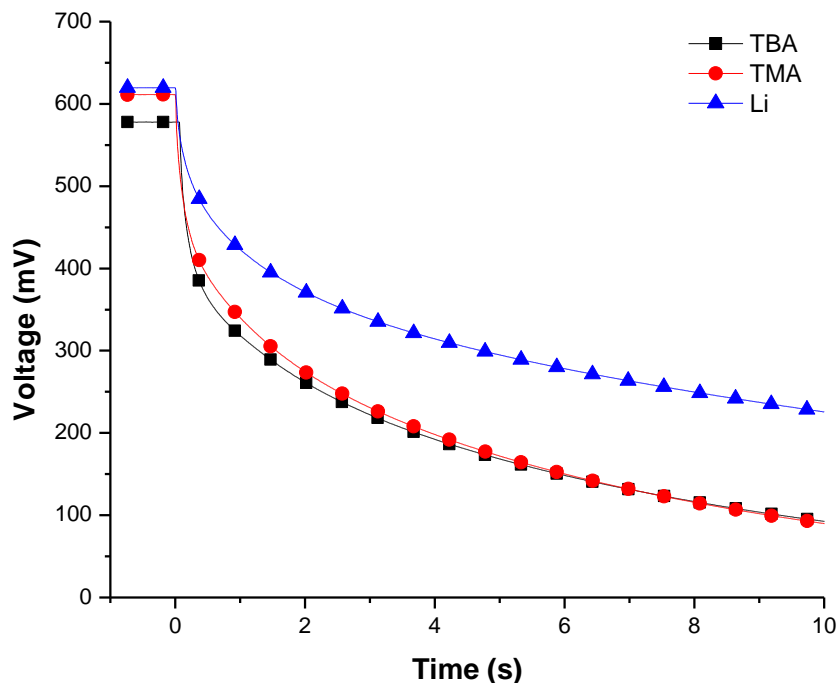


Figure 3.6. Transient voltage decays of N3 DSCs mediated by solutions of $[\text{Co}(\text{DTB})_3]^{2+/3+}$ containing supporting electrolytes of either 50 mM $\text{TBA}^+\text{ClO}_4^-$, $\text{TMA}^+\text{ClO}_4^-$, or $\text{Li}^+\text{ClO}_4^-$. Cells were the same as presented in Figures 3.4 and 3.5. See text for details.

Bisquert et al.^{14,15} have also developed a model which takes into account recombinations from the conduction band electrons, surface-trap, and bulk-trap states. This model predicts different shapes for the plot of the logarithm of the electron lifetime ($\log \tau$) vs. voltage depending

on which mechanism is dominant. Fig. 3.7 shows plots of $\log \tau$ as a function of voltage for mediator solutions containing, respectively, 50 mM TBA^+ , TMA^+ and Li^+ . The shapes of the curves in Fig. 3.7 are qualitatively different from those reported by Bisquert et al.; however, this is not particularly surprising since their results were for I^-/I_3^- electrolyte. The $[\text{Co}(\text{DTB})_3]^{2+/3+}$

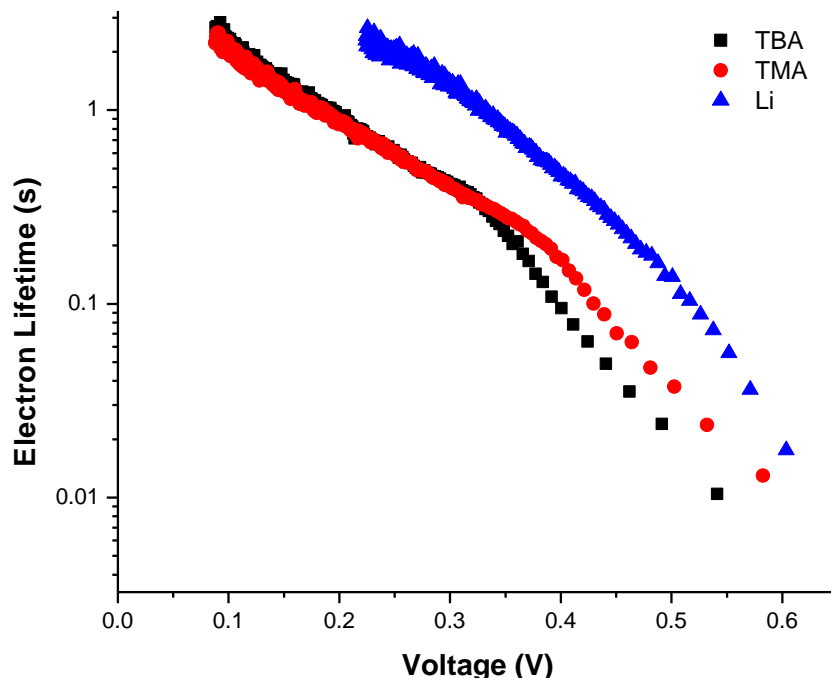


Figure 3.7. Electron lifetimes vs. voltage for N3 DSCs mediated by solutions of $[\text{Co}(\text{DTB})_3]^{2+/3+}$ containing supporting electrolytes of either 50 mM $\text{TBA}^+\text{ClO}_4^-$, $\text{TMA}^+\text{ClO}_4^-$, or $\text{Li}^+\text{ClO}_4^-$. Data is for the same cells as in Figures 3.4-3.6. See text for details.

differs from I^-/I_3^- in numerous ways, but probably most relevant in the present context is that (1) the reorganizational energy for the $[\text{Co}(\text{DTB})_3]^{2+/3+}$ process is considerably larger (ca. $\times 3$) than for I^-/I_3^- ¹⁶, and (2) the electron transfer for the $[\text{Co}(\text{DTB})_3]^{2+/3+}$ process is significantly non-adiabatic.^{7,17} Phenomenologically, from the data in Fig. 3.7, the electron lifetimes are longer for the electrolyte containing Li^+ than for the other two over the entire voltage range. The $\log \tau$ data in the Li^+ case curves down at higher potentials (i.e., increasingly shorter electron lifetimes). For TBA^+ and TMA^+ there are two sections to each curve. At large voltages the electron lifetime is

shorter for the TBA^+ solution than the TMA^+ solution; however, at ca. 350 mV the slopes change for both curves relative to the higher voltage region and these two curves coalesce. Bisquert's model predicts that, when the dominant recombination mechanism is with electrons at the conduction band edge that have been predominantly produced by thermally de-trapping from bulk-trap states (as opposed to with free, mobile electrons in the conduction band), $\log \tau$ should vary linearly with voltage. At low voltage, recombination from surface-trap states should dominate. In the latter case, $\log \tau$ vs. voltage should be parabolic in shape. Without a detailed fitting of the lifetime data to the Bisquert model (with appropriate modifications for the non-adiabaticity of the electron transfer) it is not possible to tell if the model would yield physically reasonable parameters as it does for other systems that have been tested.¹⁴⁻¹⁶ That point notwithstanding, the distinct "knee" in the curves of Fig. 3.7 for the TBA^+ and TMA^+ solutions, and possibly the downward curvature of $\log \tau$ at high voltage for the Li^+ solutions, suggest a change in the dominate recombination mechanism over the voltage range examined. Further, it seems reasonable to assume that recombination for the TBA^+ and TMA^+ cases at voltages below 350 mV are dominated by surface-traps and above 350 mV by bulk-trap electrons promoted into the conduction band. If this interpretation is correct, it is interesting that the identity of the tetraalkyl ammonium cation affects the recombination from the conduction band but not from the surface traps, whereas Li^+ appears to affect both.

Conclusions

As has been demonstrated previously, because of the large steric bulk and insulating nature of the *tert*-butyl substituents on the ligands of $[\text{Co}(\text{DTB})_3]^{2+}$, heterogeneous electron transfers at electrode surfaces are non-adiabatic.⁷ As a consequence, the Co(II/III) couple

exhibits almost unprecedented electrode-surface and electrolyte-dependent voltammetry. Consideration of a large number of different electrode materials (in addition to the ones considered here), has led to the conclusion that the electron-transfer is fastest on metallic (or metal-like) surfaces that are oxide free such as carbon or gold.^{3,18} Likewise, electron transfer appears to be dramatically slower on semiconductor oxides such as ITO, FTO, or TiO₂. Irrespective of the electrode material, the electron transfer chemistry for this couple is electrolyte dependent, being most extremely manifested on semiconductor oxide surfaces. Generally, the overpotential required to drive either the reduction or the oxidation decreases as the electrolyte cation size and lipophilicity increases. The approximate E^0 vs. SSCE for the Co(II/III) couple is ca. 0.12 V⁷; so the overpotential for oxidation of [Co(DTB)₃]²⁺ on ITO is considerably larger than for the reduction of [Co(DTB)₃]³⁺, irrespective of the electrolyte cation (Fig. 3.2). Similar but less dramatic trends are observed on other electrode materials such as Au and GC.^{7,19}

Finally, these results along with other results reported previously, are all consistent with the behavior of [Co(DTB)₃]^{2+/3+} when employed as a mediator in DSCs. For a mediator to be successful, it is necessary for it to have fast electron-transfer kinetics with both the cathode material (usually metallic) and the oxidized dye, yet slow electron-transfer kinetics with the anode conduction material (ITO, FTO, TiO₂) to prevent recombination. In these regards, [Co(DTB)₃]^{2+/3+} meets all of these requirements.

Chapter 3 References

- (1) Hagfeldt, A.; Boschloo, G.; Sun, L.; Kloo, L.; Pettersson, H. *Chem. Rev.* **2010**, *110*, 6595–6663.
- (2) Nusbaumer, H.; Moser, J.-E.; Zakeeruddin, S. M.; Nazeeruddin, M. K.; Grätzel, M. *J. Phys. Chem. B.* **2001**, *105*, 10461–10464.
- (3) Sapp, S. A.; Elliott, C. M.; Contado, C.; Caramori, S.; Bignozzi, C. A. *J. Am. Chem. Soc.* **2002**, *124*, 11215–11222.
- (4) Yella, A.; Lee, H.-W.; Tsao, H. N.; Yi, C.; Chandiran, A. K.; Nazeeruddin, M. K.; Diau, E. W.-G.; Yeh, C.-Y.; Zakeeruddin, S. M.; Grätzel, M. *Science* **2011**, *334*, 629–634.
- (5) Krivokapic, I.; Zerara, M.; Daku, M. L.; Vargas, A.; Enachescu, C.; Ambrus, C.; Tregenna-Piggott, P.; Amstutz, N.; Krausz, E.; Hauser, A. *Coordin. Chem. Rev.* **2007**, *251*, 364–378.
- (6) Palmer, R. A.; Piper, T. S. *Inorg. Chem.* **1966**, *5*, 864–878.
- (7) Gaddie, R. S.; Moss, C. B.; Elliott, C. M. *Langmuir* **2013**, *29*, 825–831.
- (8) Nelson, J. J.; Amick, T. J.; Elliott, C. M. *J. Phys. Chem. C.* **2008**, *112*, 18255–18263.
- (9) Xue, D.; Elliott, C. M.; Gong, P.; Grainger, D. W.; Bignozzi, C. A.; Caramori, S. *J. Am. Chem. Soc.* **2007**, *129*, 1854–1855.
- (10) Ashbrook, L. N.; Elliott, C. M. *J. Phys. Chem. C.* **2013**, *117*, 3853–3864.
- (11) Kelly, C. A.; Farzad, F.; Thompson, D. W.; Stipkala, J. M.; Meyer, G. J. *Langmuir* **1999**, *15*, 7047–7054.
- (12) Pelet, S.; Moser, J.-E.; Grätzel, M. *J. Phys. Chem. B.* **2000**, *104*, 1791–1795.

- (13) Benkö, G.; Kallioinen, J.; Korppi-Tommola, J. E. I.; Yartsev, A. P.; Sundström, V. *J. Am. Chem. Soc.* **2002**, *124*, 489–493.
- (14) Zaban, A.; Greenshtein, M.; Bisquert, J. *ChemPhysChem* **2003**, *4*, 859–864.
- (15) Bisquert, J.; Zaban, A.; Greenshtein, M.; Mora-Seró, I. *J. Am. Chem. Soc.* **2004**, *126*, 13550–13559.
- (16) Ondersma, J. W.; Hamann, T. W. *J. Am. Chem. Soc.* **2011**, *133*, 8264–8271.
- (17) Hamann, T. W.; Brunschwig, B. S.; Lewis, N. S. *J. Phys. Chem. B.* **2006**, *110*, 25514–25520.
- (18) Gaddie, R. S.; Elliott, C. M. *Unpublished Results*.
- (19) Xue, D. Ph.D. Dissertation, Colorado State University, 2008.

Chapter 4: Sulfide Modification of Dye-Sensitized Solar Cell Gold Cathodes for Use with Cobalt Polypyridyl Mediators^C

Introduction

Interest in alternatives to the traditional I^-/I_3^- electron transport mediator systems in dye sensitized solar cells (DSCs) has increased significantly in the last decade. This interest has been spurred by the demonstration that certain one-electron redox couples such as cobalt(II/III) polypyridine complexes can function as competent mediators in DSCs.¹⁻¹⁷ In fact, the record efficiency reported to date for a liquid-electrolyte cell employed $[\text{Co}(\text{bpy})_3]^{2+/3+}$ as the mediator.¹⁷ While cobalt complexes of a variety of types of ligands have been examined in this context, the majority of attention has been given to bipyridine (bpy) and phenanthroline (phen) type ligands likely due to their commercial availability and ease of synthetic modification.

The first cobalt-bipyridine-based mediator reported that gave IPCE values comparable to I^-/I_3^- was $[\text{Co}(\text{DTB})_3]^{2+/3+}$ (DTB = 4,4'-di-*tert*-butyl-2,2'-bipyridyl).¹⁸ The *t*-butyl substituents emanating along the apices of the octahedral coordination sphere in this complex sterically prevent strong electronic coupling between electrode and the cobalt-based redox orbitals (mediated through the ligand π -system). Consequently, the heterogeneous electron transfer is non-adiabatic resulting in a dramatic electrode surface dependence to the rate.¹⁹ For example, the apparent heterogeneous electron transfer rate constant for the $[\text{Co}(\text{DTB})_3]^{2+/3+}$ couple differs by at least ten orders of magnitude between glassy carbon and ITO.^{19,20} It is exactly this fact that allows $[\text{Co}(\text{DTB})_3]^{3+}$ to exhibit the slow recombination with photo-injected electrons in the

^C With the exception of the introduction and some minor wording changes, the remainder of this chapter was: Reproduced with permission from *J. Phys. Chem. C* **2014**, *118* (30), 16643-16650. Copyright 2014, American Chemical Society. DOI: 10.1021/jp412578a. Link: pubs.acs.org/doi/abs/10.1021/jp412578a

conduction band of the TiO₂ photoanode of a DSC while still undergoing relative rapid reduction at metallic cathodes. With smaller substituents in the 4,4'-positions of the bipyridine (e.g., methyl or protons) the ligand π -system can electronically couple to the surface of *bare* metallic electrodes much more strongly. Therefore, the electron transfer at such electrode surfaces is more nearly adiabatic and, in electrochemical terms, approximately follows standard Butler-Volmer kinetics.¹⁹

Over the period since the Elliott Group's first report¹⁸ of successful use of [Co(DTB)₃]^{2+/3+} as a DSC mediator the group has established that, generally speaking, Au and carbon cathodes are superior to Pt when combined with [Co(DTB)₃]^{2+/3+} (and other Co(bpy)₃-type complexes) as mediator. However, issues exist with reproducibility in the current-voltage behavior of DSCs employing cobalt-based mediators coupled with Au cathodes, at least some of which are clearly cathode-based. In these studies, cathodes typically employed are constructed by vapor depositing ca. 200 nm of Au either on fluorine doped tin oxide (FTO) or on glass. These cathodes are fabricated with a thin vapor deposited layer of chromium under the gold to improve the Au adherence to either substrate. Typically, when first fabricated, these cathodes show considerable variation with regard to the shape of the resulting J-V curves from batch-to-batch and even from cathode-to-cathode within the same batch. Generally, over time there is improvement particularly in the fill factor as specific cathodes are "broken in" (i.e., with repeated assembly and disassembly of cells). These observations are consistent with wide variations in electron transfer resistance (R_{CT}) at the cathode. Efforts to "clean" the cathodes by a variety of approaches (oxygen plasma, thermal annealing in O₂, solution treatments) do not generally improve reproducibility of the DSC performance and often result in poorer fill-factors (increased R_{CT}).

This chapter reports on electrochemical and DSC studies designed to shed light on the problems associated with Au cathode irreproducibility. The non-adiabatic nature of the $[\text{Co}(\text{DTB})_3]^{2+/3+}$ electron transfer at the cathode coupled with adsorption of the 4-*tert*-butylpyridine (TBP) additive on bare Au result in a large increase in R_{CT} for the $[\text{Co}(\text{DTB})_3]^{2+/3+}$ couple. Furthermore, while the electron transfer for $[\text{Co}(\text{bpy})_3]^{2+/3+}$ is fast on clean Au, the adsorption of TBP appears to interfere with electron transfer for this couple as well. However, modification of the Au surface with inorganic S^{2-} appears to block adsorption of the TBP resulting in a vastly reduced R_{CT} for either complex. Moreover, even when TBP is absent from the solution, the heterogeneous electron transfer for $[\text{Co}(\text{DTB})_3]^{2+/3+}$ is significantly faster on the Au/S^{2-} surface than on unmodified Au. While these studies do not provide a detailed unambiguous chemical answer to why some cathodes have in the past worked much better than others, they do provide considerable insight into the origin of the differences. More importantly, they provide a simple chemical solution to the irreproducibility issue which greatly increases the electron transfer rate for $[\text{Co}(\text{DTB})_3]^{2+/3+}$ and similar mediators at Au cathodes.

Experimental

Electrochemistry. Cyclic voltammetry was performed on a CHI 750D potentiostat. Au disk working electrodes used for CV measurements were constructed from Au wire (ca. 1 mm) sealed in the end of a glass tube with epoxy (Torr Seal), ground flat and polished with sub-micron alumina. Unless otherwise stated, before placing in each new solution, working electrodes were freshly polished with alumina, rinsed with DI water, and ultrasonically cleaned in absolute ethanol for approximately 1 minute.

Prior to modification with Na_2S , CV working electrodes were first polished as described above. The electrode surface was then gently swabbed for ca. 30 s using a cotton swab that had been dipped into a saturated aqueous solution of $\text{Na}_2\text{S}\cdot 9\text{H}_2\text{O}$. The electrode was then rinsed with copious amounts of DI water and blown dry with compressed air (Gust). Finally, the electrode was ultrasonically cleaned for approximately 30 s in absolute EtOH and blown dry with compressed air.

The electrochemical solvent was 0.2 M lithium triflate in γ -butyrolactone. Solutions containing TBP were 0.2 M. A two compartment electrochemical cell was employed with the reference compartment separated by a fine glass frit and Lugin capillary from the working compartment. The counter electrode was a coiled Pt wire located within the working compartment. A NaCl saturated calomel electrode (SSCE) was used as the reference.

DSC Measurements. Photoanode preparation and cell construction were accomplished as reported previously²¹ with one exception. Prior to cell construction, the photoanode was equilibrated by soaking in a γ -butyrolactone solution of 0.2 M lithium triflate / 0.2 M TBP. The cathode and photoanode, separated by a 25 μm spacers, were clamped into the cell holder. The cell holder used allows different cathodes to be sequentially mounted in the cell without disturbing the photoanode position; thus the active area of the photoanode remains the same throughout the series of measurements minimizing any changes that might be due to local inhomogeneities in anode morphology or dye uniformity.

Cathode Preparation. Au cathodes were prepared on glass by evaporating a thin layer (ca. 10 nm) of Cr onto FTO glass followed by a 200 nm layer of Au (99.97%, Alfa Aesar). Cathode modification with S^{2-} were done in essentially the same way as for Au working electrodes used in CV measurements except that the electrodes were not polished prior to

modification. The Au surface was swabbed with a saturated aqueous solution of $\text{Na}_2\text{S}\cdot 9\text{H}_2\text{O}$, rinsed with DI water and ethanol.

X-Ray Photoelectron Spectroscopy. XPS was employed to evaluate differences in surface between modified and unmodified Au cathodes. XPS measurements were conducted on a Phi-5800 spectrometer with a monochromatic (1486.6 eV) Al K α source. Samples were analyzed at an incident angle of 45° to enhance the surface sensitivity of the measurement. Spectra were shifted relative to the Au 4f_{7/2} peak set to 83.95 eV (NIST).

Results and Discussion

Cyclic voltammetry and XPS. Fig. 4.1 shows the CVs of solutions of $[\text{Co}(\text{DTB})_3]^{2+}$ (A) and $[\text{Co}(\text{bpy})_3]^{2+}$ (B) in γ -butyrolactone / 0.2 M lithium triflate electrolyte on unmodified Au with, respectively, 0.2 M TBP (red curve) and 0.0 M TBP present (black curve). In the absence of TBP both $[\text{Co}(\text{DTB})_3]^{2+/3+}$ and $[\text{Co}(\text{bpy})_3]^{2+/3+}$ are at least quasi reversible in appearance; however, the $[\text{Co}(\text{DTB})_3]^{2+/3+}$ couple is considerably less Nernstian having a $\Delta E_p > 180$ mV. With TBP present in solution the CVs of both complexes become irreversible. In the case of $[\text{Co}(\text{DTB})_3]^{2+/3+}$ the oxidation peak shifts by ca. 600 mV to more positive potentials and there is evidence of several broad reductions with the most prominent wave occurring about 300 mV more negative than the reduction peak in the absence of TBP. Qualitatively similar behavior is observed for $[\text{Co}(\text{bpy})_3]^{2+/3+}$ except that in the presence of TBP there are two distinct reduction peaks.

Fig. 4.2 again shows the CV of solutions of $[\text{Co}(\text{DTB})_3]^{2+}$ (A) and $[\text{Co}(\text{bpy})_3]^{2+}$ (B) in γ -butyrolactone / lithium triflate electrolyte / 0.2 M TBP. The red curves are for the same conditions as the red curves in Fig. 4.1 on unmodified Au (C/Au). The black curves in Fig. 4.2

are the same solutions on the same Au electrode but after modification of the Au surface with Na₂S (S/Au) as described in the Experimental section. The S²⁻ layer deposited by the modification procedure is quite robust and requires vigorous polishing with alumina to completely remove the effect.

As introduced above and covered in Chapter 3, the heterogeneous electron transfer for [Co(DTB)₃]^{2+/3+} is inherently non-adiabatic and thus presents an almost unprecedented electrode-surface- and electrolyte-dependence to its electrochemistry.¹⁹ This arises because of the insulating nature and physical size of the *t*-butyl substituents which prevents strong coupling between the relevant redox orbitals of the complex with the electrode.¹⁹ In contrast, [Co(bpy)₃]^{2+/3+} generally gives voltammetry indicative of quasireversible, adiabatic heterogeneous electron transfer. The addition of TBP to the mediator solution of a DSC results in a significant increase in the V_{OC} and is generally thought to associate with the TiO₂ surface at sites not physically blocked by dye molecules.^{22–24} Consequently, by adsorbing to these open sites the TBP molecules ostensibly block access of the oxidized mediator to the TiO₂ surface thus reducing the rate of recombination. The mechanism of action for TBP is thought to be more or less the same irrespective of whether the mediator is I[•]/I₃^{•-} or another redox couple.¹⁸

It is reasonable to hypothesize that TBP might also adsorb to the surface of bare Au and, if the coverage were sufficiently complete, that it could alter the kinetics of electron transfer between the cathode and the redox couple. This hypothesis seems to be borne out by the CV data in Fig. 4.1 for both [Co(DTB)₃]^{2+/3+} and [Co(bpy)₃]^{2+/3+}. What is odd is the structure in the voltammograms, particularly evident in the reduction scans for both complexes (but most prominent for [Co(bpy)₃]^{2+/3+}). This observation will be revisited below; however, the presence of TBP in the solution clearly and significantly impedes the electron transfer for the Co^{2+/3+}

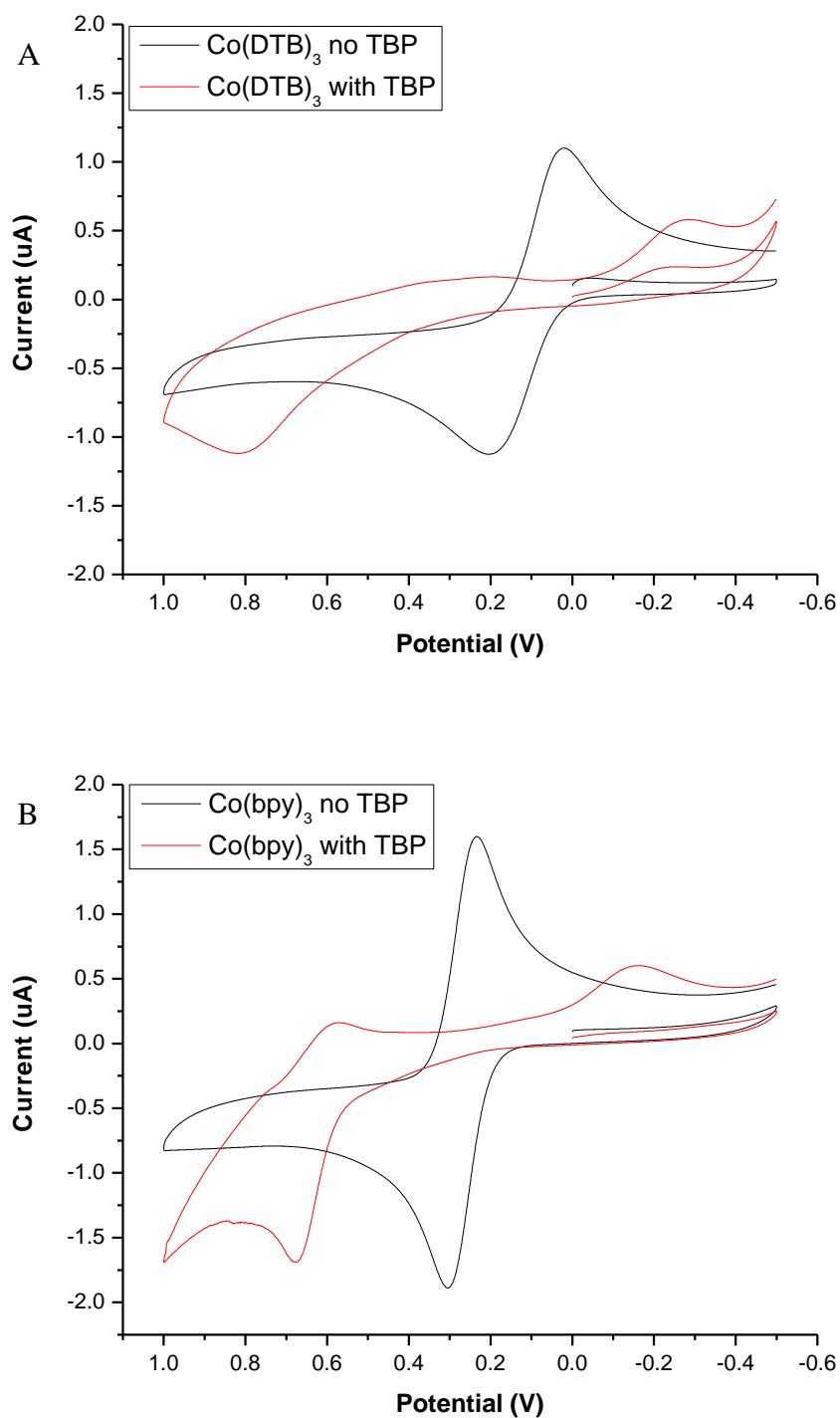


Figure 4.1. Effect of TBP presence on electrochemical reversibility of $[\text{Co}(\text{DTB})_3]^{2+}$ (A) and $[\text{Co}(\text{bpy})_3]^{2+}$ (B) on a clean Au working electrode.

couple of both complexes presumably through TBP's interaction with the Au surface. However, the adsorption of TBP to the Au surface appears to be reversible. Rinsing the Au surface with solvent is sufficient to recover the original voltammetry of the $[\text{Co}(\text{bpy})_3]^{2+/3+}$ (i.e., the voltammetry observed in the absence of TBP). In contrast, modification of the Au surface with S^{2-} is a highly irreversible process which appears to block TBP (and perhaps other Lewis bases) from adsorbing to the Au surface.

The deposition of a monolayer of S^{2-} on the Au surface appears to not only prevent TBP adsorption but also increases the rate of electron transfer between the Au and $[\text{Co}(\text{DTB})_3]^{2+/3+}$ in the absence of TBP. Comparing the CVs in Figs. 4.1A and 4.2A in the absence of TBP, the ΔE_p for $[\text{Co}(\text{DTB})_3]^{2+/3+}$ on C/Au is 185 mV while on S/Au it is only 80 mV. Thus the presence of the S^{2-} layer significantly enhances the rate of heterogeneous electron transfer for this couple relative to unmodified Au. Also, the shape and magnitude of the voltammogram for both $[\text{Co}(\text{DTB})_3]^{2+/3+}$ and $[\text{Co}(\text{bpy})_3]^{2+/3+}$ are Nernstian. The data in Figs. 4.1 and 4.2 when TBP is present were obtained under identical conditions except for the electrode modification with S^{2-} . Therefore, it must be concluded that the structure in the cathodic scans on the C/Au electrodes noted above is purely a surface phenomenon; in other words, it is not due to any chemical processes involving TBP and $[\text{Co}(\text{LL})_3]^{2+/3+}$ in solution, otherwise multiple reduction peaks should be observed on both C/Au and S/Au. The simplest hypothesis is thus that the multiple reduction "peaks" in the C/Au CVs are the result of surface inhomogeneities that give rise to different rates of heterogeneous electron transfer. If this hypothesis is correct, it could have ramifications to the DSC behavior of C/Au cathodes.

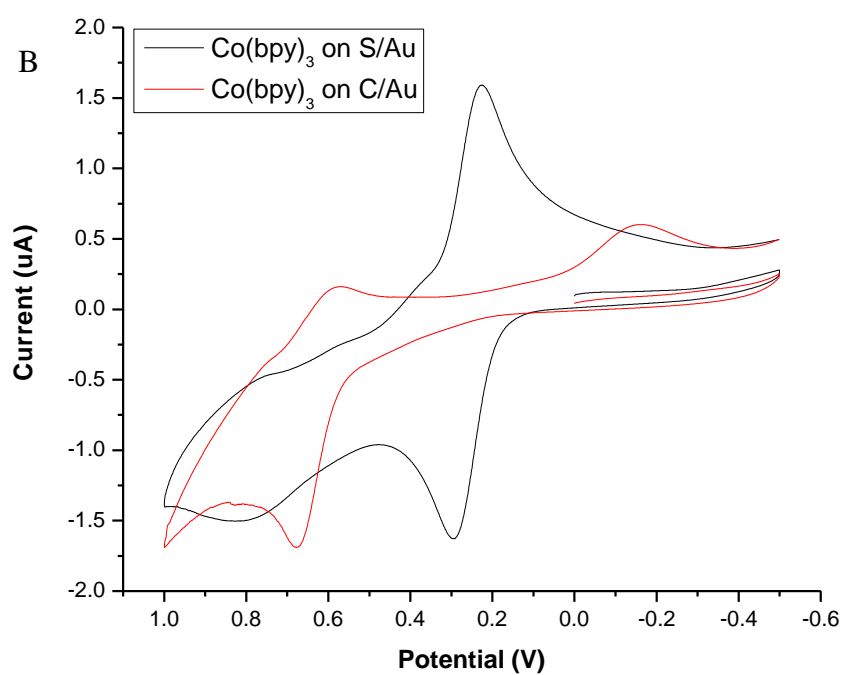
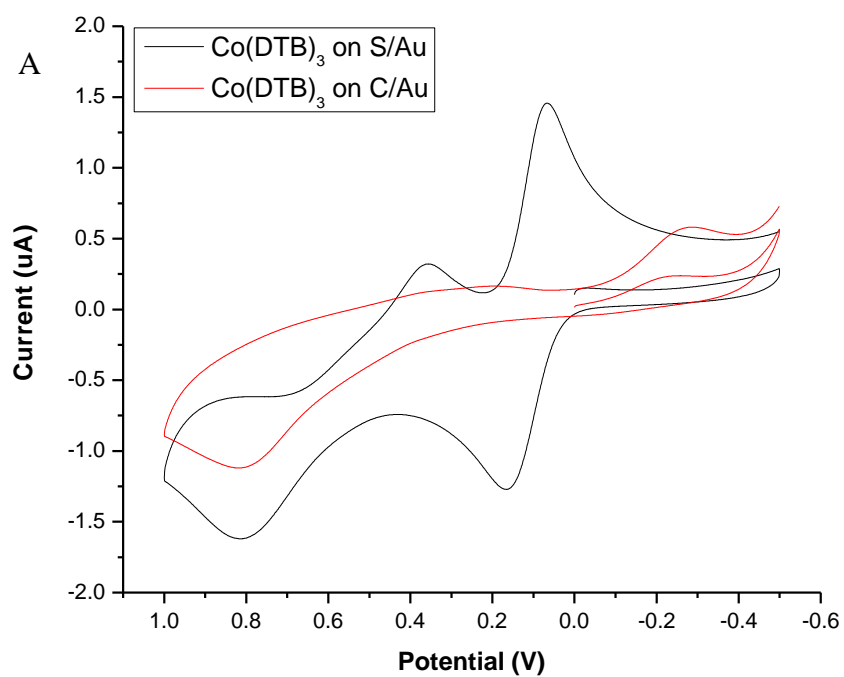


Figure 4.2. Effect of modifying a Au working electrode with S^{2-} on the electrochemistry of $[Co(DTB)_3]^{2+}$ (A) and $[Co(bpy)_3]^{2+}$ (B).

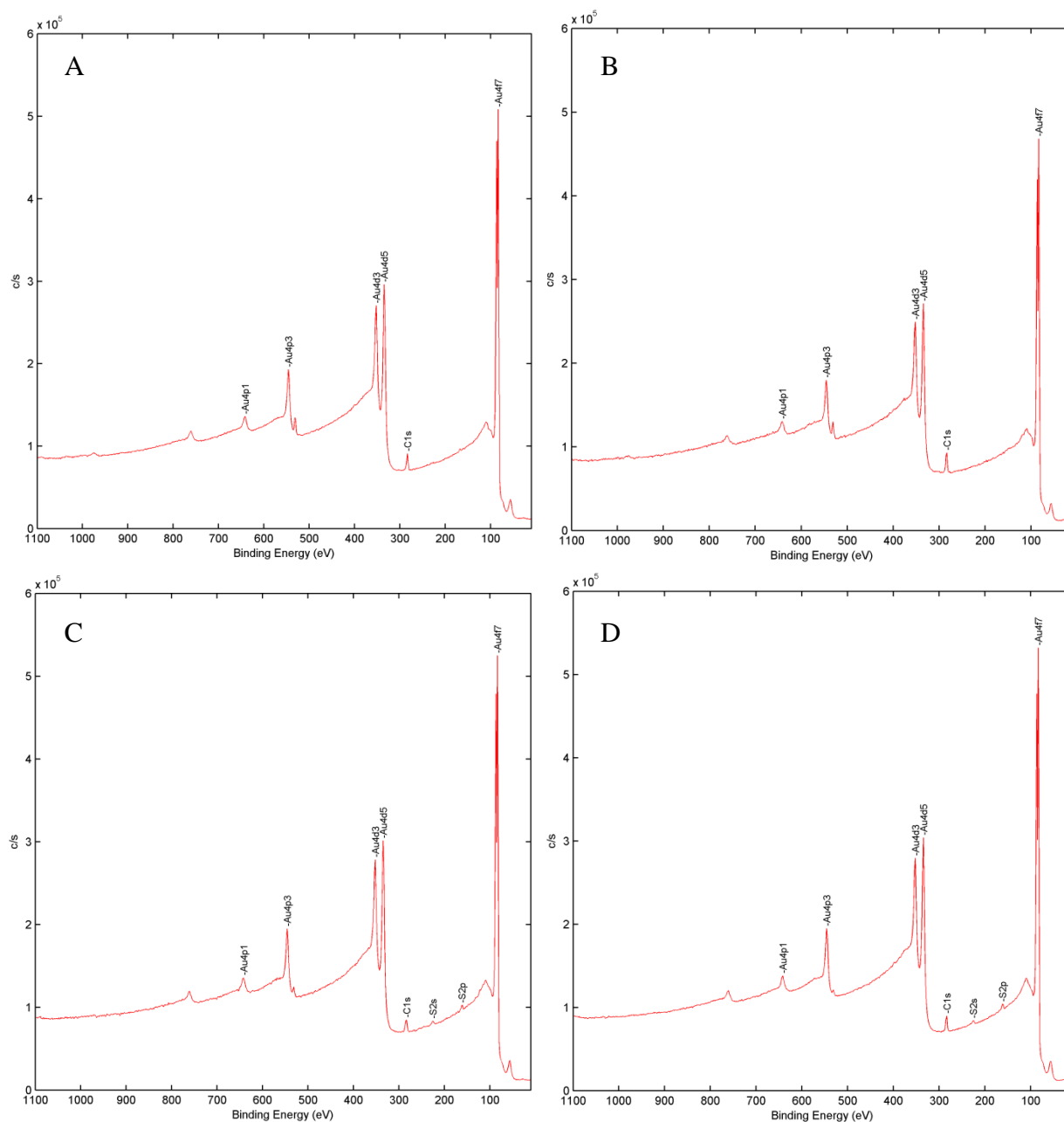


Figure 4.3. XPS survey scans of gold cathode surfaces untreated (A,B) and treated with Na₂S (C,D). B and D also were exposed to a similar electrolyte solution to that present in a DSC. Prominent sulfur 2s and 2p peaks are observed in the S/Au cases below 300 eV.

The dramatic differences in the electrochemistry of the [Co(LL)₃]^{2+/3+} complexes on C/Au and S/Au prompted surface analyses of both untreated and treated gold cathodes using

XPS. Fig. 4.3 presents low resolution survey scans on C/Au by itself (A) and after treating with mediator solution (B) as well as on S/Au by itself (C) and after treating with mediator solution (D). The sample surfaces shown in Figs. 4.3B and 4.3D were exposed to a solution of 0.2 M lithium triflate / 0.2 M TBP / 2 mM $[\text{Co}(\text{DTB})_3]^{2+}$ for a few minutes, then rinsed with absolute ethanol and blown dry with compressed air. In both S/Au scans, the S 2s and 2p peaks are prevalent at low binding energies. These peaks are not observed on the similar scans of C/Au gold cathode surfaces. Additionally, Figs. 4.3A and 4.3B are essentially the same within experimental error, backing up the earlier supposition that adsorption of TBP to the gold surface is a reversible process (and therefore fairly weak).

The nature of the sulfur species on Au is of relevance. Gao and coworkers studied the adsorption of S^{2-} from aqueous solution onto Au surfaces under potentiostatic control.^{25,26} Based on a combination of electrochemistry, SERS and STM they were able to determine the form of the sulfur add-layer as a function of potential and pH. At the most negative potentials (i.e., just prior to the onset of proton reduction) they proposed that the sulfur exists as adsorbed HS^- . As the potential was moved to more positive values the adsorbed HS^- was oxidized by $2e^-$ with the loss of a proton to give neutral, adsorbed, monomeric sulfur atoms. From STM studies on Au (111) they determined the S layer to consist of a 1/3 fractional monolayer (relative to Au surface atoms) where the sulfur atoms sit in threefold hollows.²⁶ (Hoffman et al. later reported the preference of sulfur for these hollows and that the interaction was purely surface oriented.²⁷) The resonance Raman spectrum on polycrystalline Au was consistent with an analogous surface structure. In Gao's experiments the bulk solution contained S^{2-} and at still more positive potentials the oxidation of S^{2-} from solution resulted in the deposition of bulk sulfur on the Au surface.

In the current experiments, the application of the S^{2-} is not done under potentiostatic control and subsequent electrochemistry is done in aprotic solvent in the absence of bulk S^{2-} . Consequently, it was necessary to attempt to establish what form the adsorbed sulfur is in initially. The survey scan for the S^{2-} modified surface (Fig. 4.3C) shows clear sulfur peaks with appropriate intensity to support a sub-monolayer of surface coverage. Moreover, there is no experimentally significant Na peak, suggesting there is no charge balancing Na^+ associated with the sulfur on the surface. The sensitivity factor of sodium is significantly larger than that of sulfur, so any Na^+ present would surely be observable given the obvious presence of sulfur.²⁸ While this does not constitute definitive evidence, it suggests that the form of the sulfur in the as-formed film is not anionic. In the subsequent electrochemistry of S/Au electrodes the first observable oxidation begins at ca. 0.4 V vs. SSCE suggesting that the form of the sulfur layer is as monomeric sulfur atoms which remain in this form out to potentials of at least 0.4 V vs. SSCE.

The high-resolution XPS measurement (Fig. 4.4) shows the apparent splitting of the sulfur $2p_{3/2}$ binding energy with a separation of ca. 1 eV which could suggest the possibility of multiple sulfur binding environments. While this possibility cannot be completely ruled out, the CV results in Fig. 4.2 suggest otherwise, at least in so far as the formal oxidation and protonation state of the sulfur is concerned. The fact that only one set of oxidation and reduction waves associated with the surface modification is observed suggests the presence of only one type of sulfur on the surface within the potential window between -0.6 V and ca. 0.4 V.

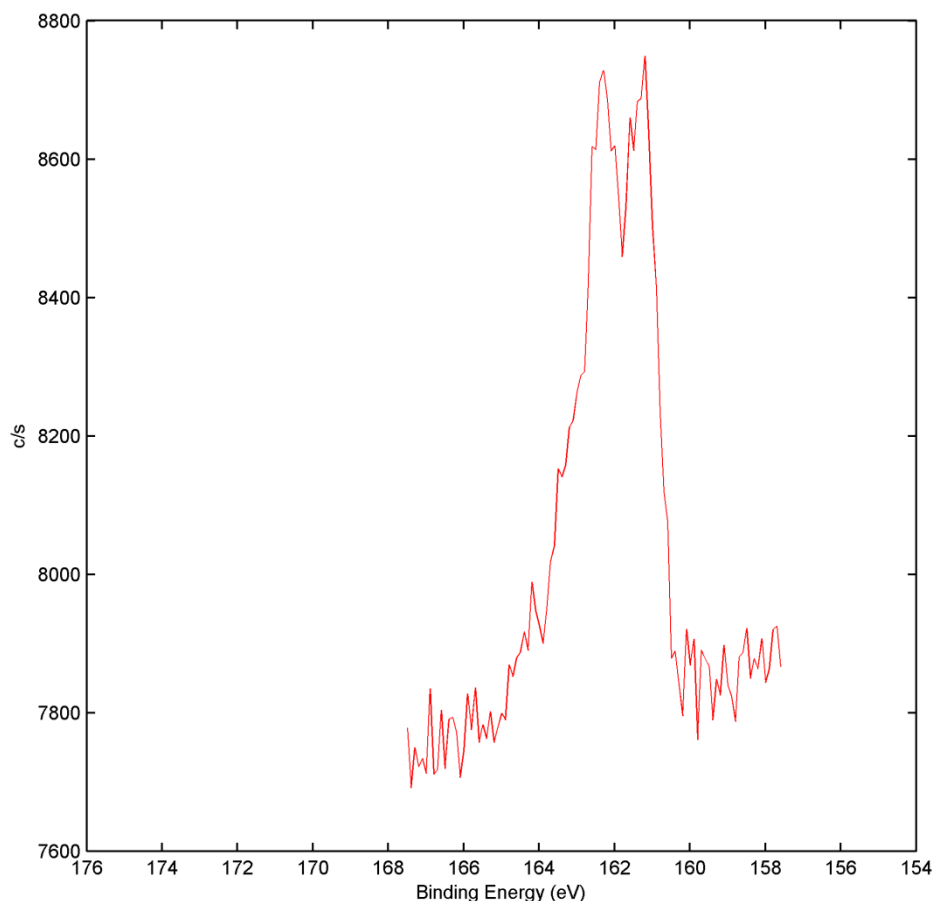


Figure 4.4. High resolution scan of the S/Au surface focused on the S 2p peak. The splitting of the peak seems to indicate the presence of more than one binding environment which is not supported by the electrochemical result of a single redox process.

In order to effectively employ S/Au cathodes in DSCs, the stability of the surface must be determined. Fig. 4.5 shows the multiple scan CV (12 cycles) of $[\text{Co}(\text{DTB})_3]^{2+}$ on S/Au with two different positive potential limits: 0.4 V (A) and 1.0 V (B). There is essentially no change in the voltammetry with multiple cycling with the 0.4 V anodic limit. However, when the potential is repeatedly cycled to 1.0 V the peak separation for the $[\text{Co}(\text{DTB})_3]^{2+/3+}$ couple ($E_{1/2} = \text{ca. } 0.1 \text{ V}$) increases with each cycle and the voltammetry becomes progressively less reversible. The oxidation peak at ca. 750 mV and the corresponding reduction at ca. 400 mV are associated with the S^{2-} on the Au surface. Upon multiple scans out to 1.0 V the peak currents decrease with each successive scan and the peaks shift apart.

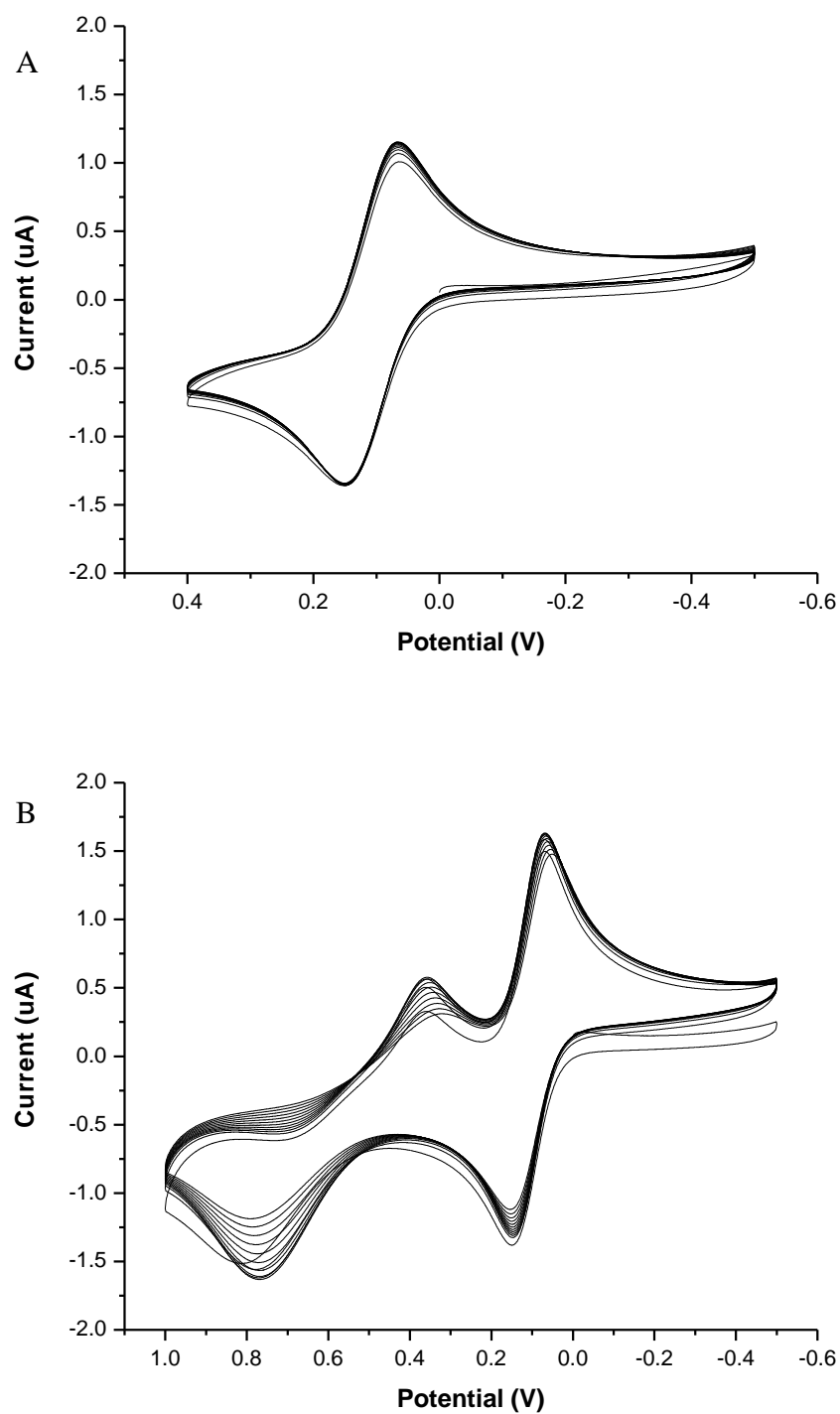


Figure 4.5. Effect of multiple cycles on the electrochemistry of $[\text{Co}(\text{DTB})_3]^{2+}$ on a modified cathode in the presence of TBP with anodic limits of +0.4 V (A) and +1.0 V (B). Both the reduction and oxidation become more irreversible with cycling out to large anodic potentials.

The voltammetric waves at potentials more positive than 0.4 V are a result of the sulfur layer. Because there is no S^{2-} in solution, this wave is not due to the formation of bulk sulfur on the surface – at least not in the same fashion as was observed by Gao et al.^{25,26} At this point, any attempt to explain this oxidation would be purely speculation. Suffice it to say that whatever process it does involve, it is not fully reversible on the time scale of these voltammetry experiments when the potential is cycled out to 1.0 V. However, based on the voltammetry shown in Fig. 4.5, if the potential is maintained at values less positive than ca. 0.4 V then the surface appears to be stable. This fact is relevant in terms of using S/Au as a cathode in a DSC because the potential of the cathode should never become significantly more positive than the $E_{1/2}$ for the respective $[Co(LL)_3]^{2+/3+}$ couple present in the mediator.

With regard to how the S modification affects the electrochemistry of $[Co(LL)_3]^{2+/3+}$ there are several possibilities. First, irrespective of the actual oxidation state of the sulfur monolayer, as suggested earlier, it is likely that TBP and similar Lewis bases would have little affinity for binding to such a surface. Even with the sulfur formally as S^0 , the surface dipole would be oriented to disfavor TBP binding. Also, the surface dipole would favor electrostatic interactions with the cationic $[Co(LL)_3]^{2+/3+}$. Dipolar interactions notwithstanding, the higher rate of heterogeneous electron transfer for $[Co(DTB)_3]^{2+/3+}$ at S/Au compared to C/Au could be rationalized in part on the basis of the higher microscopic roughness of the sulfur modified surface. If the sulfur is present as a sub-monolayer, this packing could allow $[Co(DTB)_3]^{2+/3+}$ to more closely approach (and thus better couple to) the electrode than would be possible for a close packed layer of Au atoms. Irrespective of the detailed mechanism, the sulfur modified Au surface clearly couples more strongly with the $[Co(DTB)_3]^{2+/3+}$ than does nominally clean Au, rendering the heterogeneous electron transfer considerably more adiabatic.

DSC Testing. Given the promising electrochemical results of $[\text{Co}(\text{LL})_3]^{2+/3+}$ complexes on sulfide-treated gold cathodes, DSCs were fabricated and tested to determine if any benefits were manifested in cell performance. Fig. 4.6 shows J-V curves obtained with a single mesoporous TiO_2 photoanode dyed with N3. The electrolyte in all cases is $[\text{Co}(\text{DTB})_3]^{2+/3+}$ (0.135 M / 0.015 M), 0.2 M lithium triflate, and 0.2 M TBP in γ -butyrolactone. The dashed blue trace is with a typical, new unmodified Au film cathode. The solid blue trace is for the same cell after it has been illuminated at approximately 1 sun for 15 minutes at open circuit. The dashed and solid red traces are for the same photoanode coupled with a S/Au cathode. The dashed red

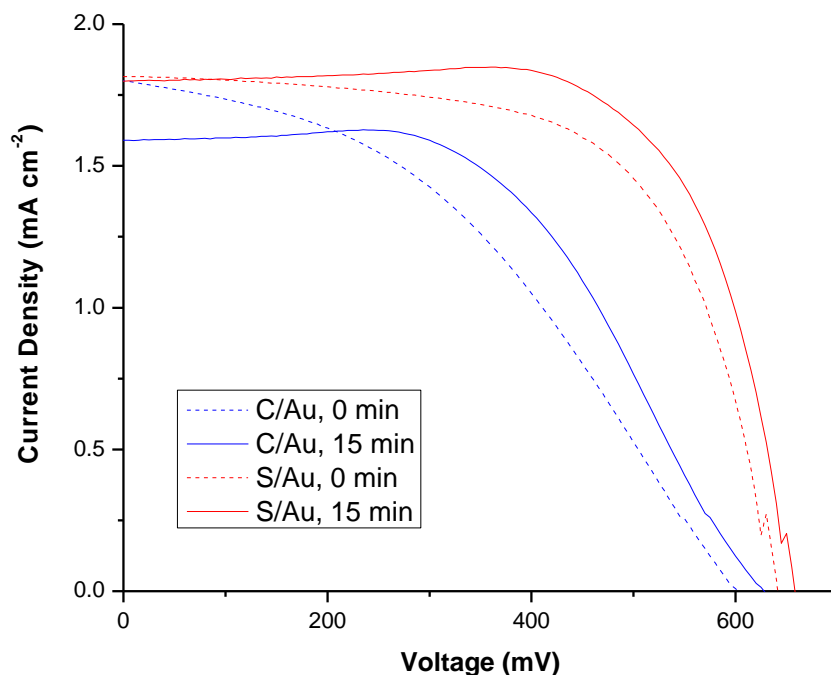


Figure 4.6. Current density – voltage curves for cells constructed with a Au cathode before (C/Au) and after (S/Au) modification. The cells were held at open circuit and illuminated for 15 min. with approximate 1-sun radiation. The same anode was used for both cathode cases.

curve was obtained initially after the cell is first assembled. The solid red curve is after 15 minutes of illumination (ca. 1 sun) at open circuit. Fig. 4.7 shows typical dark current traces

with the same electrolyte as in Fig. 4.6 for a new, C/Au cathode (blue trace) and a S/Au cathode (red trace). The insert shows a blow up of the same data.

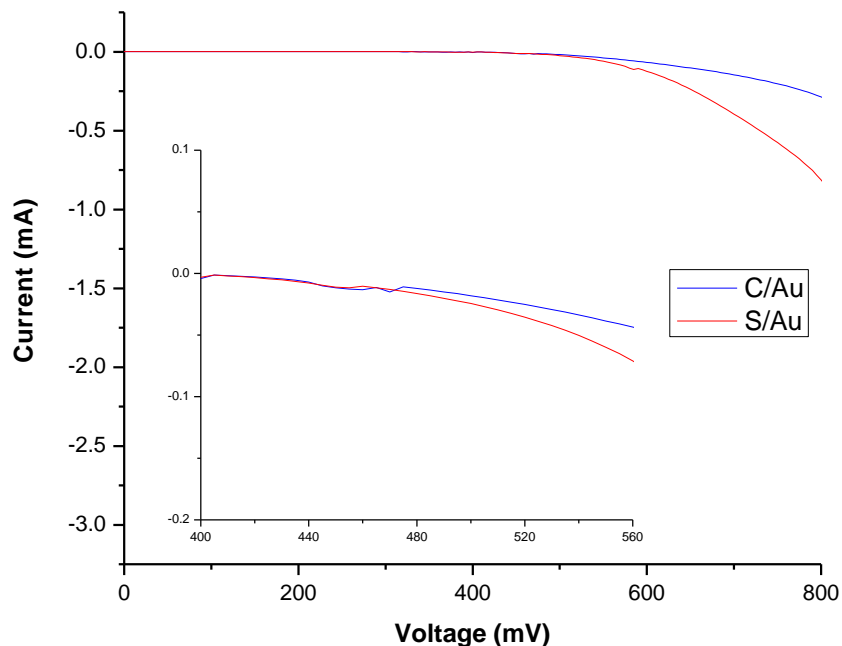


Figure 4.7. Dark current-voltage curves of $[\text{Co}(\text{DTB})_3]^{2+/3+}$ -mediated DSCs utilizing a Au cathode before (C/Au) and after (S/Au) modification with S^{2-} . The inset is the same plot focused at the potential where negative current begins to be observed.

Fig. 4.8 shows plots of J_{SC} vs. time in experiments where the light (ca. 1 sun) is abruptly pulsed on. Data is given for the same cells considered in Fig. 4.6. The initial, instantaneous current is reflective of the current density before the mass transport of the oxidized mediator becomes rate limiting in the cell. The steady state current density obtained after ca. 1 s is reflective of the mass-transport limited current.

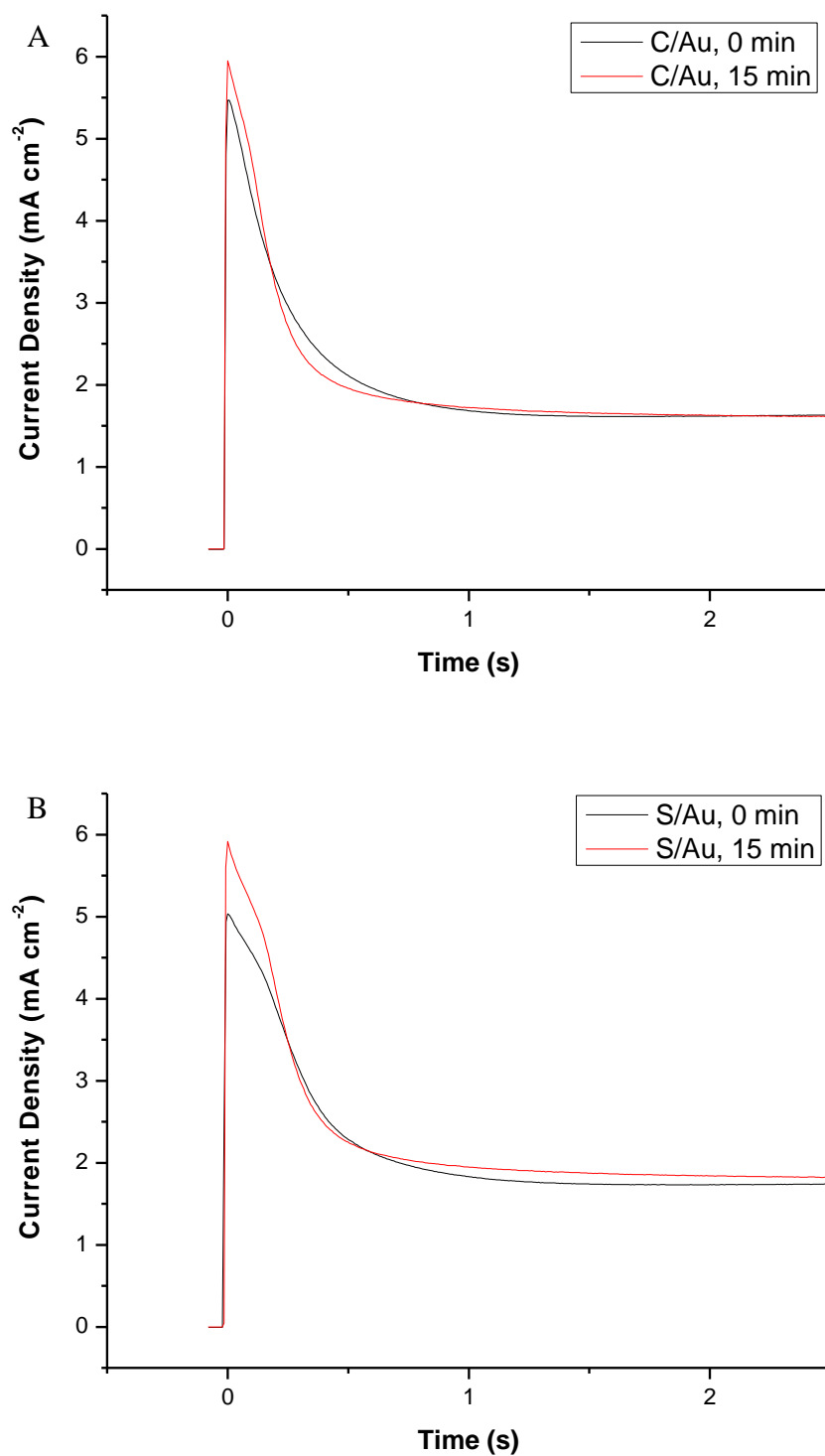


Figure 4.8. Short-circuit current density (J_{SC}) as a function of time in the light for $[\text{Co}(\text{DTB})_3]^{2+/3+}$ coupled with C/Au (A) and S/Au (B) immediately after cell assembly and after 15 minutes of irradiation at ca. 1 sun at open circuit. These traces correspond to the same cells as Fig. 6.

For a DSC mediated with either $[\text{Co}(\text{DTB})_3]^{2+/3+}$ or $[\text{Co}(\text{bpy})_3]^{2+/3+}$ two things are typically observed when comparing the J-V curves obtained from a single photoanode paired, respectively, with a new C/Au cathode and with a S/Au cathode: (1) The fill factor is significantly better with the S/Au cathode and (2) the V_{OC} increases by a modest amount (ca. 30 mV) with the S/Au cathode relative to C/Au. However, the increase in V_{OC} is likely an experimental artifact of disassembling and reassembling the cell with fresh electrolyte and not the result of modifying the cathode surface, as a similar increase in V_{OC} is observed with unmodified cathodes as well. The J-V curves shown in Fig. 4.6 are typical with the additional caveat that there is a fair amount of variability from cathode-to-cathode in the shape (and thus fill factor) for C/Au but there is much less variability in comparable data with different S/Au cathodes. The distinctive "S" shape in the J-V curves for the C/Au cathode in Fig. 4.6 is indicative that charge transfer at the cathode is becoming rate limiting at higher cell voltages. This can also be seen by comparing the dark currents for the two different cells in Fig. 4.7. At lower voltages the dark currents are comparable (Fig. 4.7, insert) but diverge as the oxidation of $[\text{Co}(\text{DTB})_3]^{2+}$ at the cathode becomes rate limiting on C/Au.

Both cells represented in Fig. 4.6 show modest changes in shape over the first 15 minutes of illumination after assembly; however, the shapes are generally similar for the given type of cathode. Normally, such changes in the J-V with time or illumination are assumed to result from changes occurring only at the photoanode. An important consideration in discussing the J-V curves for these cells is, however, that short circuit current density is significantly limited by mass transport of $[\text{Co}(\text{LL})_3]^{3+}$. Moreover, the mass-transport limitation is particularly significant for the relatively large $[\text{Co}(\text{DTB})_3]^{3+}$. J_{SC} vs. time transients obtained from pulsed light experiments (Fig. 4.8) indicate that the steady state current is only ca. 1/3 of what it would be in

the absence of mass-transport limitations for $[\text{Co}(\text{DTB})_3]^{3+}$ (i.e., compare $J_{\text{SC}}(t = 0)$ with $J_{\text{SC}}(t = 2 \text{ s})$ in Fig. 4.8). The point here is that mass-transfer effects on J-V curves for these mediator systems cannot be ignored and they can mask other effects such as changes in recombination rates. That caveat notwithstanding, the initial currents in the J_{SC} vs. time plots of Fig. 4.8 are larger after the 15 minute illumination period for both C/Au and S/Au cathodes. The V_{OC} is also larger. Increases in V_{OC} and initial current density are both consistent with modestly slower recombination. The hypothesis for this is that the initial kinetic distribution of TBP on the TiO_2 surface may not be optimal for blocking recombination. With time during the illumination the TBP/ TiO_2 interactions possibly "anneal" in a way that reduces recombination at the photoanode surface. Finally, the change in shape between the 0 and 15 minute curves for the S/Au cathode could simply be due to a change in viscosity of the solution as the cell warms under illumination.

For the C/Au cathodes things are more complicated. At short circuit, the current is again limited by mass transport of $[\text{Co}(\text{DTB})_3]^{3+}$ (Fig. 4.8A) but, as the voltage approaches V_{OC} , the current becomes limited by slow electron transfer at the cathode. Again, the data in Fig. 4.8A sheds some light on the difference in J_{SC} between the initial scan and the scan after 15 minutes of illumination. As was the case for the S/Au cathode discussed above, after the 15 minute period of illumination the initial current, $J_{\text{SC}}(t = 0)$, in Fig. 8A is actually larger than prior to illumination (consistent with less recombination). It is the mass-transport limited current in Fig. 4.6 that is smaller. As argued above, one obvious change in the cell under illumination is that the solution should warm up to some degree. However, that should speed up mass transport rather than slow it down. There is currently no good hypothesis for how illumination could affect the $[\text{Co}(\text{DTB})_3]^{3+}$ mass transport in the way it does. Nonetheless, the effect of illumination on

the current in the J-V plots is at least partially reversible. After the cell sits in the dark for an extended period the current recovers.

Conclusion

The common DSC solution additive 4-*tert*-butylpyridine not only adsorbs to recombination sites on TiO₂ photoanodes, it also adsorbs on the surface of clean Au cathodes. Moreover, this adsorption can drastically hamper the electron transfer between the electrode and [Co(LL)₃]^{2+/3+}-type mediators. Exposing the Au surface to aqueous S²⁻ irreversibly modifies that surface. The sulfur likely resides on the surface as formally neutral monomeric sulfur atoms in sub-monolayer coverage. The effect of this modification is several fold: first, it appears to prevent strong adsorption of TBP to the Au surface and, second, it actually acts as an electron-transfer catalyst for [Co(DTB)₃]^{2+/3+} relative to clean Au. As a consequence, in DSCs mediated with [Co(LL)₃]^{2+/3+}, Au cathodes modified in this way are more reproducible and typically give better fill factors than their unmodified counter parts. Interestingly, similar attempts to modify Au electrodes with CN⁻ (another strongly Au-binding anion) produced no similar effects in the voltammetry.

Finally, this study was initially undertaken because of a decade long problem with batch-to-batch variations in Au DSC cathodes. Initially the hypothesis was that the surface of these "bad" electrodes contained some contaminant which was hampering the electron transfer of [Co(LL)₃]^{2+/3+}. In light of the current results, that hypothesis is almost certainly incorrect. In fact, the current hypothesis is that the electrodes which were found to work best were the ones which had been contaminated, specifically with some species which was preventing TBP from adsorbing and blocking the electron transfer at the cathode. Furthermore, this new hypothesis is

consistent with the observation that unmodified cathodes tend to improve with multiple usage (i.e., assembly and disassembly of cells).

Chapter 4 References

- (1) Cai, N.; Li, R.; Wang, Y.; Zhang, M.; Wang, P. *Energy Environ. Sci.* **2013**, *6*, 139.
- (2) Xie, Y.; Hamann, T. W. *J. Phys. Chem. Lett.* **2013**, *4*, 328–332.
- (3) Ondersma, J. W.; Hamann, T. W. *Coord. Chem. Rev.* **2013**, *257*, 1533–1543.
- (4) Feldt, S. M.; Lohse, P. W.; Kessler, F.; Nazeeruddin, M. K.; Grätzel, M.; Boschloo, G.; Hagfeldt, A. *Phys. Chem. Chem. Phys.* **2013**, *15*, 7087.
- (5) Salvatori, P.; Marotta, G.; Cinti, A.; Anselmi, C.; Mosconi, E.; De Angelis, F. *J. Phys. Chem. C* **2013**, *117*, 3874–3887.
- (6) Hamann, T. W. *Dalton Trans.* **2012**, *41*, 3111.
- (7) Mosconi, E.; Yum, J.-H.; Kessler, F.; Gómez García, C. J.; Zuccaccia, C.; Cinti, A.; Nazeeruddin, M. K.; Grätzel, M.; De Angelis, F. *J. Am. Chem. Soc.* **2012**, *134*, 19438–19453.
- (8) Xu, M.; Zhang, M.; Pastore, M.; Li, R.; De Angelis, F.; Wang, P. *Chem. Sci.* **2012**, *3*, 976.
- (9) Bai, Y.; Zhang, J.; Zhou, D.; Wang, Y.; Zhang, M.; Wang, P. *J. Am. Chem. Soc.* **2011**, *133*, 11442–11445.
- (10) Liu, J.; Zhang, J.; Xu, M.; Zhou, D.; Jing, X.; Wang, P. *Energy Environ. Sci.* **2011**, *4*, 3021.
- (11) Zhou, D.; Yu, Q.; Cai, N.; Bai, Y.; Wang, Y.; Wang, P. *Energy Environ. Sci.* **2011**, *4*, 2030.
- (12) Feldt, S. M.; Wang, G.; Boschloo, G.; Hagfeldt, A. *J. Phys. Chem. C* **2011**, *115*, 21500–21507.

- (13) Gibson, E. A.; Smeigh, A. L.; Le Pleux, L.; Hammarström, L.; Odobel, F.; Boschloo, G.; Hagfeldt, A. *J. Phys. Chem. C* **2011**, *115*, 9772–9779.
- (14) Liu, Y.; Jennings, J. R.; Huang, Y.; Wang, Q.; Zakeeruddin, S. M.; Grätzel, M. *J. Phys. Chem. C* **2011**, *115*, 18847–18855.
- (15) Feldt, S. M.; Gibson, E. A.; Gabrielsson, E.; Sun, L.; Boschloo, G.; Hagfeldt, A. *J. Am. Chem. Soc.* **2010**, *132*, 16714–16724.
- (16) Klahr, B. M.; Hamann, T. W. *J. Phys. Chem. C* **2009**, *113*, 14040–14045.
- (17) Yella, A.; Lee, H.-W.; Tsao, H. N.; Yi, C.; Chandiran, A. K.; Nazeeruddin, M. K.; Diau, E. W.-G.; Yeh, C.-Y.; Zakeeruddin, S. M.; Gratzel, M. *Science* **2011**, *334*, 629–634.
- (18) Sapp, S. A.; Elliott, C. M.; Contado, C.; Caramori, S.; Bignozzi, C. A. *J. Am. Chem. Soc.* **2002**, *124*, 11215–11222.
- (19) Gaddie, R. S.; Moss, C. B.; Elliott, C. M. *Langmuir* **2013**, *29*, 825–831.
- (20) Xue, D.; Ashbrook, L. N.; Gaddie, R. S.; Elliott, C. M. *J. Electrochem. Soc.* **2013**, *160*, H355–H359.
- (21) Ashbrook, L. N.; Elliott, C. M. *J. Phys. Chem. C* **2013**, *117*, 3853–3864.
- (22) Koh, T. M.; Nonomura, K.; Mathews, N.; Hagfeldt, A.; Grätzel, M.; Mhaisalkar, S. G.; Grimsdale, A. C. *J. Phys. Chem. C* **2013**, *117*, 15515–15522.
- (23) Boschloo, G.; Häggman, L.; Hagfeldt, A. *J. Phys. Chem. B* **2006**, *110*, 13144–13150.
- (24) Nazeeruddin, M. K.; Kay, A.; Rodicio, I.; Humphry-Baker, R.; Mueller, E.; Liska, P.; Vlachopoulos, N.; Grätzel, M. *J. Am. Chem. Soc.* **1993**, *115*, 6382–6390.
- (25) Gao, X.; Zhang, Y.; Weaver, M. J. *J. Phys. Chem.* **1992**, *96*, 4156–4159.
- (26) Gao, X.; Zhang, Y.; Weaver, M. J. *Langmuir* **1992**, *8*, 668–672.

- (27) Tachibana, M.; Yoshizawa, K.; Ogawa, A.; Fujimoto, H.; Hoffmann, R. *J. Phys. Chem. B* **2002**, *106*, 12727–12736.
- (28) Wagner, C. D.; Davis, L. E.; Zeller, M. V.; Taylor, J. A.; Raymond, R. H.; Gale, L. H. *Surf. Interface Anal.* **1981**, *3*, 211–225.

Chapter 5: Donor-Appended N3-Type Sensitizers

Introduction

Given the success of phenothiazine-type (PTZ) donors in both ruthenium D-C-A triads¹⁻⁴ and the work with copper dyes⁵ (see Chapter 2), a natural progression was to explore the efficacy of these donors in $[\text{Ru}(\text{LL})_3]^{2+}$ -type dyes (where LL = 2,2'-bipyridine or 1,10'-phenanthroline). Reducing these sensitizers by Γ^- is relatively fast and occurs on the timescale of 100 ns to 10 μs .⁶ $[\text{Co}(\text{LL})_3]^{2+}$ complexes have a competitive regeneration rate but suffer from additional complexities due to their substantially larger size and slower mass transport within the TiO_2 framework.⁷ Without the slow self-exchange derived from the spin change between oxidation states, these complexes would probably only function competently as mediators under very select circumstances like ferrocene.⁸

Typically the largest loss mechanism in a dye-sensitized solar cell (DSC) is electron recombination, either from the TiO_2 or conductive glass. Fewer electrons in the conduction band clearly leads to less collected photocurrent, but also results in a positive shift of the Fermi energy and therefore limits the photovoltage as well. Reducing the recombination rate can therefore yield substantial gains in solar cell performance. Recombination from the conductive glass can be effectively blocked by deposition of a thin (< 100 nm) dense TiO_2 layer prior to the mesoporous layer.⁷ This blockage allows electrical conductivity throughout the whole system but prevents mediator molecules from physically reaching the glass. Chemical vapor deposition of alumina has been shown to drastically inhibit recombination from the TiO_2 .⁹ The alumina layer is kept thin enough (on the order of a monolayer) to still allow electron injection and

insulating enough to prevent electron capture by oxidized mediator before diffusion to the conductive glass.

As noted in Chapter 2, Argazzi and coworkers showed proof of concept for a $[\text{Ru}(\text{LL})_3]^{2+}$ system with a covalently bound electron donor.¹⁰ This system yielded a V_{OC} value 100 mV larger than that of a similar species that lacked a donor. The larger V_{OC} was attributed to the increased spatial separation of the electron-hole pair being responsible for a slower recombination rate. The application of this concept to an N3-type dye (i.e., a $\text{Ru}(\text{LL})_2(\text{SCN})_2$ -type system), however, was not attempted in that study. Nevertheless, this method represents a complementary technique to those mentioned above to reduce combination.

It is assumed that the ground-state redox potential of the dyes investigated in this chapter should be approximately the same as that of N3 (0.85 V vs. SCE)¹¹ and therefore about 400 mV negative of a $[\text{Ru}(\text{bpy})_3]^{2+}$ -type system such as that studied by Argazzi et al.¹⁰ Still, a moderately sized driving force of ca. 150 mV should exist for reduction of the oxidized metal center even when the donor is covalently bound to a ligand. (Recall from Chapter 2 that the redox potential shifts ca. 100 mV positive when attached through the nitrogen so reduction would occur from something akin to *N*-methyl PTZ, $E_{1/2} \approx 700$ mV vs. SCE). Therefore, modification of the PTZ species in order to further shift the $E_{1/2}$ negatively as in Chapter 2 is not necessary.

This chapter reports on two newly synthesized dyes, RD1 and RD2 (Fig. 5.1), coupled with cobalt polypyridyl mediators. These dyes incorporate PTZ donors covalently bound through the nitrogen on the center heterocycle. The steric footprint of these dyes is substantially larger than that of N3, which potentially has consequences on the rate of regeneration by the large $[\text{Co}(\text{LL})_3]^{2+}$ species. The performance of these dyes with cobalt mediators is benchmarked against the widely investigated N3 and Z-907 sensitizers.

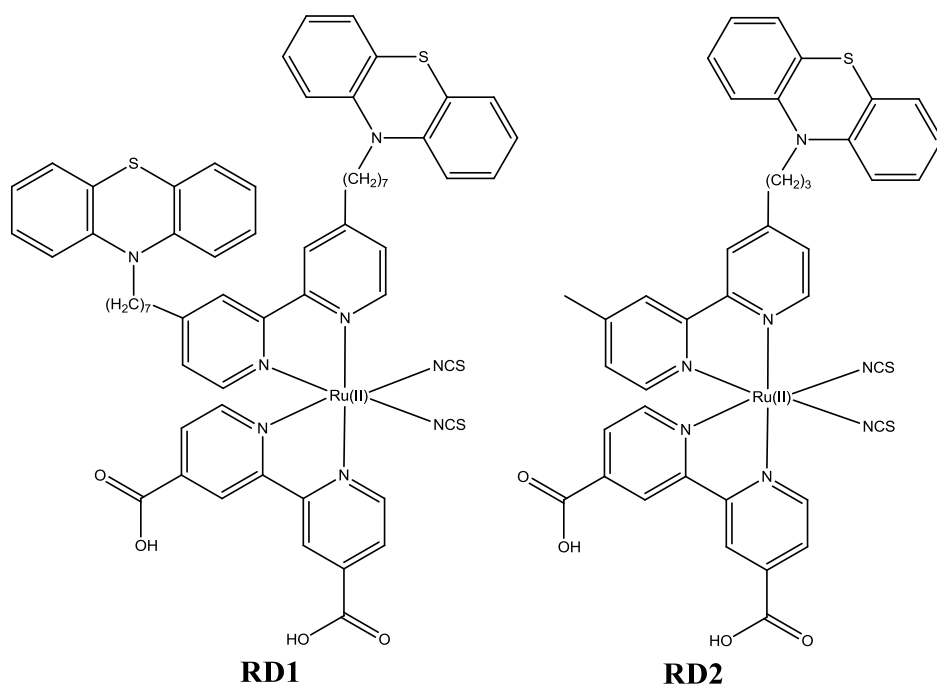
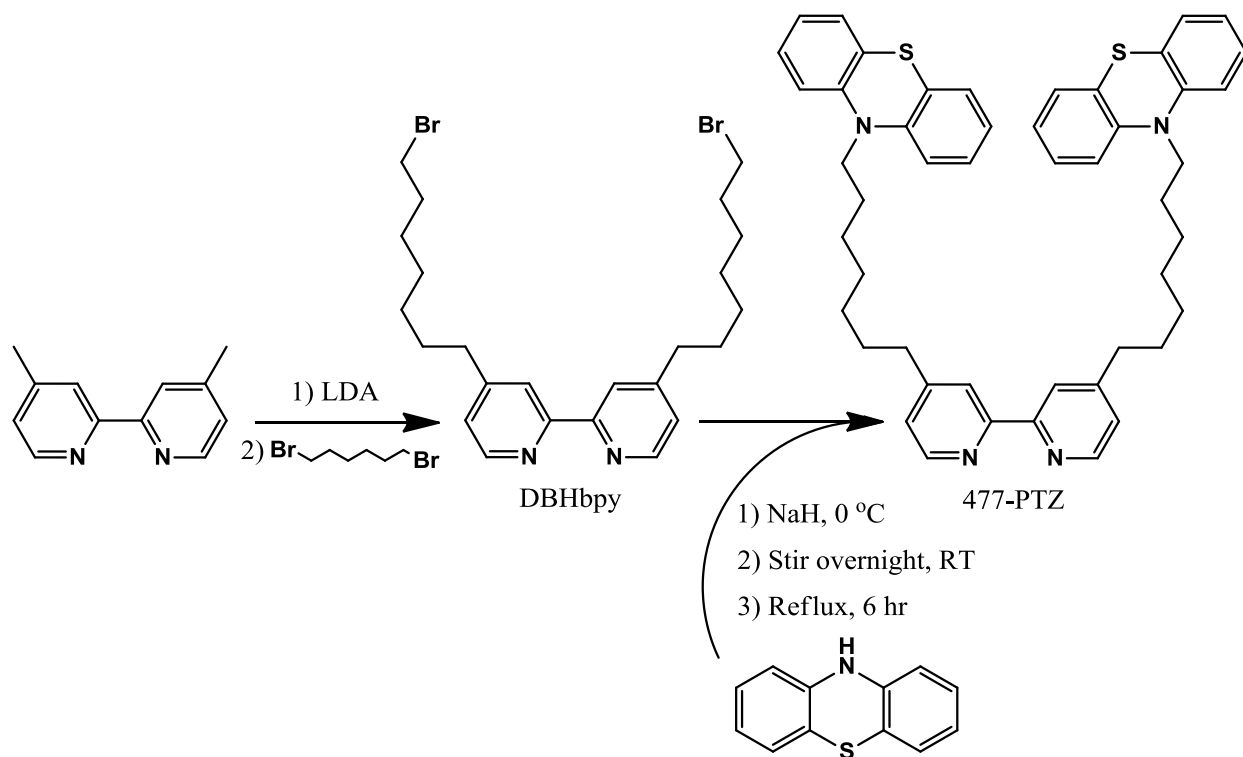


Figure 5.1. Structures of RD1 and RD2.

Experimental

Detailed syntheses of the ruthenium-based sensitizers are described below. Dry THF was obtained by distillation from commercial THF, benzophenone, and sodium metal. 4-methyl-4'-(3-(phenothiazino)propyl)-2,2'-bipyridine (43-PTZ) and 4,4'-dicarboxy-2,2'-bipyridine (dcbpy) were synthesized previously.^{1,12} The complete synthesis of 477-PTZ (the ligand used to make RD1) is described in Scheme 5.1. Ammonium thiocyanate was recrystallized from acetonitrile. All other materials were obtained through commercial sources and used without further purification.

Scheme 5.1. Complete synthesis of 477-PTZ, the ligand used in sensitizer RD1.



Synthesis of 4,4'-bis(7-bromoheptyl)-2,2'-bipyridine (DBHbpy). A round bottom flask under active N₂ flow was charged with diisopropyl amine (16 mL, 0.11 mol) and 25 mL THF. The flask was placed in a dry ice/acetone bath and n-BuLi (68 mL, 0.11 mol) was added via cannula to make lithium diisopropylamide (LDA). Separately, 4,4'-dimethyl-2,2'-bipyridine (DMB, 10 g, 0.054 mol) was dissolved in 350 mL THF. The DMB solution was added slowly to the LDA solution while stirring over a period of 20 minutes. The solution immediately turned dark brown on addition. The reaction was subsequently stirred for three hours during which the color gradually changed to bright red.

In a separate flask, 1,6-dibromohexane (72 mL, 0.57 mol) was diluted into an additional 350 mL THF under N₂ and then added to the DMB/LDA solution via cannula. Initially the resultant mixture was a murky red color. It was allowed to stir for one hour, and then removed

from the dry ice/acetone bath. The reaction mixture was a milky light green at this point, and turned milky yellow upon warming to room temperature.

The reaction (and specifically unreacted LDA) was quenched with 150 mL H₂O. Extractions with 100 mL diethyl ether and 3× 100 mL dichloromethane (DCM) yielded a bright yellow liquid after 75% volume reduction via rotary evaporation. TLC (10% ethyl acetate in DCM) yielded two major spots at $R_f = 0.85$ and $R_f = 0.2$ corresponding to the di-substituted and mono-substituted ligand, respectively. Column chromatography on 200-400 mesh silica gel (DCM to remove excess dibromohexane, then 10% ethyl acetate in DCM) yielded the dibromoheptyl-substituted bipyridine (DBHbpy). ¹H NMR in CDCl₃, δ in ppm: 8.59 (2H, d), 8.26 (2H, s), 7.16 (2H, m), 3.44 (4H, t), 2.74 (4H, t), 1.89 (4H, m), 1.74 (4H, m), 1.42 (12H, m).

Synthesis of 4,4'-bis(7-(10H-phenothiazin-10-yl)heptyl)-2,2'-bipyridine (477-PTZ). PTZ (2.34 g, 12 mmol) and NaH (0.4227 g of a 60% dispersion in oil, 10.5 mmol) were combined in a round bottom flask under N₂, after which the flask was placed in an ice water bath. THF (35 mL) was added and the solution was allowed to stir for two hours. The solution turned a yellow/gold color. Separately, DBHbpy (0.5 g, 1 mmol) was dissolved in 50 mL THF and then added dropwise to the deprotonated PTZ solution over the course of 15 minutes. The ice water bath was removed and the solution was allowed to stir overnight under N₂, during which it turned a yellow-orange color similar to orange juice. This solution was then refluxed for six hours, though TLC (5% acetone in DCM) suggested no significant change after two hours. During reflux the color changed from orange to maroon to dark brown. After cooling the reaction was quenched with ca. 40 mL H₂O. The product was extracted with 2× 50 mL diethyl ether and 2× 50 mL CHCl₃. The organic fractions were combined and dried with anhydrous MgSO₄, filtered, and then purified using column chromatography on 200-400 mesh silica gel

(DCM to remove excess PTZ, then 10% ethyl acetate in DCM). The desired product was isolated as a tan-colored oil. ^1H NMR in CDCl_3 , δ in ppm: 8.59 (2H, d), 8.24 (2H, s), 7.15 (10H, m), 6.90 (8H, m), 3.87 (4H, t), 2.69 (4H, t), 1.83 (4H, m), 1.70 (4H, m), 1.44 (12H, m).

Synthesis of Ruthenium Dyes. RD1, RD2, and Z-907 were synthesized as follows using the original Z-907 preparation as a guide.¹³ Two equivalents of the desired ligand (477-PTZ, 43-PTZ, or 4,4'-dinonyl bipyridine respectively) and one equivalent of $[\text{RuCl}_2(\text{p-cymene})]_2$ were combined in DMF under N_2 and allowed to stir at ca. 70 °C for four hours. Two equivalents of dcbpy were added and the reaction temperature was increased to 140-150 °C. The reaction gradually turned black after another four hours of stirring. A large excess (ca. 20× equiv.) of NH_4SCN was then added and the reaction was allowed to stir for another four hours. DMF was removed by rotary evaporation and the products were re-dissolved in DCM and filtered. The first dye synthesized in this manner was RD1 and was initially used without further purification. Preliminary results (see Results and Discussion) suggested that further purification was required, and RD1, RD2, and Z-907 were all subjected to chromatography on 200-400 mesh silica gel columns. For RD1 and RD2, elution was with a solvent mixture of 93% DCM, 5% ethanol, and 2% acetic acid by volume. For Z-907, elution was with a $\text{CHCl}_3/\text{EtOH}$ mixed solvent where the proportion of ethanol was gradually increased from 0% to 100% by volume.

DSC Testing. Bare photoanodes were prepared as previously described in Chapters 2-4. Photoanodes were dyed in 0.5-2.0 mM solutions; 90/10 DCM/EtOH (v/v) for RD1, neat MeOH for RD2, or 80/20 $\text{CHCl}_3/\text{EtOH}$ (v/v) for Z-907. All anodes were dyed for at least 24 hours but no longer than one week due to the possibility of long-term surface equilibria (e.g., aggregation) resulting in reduced cell performance. Mediators consisted of 0.135 M $[\text{Co}(\text{LL})_3]^{2+}$, 0.015 M $[\text{Co}(\text{LL})_3]^{3+}$, 0.2 M lithium triflate, and 0.2 M 4-*tert*-butylpyridine (TBP) in γ -butyrolactone,

where LL = 4,4'-di-*tert*-butyl-2,2'-bipyridine (DTB) or 2,2'-bipyridine (bpy). Initial experiments on unpurified RD1 dye were conducted with photoanode and an unmodified gold-on-glass cathode separated by a 25 micron spacer. All other cells were constructed with photoanode and 200 nm gold-on-chromium-on-FTO cathode separated by a 25 micron spacer. In these latter cases, the cathode remained the same throughout and was also modified by dilute aqueous Na₂S as described previously.¹⁴ The mediator was introduced to the edge of the cathode and wicked in through capillary forces. All anodes were pretreated for approximately 10 minutes by exposing them to DTB mediator solution (which already contained 0.2 M lithium triflate/TBP) in order to increase reproducibility. This procedure is adapted from one utilized by Ondersma and Hamann in which anodes were pre-treated in 0.1 M LiClO₄ overnight.¹⁵

Kinetic Measurements. Transient absorption (TA) measurements were used to evaluate recombination kinetics involving injected electrons. A 530 nm OPO laser (Opotek, ca. 30 mW, 20 Hz) was used to excite a pseudo-photoanode consisting of a 3× layer of dyed TiO₂ on a microscope slide. A 100 W xenon arc lamp (Oriel) beam oriented at 45° to the pump beam was used as the probe. A 5 kΩ resistor was connected in parallel with the 1 MΩ input impedance (for a total input impedance of ca. 4975 Ω) on a Tektronix TDS 620B oscilloscope to obtain signal gain at a cost of time resolution. Detection was accomplished with a Hamamatsu R2496 photomultiplier tube attached to the exit slit on a monochromator. Data points are the result of at least 500 averages. Measurements were conducted either with no mediator, in which a drop of 0.2 M lithium triflate / 0.2 M TBP solution in γ-butyrolactone was sandwiched between the pseudo-photoanode and a slide cover, or with mediator where 0.135 M of the appropriate [Co(LL)₃]²⁺ complex was part of the solution as well. The oxidized component of the active

redox couple was not needed in these cases since it would only serve to capture photo-injected electrons.

Results and Discussion

The redox potential of the PTZ donor is more or less invariant past three methylene linkages³, so it can be safely assumed that the driving force for regeneration of the Ru(II) center is approximately equivalent in both RD1 and RD2. RD1 was designed to be very hydrophobic with long alkyl chains extending out into solution. The lengths of these chains were chosen to mimic those in Z-907, where nonyl chains serve to increase long-term stability in the presence of water (ostensibly by preventing SCN⁻ loss).¹³

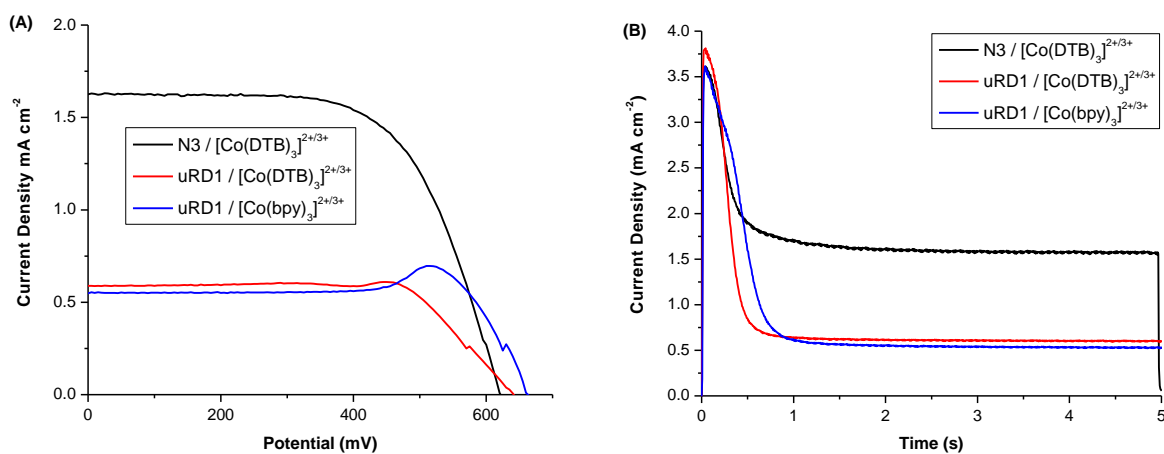


Figure 5.2. J-V curves (A) and current transients (B) for N3 and impure RD1 (uRD1) dyes mediated by cobalt polypyridyl complexes. The [Co(DTB)₃]^{2+/3+} mediator was identical for both N3 and uRD1 cells. The cathode employed was a gold-on-chromium-on-glass film. The drastic differences in J_{SC} values between N3 and uRD1 coupled with similar initial current values in the current transients indicate a severe mass transport limitation of the mediator through the TiO₂ film.

Initially, RD1 was left unpurified with the belief that workup was sufficient to isolate the desired complex in large quantity relative to any impurities. TLC indicated several impurities,

one of which did not move off the origin of the plate. These were all highly colored and were clearly other ruthenium complexes, but were substantially less concentrated than the desired product. Two impurities were purple in color, indicating photo-oxidized PTZ. These impurities were even less concerning since, in an operational DSC, these species would be reduced by mediator. At worst, slightly different equilibrium concentrations of reduced and oxidized mediator species would be expected. Still, the identity of the impurities and their steric footprints was unknown. Thus, RD1 was isolated from all impurities as described in the experimental section.

As shown in Fig. 5.2A, J-V curves of unpurified RD1 (uRD1) mediated by several cobalt mediators had universally poor J_{SC} values compared to a $[Co(DTB)_3]^{2+/3+}$ -mediated N3 cell on the same cathode. The origin of the irregular shapes in the $[Co(DTB)_3]^{2+/3+}$ and $[Co(bpy)_3]^{2+/3+}$ RD1 curves is unknown, though they are assuredly dye related since otherwise equivalent cells utilizing N3 dye exhibit normal shapes. Examining the $[Co(DTB)_3]^{2+/3+}$ -mediated cases of RD1 and N3, it appears that although current is poor for RD1, there is a moderate improvement in V_{OC} . Subsequent current transient measurements presented in Fig. 5.2B indicate similar initial currents for both N3 and uRD1 regardless of mediator despite the drastically different J_{SC} values. The steep drop-off in current within a second after light exposure is indicative of mass transport limitation.⁷

The smaller RD2 sensitizer was synthesized as an alternative to RD1. It stands to reason that a larger complex would lead to a more congested surface and hence a greater limitation on current due to mass transport. This is consistent with the behavior observed in Fig 5.2B where an initially high current density rapidly decays to a lower steady-state value. Specifically, it has previously been shown that restricted movement of the *oxidized* cobalt mediator through the

TiO₂ framework negatively affects this steady-state current.⁷ In addition, the mass transport limitation could be compounded not only by the size of the dye itself but also the freedom of movement of the heptyl-PTZ species. Although the mediator should be reducing oxidized PTZs rather than metal centers in the RD1 dye, the chains could possibly kink and create a physical barrier. Furthermore, a PTZ species could be completely buried within a “blanket” of alkyl groups since one is pointed equatorially from the Ru(II) center when bound to the surface. RD2 was thus designed to preserve donor functionality while reducing the footprint of the dye.

Reproduction of results in DSC experiments tends to be tedious even in the simplest systems due to the large number of variables concerning the working operation of the cell. Even with initial results of the purified compound showing great promise, large variations in cell performance were observed with RD1 cells in particular. The presumed reasoning for this is the steric “blanket” that can form along the TiO₂ surface with equatorial heptyl-PTZ chains (*vide supra*). While a similar effect can occur in Z-907 cells, the oxidized ruthenium center is *always* the species being reduced in that case. In RD1, this blanket could serve to physically prevent reduction of the Ru(III) center by PTZ. Indeed, the most common inconsistency in these experiments was the J_{SC}, which one would expect to vary with the rate of regeneration and thus the access of the mediator to the reduction site. Without hole transfer to the PTZ, this site would be the Ru(III) center and the system would essentially be equivalent to an overly bulky case of Z-907.

Thus, the first issue to address is whether oxidation of PTZ by Ru(III) is taking place at all. A convenient means testing for PTZ oxidation is transient absorption spectroscopy (TAS), which has strong literature precedent over the past two decades as a tool in determining the kinetics of various DSC processes.^{16–20} Taking *N*-methyl PTZ as a model system, there is no

appreciable absorption in the visible region for the zero valent form of the compound. However, oxidized *N*-methyl PTZ has a strong absorption ($\epsilon \approx 10,000 \text{ M}^{-1}\text{cm}^{-1}$) near 520 nm.²¹ Thus, any signal due to oxidized PTZ would be washed out by the strong Ru dye bleach in the 400-600 nm region.

Observation at low wavelengths in the absence of mediator (380-420 nm, Fig. 5.3) reveals a small positive absorption signal in the case of RD1 that gradually transitions to the

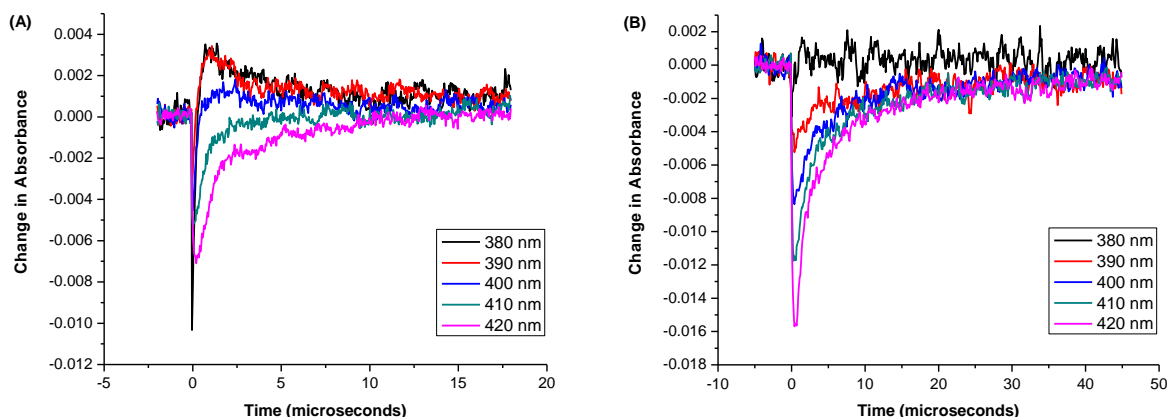


Figure 5.3. Transient absorption spectra of RD1 (A) and Z-907 (B) pseudo-photoanodes in the presence of 0.2 M lithium triflate and TBP in γ -butyrolactone (i.e., “no mediator” control). The significant quenching effect and presence of a positive absorption peak attributed to oxidized PTZ in the RD1 signal are taken as evidence of hole transfer to the PTZ species.

negative bleach signal as monitoring wavelength increases. Since oxidized *N*-methyl PTZ does have a small absorption in this region, the positive signal is consistent with hole transfer to the appended PTZ. Furthermore, this absorption is not observed in the case of Z-907 where PTZ is not present. However, an absorption signal near these wavelengths *has* been reported in the absence of mediator by Boschloo and Hagfeldt for the case of N3 bound to a TiO_2 film.¹⁸ Several attempts to reproduce this result for both N3 and Z-907 proved unsuccessful. Interestingly, addition of mediator solution results in an enhanced absorption signal for RD1 and the growth of a small positive signal for Z-907 as shown in Fig. 5.4. The positive signal for

Z-907 does not have a defined peak-like shape as would be expected and more closely resembles either a shift in baseline or a very long-lived process. Although the latter case cannot be completely ruled out, the signal does not regress back to the original baseline over the entire maximum data collection window (> 1 ms). In addition, the enhanced RD1 signal in 5.4A appears to be largely due to the same type of baseline shift and is somehow related to mediator addition. Any absorbance contribution from the Co complex itself can be ruled out given its low molar extinction coefficient (ca. $100 \text{ M}^{-1} \text{ cm}^{-1}$ for 2+ form), leaving only the dye.

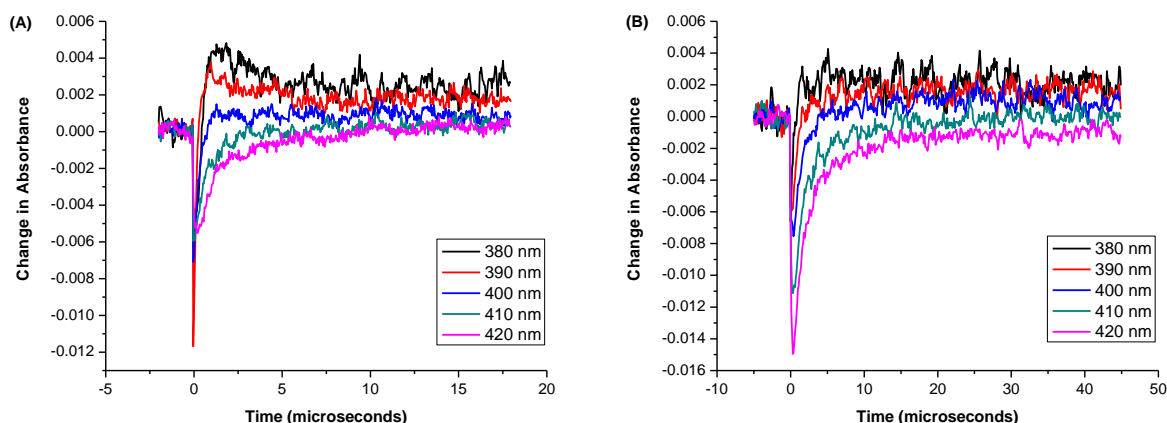


Figure 5.4. Transient absorption spectra of RD1 (A) and Z-907 (B) pseudo-photoanodes in the presence of 0.2 M lithium triflate, 0.2 M TBP, and 0.135 M $[\text{Co}(\text{DTB})_3]^{2+}$ (“with mediator”). The pseudo-photoanodes are the same as in Fig. 5.3, and the photo-active area was kept approximately the same.

Comparing the intensities of the RD1 and Z-907 curves also indirectly supports the case for hole transfer to the PTZ. When mediator is added to either system, the bleach signal is slightly quenched. This is due to the population of oxidized dye being rapidly regenerated by the mediator. When comparing signal intensities between RD1 and Z-907 without mediator, a much larger quenching effect is observed. Specifically, the RD1 bleach signals at the longer wavelengths presented here are up to $> 60\%$ smaller than that of Z-907 in Fig. 5.3A. As with the case of adding mediator, a smaller signal is indicative of regenerated dye. This quenching effect could also in principle be interpreted as being due to a smaller population of the dye being photo-

excited by the laser pulse, but the intensity of the laser at the dye's λ_{max} coupled with the presence of the positive absorption peak at shorter wavelengths makes a more powerful case for regeneration by PTZ.

Having established that hole transfer to the PTZ most likely occurs, detailed solar cell measurements were then conducted in order to further explore this donor-acceptor-type interaction. Strong efforts were made to ensure that each cell was equivalent. Mediator solutions were made fresh before each round of cell testing to combat possible degradation and the same gold cathode was employed throughout. The gold cathode was carefully modified as in Chapter 4 with fresh dilute aqueous Na_2S solution prior to evaluation of each mediator. Each anode was also pretreated with DTB solution to allow lithium triflate and TBP to equilibrate on the TiO_2 surface prior to cell evaluation. Even so, only ca. 50% of RD1 cells exhibited similar behavior. These cells were taken as the “typical” expected behavior and are used below to make meaningful comparisons to other dyes. For the sake of these comparisons, the same conditions apply to all cells using all dyes: fresh mediator, freshly modified cathode, and identical pretreatment regimen.

Fig. 5.5 displays the J-V curves for RD1 (black), RD2 (red), Z-907 (blue), and N3 (cyan) on the same modified gold cathode. These experiments were conducted with both $[\text{Co}(\text{DTB})_3]^{2+/3+}$ (A) and $[\text{Co}(\text{bpy})_3]^{2+/3+}$ (B) mediators. Addressing the DTB curves first, J_{SC} values for PTZ-containing dyes are lower than those for N3 or Z-907. Therefore, it appears that hole transfer to the PTZ does not offer any gains in current. In addition, V_{OC} values appear to be clustered into two separate groups based on similar sensitizer size: N3/RD2 and Z-907/RD1. Cell figures of merit for RD1 are also consistent with a previous study where free PTZ was used as a co-mediator with $[\text{Co}(\text{DTB})_3]^{2+}$ in conjunction with the Z-907 dye.²² As shown in Fig. 5.6,

a delay in dark current onset for Z-907 and RD1 to an overpotential ca. 50 mV greater than that of N3 or RD2 appears to be directly responsible for the increase in V_{OC} . This appears to support the conclusion that exclusion of the oxidized mediator from the TiO_2 surface results in significant improvement in voltage. Alternatively stated, the charge-transfer resistance at the TiO_2 /electrolyte interface increases by preventing $[Co(DTB)_3]^{3+}$ from getting close enough to electronically couple to the surface effectively.

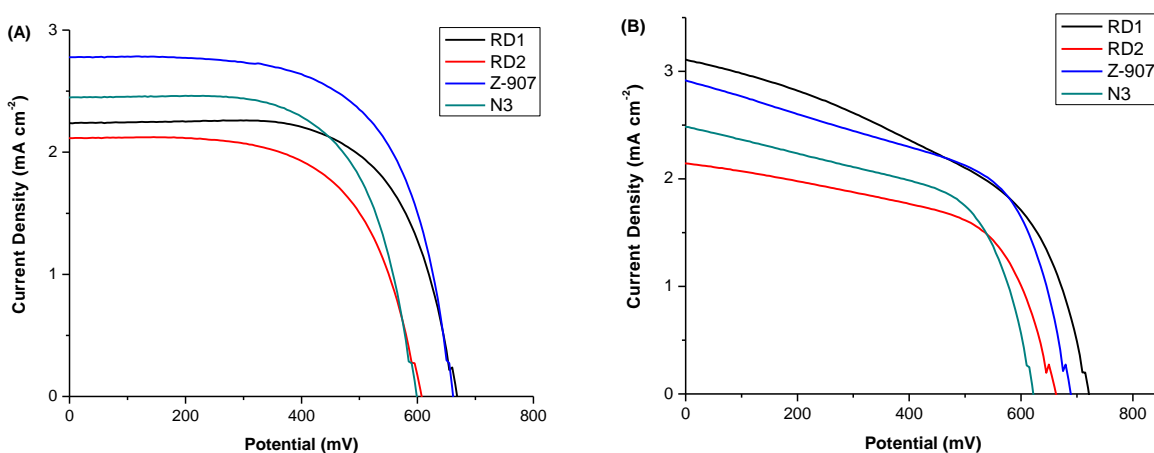


Figure 5.5. J-V curves for ruthenium dyes mediated by $[Co(DTB)_3]^{2+/3+}$ (A) and $[Co(bpy)_3]^{2+/3+}$ (B). Photoanodes for a given dye are the same; photoanodes were first evaluated with $[Co(DTB)_3]^{2+/3+}$, disassembled and rinsed with acetonitrile, then clamped back together and evaluated with $[Co(bpy)_3]^{2+/3+}$. V_{OC} consistently increases when moving between mediators, and fill factors are worse for $[Co(bpy)_3]^{2+/3+}$ -mediated cells.

Note, however, that the dark currents for both RD2 and Z-907 converge at higher potentials, implying a similar impedance to charge transfer even with greater driving force. Combined with electron lifetime data extracted from voltage transient measurements^{23,24} in Fig. 5.7A, it is clear that RD2 has a desirable effect on recombination between injected electrons and $[Co(DTB)_3]^{3+}$. Injected electrons live longer at higher potentials with RD2 than with N3, which can be interpreted as slower recombination involving conduction band electrons.^{23,24} However, surface and bulk trapped electrons live slightly longer with Z-907. This effect can be rationalized in terms of the sensitizer size physically inhibiting electron scavenging by the

oxidized mediator. Electrons live substantially longer when RD1 is the dye regardless of what TiO_2 energetic state they are in, which further supports the notion that hole transfer to a PTZ moiety occurs.

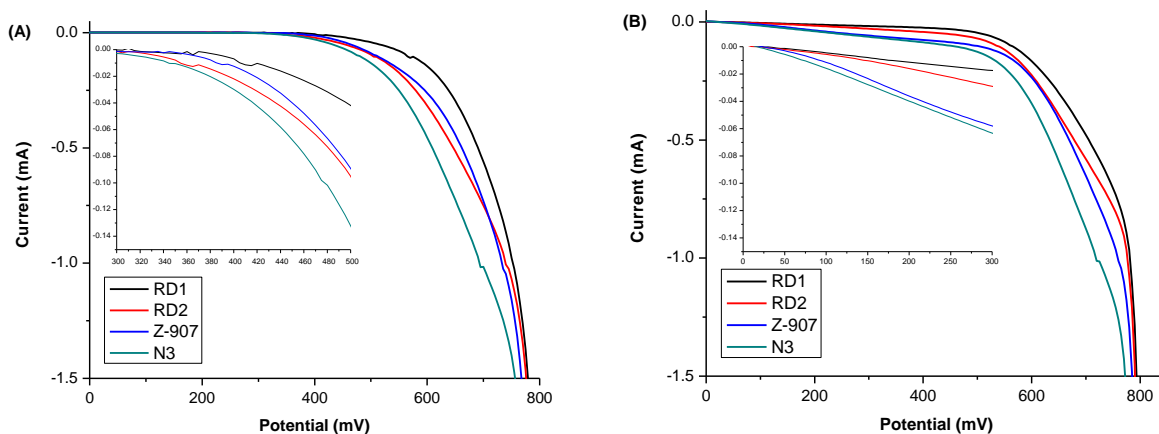


Figure 5.6. Dark J-V plots for the same photoanodes in Fig. 5.5 mediated again by $[\text{Co}(\text{DTB})_3]^{2+/3+}$ (A) and $[\text{Co}(\text{bpy})_3]^{2+/3+}$ (B).

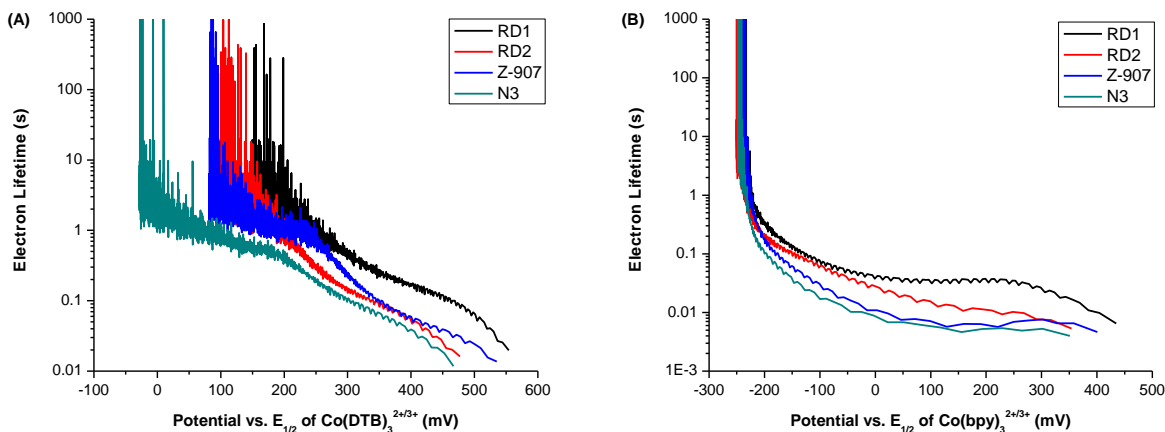


Figure 5.7. Lifetime of injected electrons presented as a function of the driving force for recombination with mediators $[\text{Co}(\text{DTB})_3]^{2+/3+}$ (A) and $[\text{Co}(\text{bpy})_3]^{2+/3+}$ (B). Recombination occurs directly through the TiO_2 conduction band for high voltages, through thermal de-trapping of bulk trap states at intermediate voltages, and through thermal de-trapping of surface trap states at low voltages.

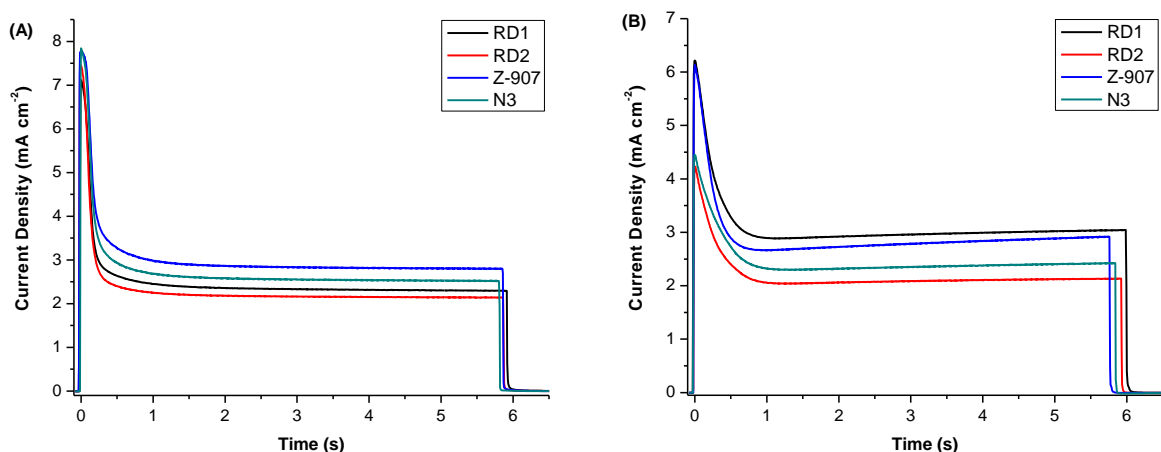


Figure 5.8. Current transient plots of ruthenium dyes mediated by [Co(DTB)₃]^{2+/3+} (A) and [Co(bpy)₃]^{2+/3+} (B). Generally speaking and for a given dye, the peak current initially reached due to the immediate surface concentration of mediator is higher for [Co(DTB)₃]^{2+/3+}. In systems employing a relatively small dye as with N3 or RD2, similar steady-state currents are reached for either mediator. However, in especially sterically hindered systems such as with Z-907 or RD1, [Co(bpy)₃]^{2+/3+}-mediated systems will still exhibit a smaller peak current but a higher steady-state current due to hampered recombination from injected TiO₂ electrons.

Current transients for the four dyes are presented in Fig. 5.8 when coupled with [Co(DTB)₃]^{2+/3+} (A) and [Co(bpy)₃]^{2+/3+} (B) mediators. Again addressing only the [Co(DTB)₃]^{2+/3+} case for now, all four dyes reach similar peak currents but decay to various steady-state currents. This translates to similar IPCE values (ca. 55%, data not shown) but very different J_{SC} values in the J-V curves presented in Fig. 5.5A. Argazzi et al. briefly discussed the highly efficient electron transfer between TiO₂ injected electrons and oxidized PTZ, which limited the current efficiencies of their [Ru(LL)₃]²⁺ dyes coupled with solution-free PTZ.¹⁰ It appears this issue motivated the appendage of PTZ to the dye by a short methylene linkage, which resulted in more respectable IPCE values. RD1 and RD2, however, have heptyl and propyl linkages, respectively. One might then expect substantial current losses from direct scavenging by oxidized PTZ in these systems. On the other hand, the electron lifetime data in Fig. 5.7A seems to contradict this possibility, especially in the case of RD1 (which would also be

expected to have the highest degree of electron scavenging given the size and flexibility of the linkage).

A more plausible explanation lies in the likelihood of inefficient dye regeneration by PTZ. Previous studies on D-C-A triads involving $[\text{Ru}(\text{LL})_3]^{2+}$ -type complexes demonstrated a maximum Φ_{CSS} centered around $n = 4$ methylene linkages.¹ Unfortunately, the Φ_{CSS} drops by ca. 50% when $n = 3$ or $n = 7$ (as in the cases of RD2 and RD1, respectively).¹ This electron transfer was also found to exponentially decrease with increasing donor-acceptor distance in conjugated donor-bridge-acceptor complexes linked by 1-4 *p*-xylene species.²⁵ Inefficient regeneration would explain the lower steady-state currents in Fig. 5.8A for RD1/RD2 relative to Z-907/N3, as oxidized dye cannot participate in further electron injection.

Donor effects are far more pronounced when the dyes are coupled with a $[\text{Co}(\text{bpy})_3]^{2+/3+}$ mediator solution. $[\text{Co}(\text{bpy})_3]^{2+/3+}$ is smaller and less lipophilic than $[\text{Co}(\text{DTB})_3]^{2+/3+}$ and can therefore better navigate the TiO_2 /lipophilic dye network. In addition, electron transfer to $[\text{Co}(\text{bpy})_3]^{2+/3+}$ is adiabatic unlike $[\text{Co}(\text{DTB})_3]^{2+/3+}$. Generally this is a nuisance due to its far more efficient electron scavenging with injected electrons, but in this case it allows a further deconvolution of effects due to mass transport versus hole transfer.

J-V curves for $[\text{Co}(\text{bpy})_3]^{2+/3+}$ cases are presented in Fig. 5.5B. Fill factors are universally poorer than $[\text{Co}(\text{DTB})_3]^{2+/3+}$ due to the aforementioned efficient recombination. Generally, better fill factors are observed as the cells are exposed to light over long times at open circuit while J_{SC} and V_{OC} remain largely unaffected. This allows the forward injection rate and the backward recombination rate to equilibrate. However, this can take hours in some cases and as such the cells were only light-soaked for 15 minutes to better compare with $[\text{Co}(\text{DTB})_3]^{2+/3+}$ cells. Interesting, the RD1 trace in Fig. 5.5B exhibits a ca. 33% increase in current relative to

that of the similar $[\text{Co}(\text{DTB})_3]^{2+/3+}$ case in Fig. 5.5A. Z-907 coupled with $[\text{Co}(\text{bpy})_3]^{2+/3+}$ also exhibits a slight current increase over that of $[\text{Co}(\text{DTB})_3]^{2+/3+}$. That this increase is fairly small indicates that limiting the mass transport of $[\text{Co}(\text{bpy})_3]^{3+}$ to the TiO_2 surface cannot be solely responsible.

The origins of the voltage increases in Fig. 5.5B are fundamentally different than in Fig. 5.5A. The $2+/3+$ redox couple for $\text{Co}(\text{bpy})_3$ lies ca. 150 mV more positive than that of $\text{Co}(\text{DTB})_3$, which should translate to an increase in the maximum achievable V_{OC} but also an increase in the overpotential for electron recombination with injected electrons. In the absence of appended PTZ, the V_{OC} for Z-907 and N3 appears to increase by approximately 25 mV relative to Fig. 5.5A, which can be taken as an effect of the positively shifted mediator redox potential. However, RD1 and RD2 systems both exhibit a ca. 55 mV increase relative to Fig. 5.5A. Thus, hole transfer to the PTZ appears to be responsible for an approximate 30 mV increase in V_{OC} . Dark currents in Fig. 5.6B reflect this as well, with the onset of appreciable negative current being shifted to significantly higher overpotentials in the presence of an appended PTZ donor. For instance, for -20 μA to flow through the cell mediated by $[\text{Co}(\text{bpy})_3]^{2+/3+}$, the RD1 system requires 150 mV more driving force than the Z-907 system. Indeed, Z-907 and N3 both exhibit significant current with nearly no overpotential whatsoever.

Unsurprisingly, TiO_2 electron lifetimes are very short in all $[\text{Co}(\text{bpy})_3]^{2+/3+}$ cases presented in Fig. 5.7B due to efficient electron scavenging by $[\text{Co}(\text{bpy})_3]^{3+}$. Nevertheless, it is clear that lifetimes are prolonged in the cases where a PTZ species is present. Interestingly, lifetimes for RD2 systems are generally longer than those of Z-907 systems, indicating the larger electron-hole distance has a greater effect than simply blocking the surface. Still, it should be emphasized again that these effects are not mutually exclusive. Indeed, as in the $[\text{Co}(\text{DTB})_3]^{2+/3+}$

case, RD1 exhibits greatly enhanced lifetimes in the presence of $[\text{Co}(\text{bpy})_3]^{2+/3+}$ due to the combination of both electron donor presence *and* sensitizer lipophilicity.

Current transients for $[\text{Co}(\text{bpy})_3]^{2+/3+}$ -mediated cells (Fig. 5.8B) are also qualitatively different than current transients for $[\text{Co}(\text{DTB})_3]^{2+/3+}$ (Fig. 5.8A). RD1 and Z-907 appear to have clustered peak and steady-state current values, as do Z-907 and N3. Because $[\text{Co}(\text{DTB})_3]^{2+/3+}$ has built-in insulation in the form of *t*-butyl groups and exhibits relatively slow recombination with injected electrons, the size of the dye does not have a dramatic effect on the peak current. This is not so for $[\text{Co}(\text{bpy})_3]^{2+/3+}$, which is why peak current for a PTZ-appended dye only reaches that of Z-907 when it is also of approximate size to Z-907. When the dye is not of sufficient bulk to suitably inhibit access of $[\text{Co}(\text{bpy})_3]^{3+}$ to the TiO_2 surface, the presence of the donor has very little effect on peak current.

On the other hand, the steady-state current is another matter entirely. Peak currents for $[\text{Co}(\text{DTB})_3]^{2+/3+}$ are always greater than those of $[\text{Co}(\text{bpy})_3]^{2+/3+}$ for a given dye because of slow recombination. These conditions are reflective only of the localized presence of reduced mediator in proximity to the dyed TiO_2 surface. When the light is abruptly cycled on, the mediator is thus positioned at the surface to regenerate all excited dye species and yield the maximum achievable current. Immediately following this, the now-oxidized mediator must diffuse out of the mesoporous layer and to the cathode. Therefore, the steady-state current reflects the mass-transport limited current. Because $[\text{Co}(\text{bpy})_3]^{2+/3+}$ is so much smaller than $[\text{Co}(\text{DTB})_3]^{2+/3+}$, the steady-state current values of $[\text{Co}(\text{bpy})_3]^{2+/3+}$ cells are always higher than those of otherwise equivalent $[\text{Co}(\text{DTB})_3]^{2+/3+}$ cells. IPCE values for $[\text{Co}(\text{bpy})_3]^{2+/3+}$ are generally lower than $[\text{Co}(\text{DTB})_3]^{2+/3+}$ values for a similar cell and can be somewhat misleading since those conditions reflect light levels at which mass transport limitations have not set in and

current is instead limited by photon flux. Thus, current transients were elected to more appropriately compare the behavior of the chosen dyes with the two mediators.

Future Directions

Although the effect of an appended donor moiety in these systems is apparent, additional studies would serve to further separate that effect from that imposed by simple sterics. Previous electrochemical studies by Nelson et al. with custom-made rotating disk electrodes (RDEs) were responsible for the realization that cell current was limited by mass transport of oxidized Co complexes.⁷ These electrodes consisted of TiO_2 films on platinized glass which were masked to roughly circular area and encased in Teflon. Cobalt species were thus forced to navigate the mesoporous framework to be reduced or oxidized as shown in Fig. 5.9.

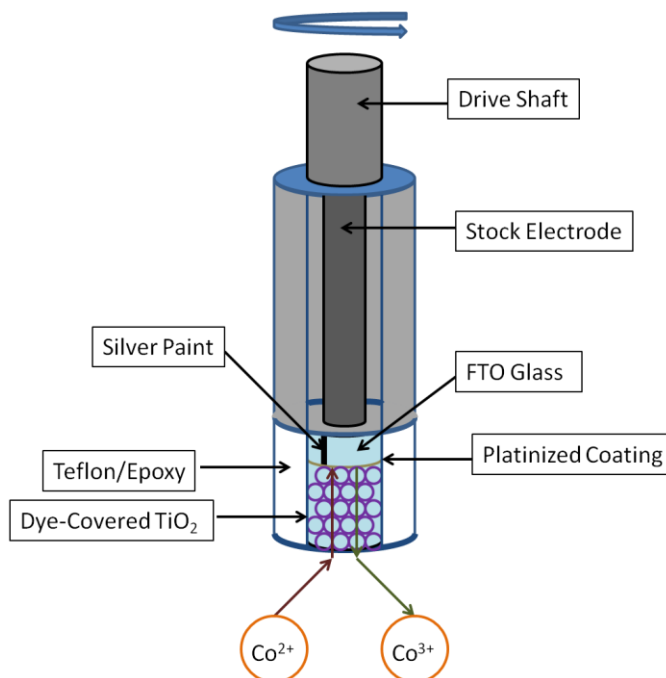


Figure 5.9. Schematic representation of a custom rotating disk electrode. A photoanode is imbedded within Teflon or epoxy and electrically connected to a stock RDE via conductive paint. The photoanode is then dyed and the diffusion coefficient of a cobalt mediator complex can be determined.

The study by Nelson et al. was performed with bare TiO₂ as opposed to dyed. The diffusion coefficients obtained for cobalt species in this manner most likely vary slightly from those in a working DSC due to the additional pore space occupied by dye molecules. By taking an electrode of this type and dyeing it, the diffusion of the cobalt complexes through the TiO₂/lipophilic dye framework can be evaluated. This dye can then be stripped and the electrode can be re-dyed in another sensitizer. The dye would have no function in these experiments other than inhibiting mass transport of cobalt complexes through the framework, and thus this would be a “dark” experiment. As with linear sweep voltammetry, the voltage would be scanned and the current measured. On an ideally planar RDE, the limiting current measured for the process $\text{Co}^{2+} \rightarrow \text{Co}^{3+} + \text{e}^-$ is given by Eq. 5.1:

$$i_l = nFADC\omega^{1/2}\nu^{-1/6} \quad \text{Equation 5.1}$$

where n is the number of electrons involved in the process (1 in the case of $\text{Co}^{2+/3+}$), F is the Faraday constant, A is the active area of the electrode, D is the diffusion coefficient, ω is the angular velocity of the electrode, ν is the kinematic viscosity of the solvent, and C is the initial concentration of Co^{2+} . By conducting the experiment at several rotation speeds, a Levich plot (i vs. $\omega^{1/2}$) can be constructed. The slope of this plot can subsequently be used to find the diffusion coefficient of the cobalt complex. Given the results presented above, the expectation in such an experiment would be that diffusion of a particular cobalt complex through RD1 and Z-907-dyed anodes would be similarly slow, and diffusion through RD2 and N3-dyed anodes would be similarly fast.

The mass transport limitation on current is only problematic when focusing on mediator species that are large enough to have mobility issues through the TiO₂ framework. An obvious method of decoupling donor and mass transport effects is to use the I^-/I_3^- couple, which does not

generally exhibit any limitations due to size. This experiment was attempted with a homemade mediator solution but resulted in strangely shaped J-V curves indicative of large charge transfer resistance on both Pt film and platinized FTO (which have both performed well in the past). Additives and solvent were the same purity as those used in cobalt mediators. Repetition of this experiment for all dyes using a commercially available standardized I^-/I_3^- mediator should serve to highlight the effect of larger electron-hole separation.

Branching out beyond the current selection of dyes, it would also be beneficial to investigate PTZ-appended Ru(II/III) sensitizers with more optimal linkages (ie., $n = 4$ or 5). If quantum yield increases by ca. 50% as with the D-C-A cases¹, then it should have a noticeably positive impact on J_{SC} . In addition, TAS studies would show a more pronounced peak at low wavelength monitoring and a more remarkable quenching effect on the dye bleach throughout most of the visible region.

Conclusions

N3-like dyes with appended PTZ moieties were evaluated against both N3 and Z-907. Hole transfer from Ru(III) to PTZ was observed in both RD1 and RD2 cells, though the effects are subtle and do not necessarily translate to improved cell performance. The most noticeable improvements occurred when $[Co(bpy)_3]^{2+/3+}$ was employed, where photovoltage was improved when a PTZ species was bound to the dye. When recombination is limited via steric congestion of the TiO_2 surface by the sensitizer (as with the long heptyl tethers on RD1) and when coupled with $[Co(bpy)_3]^{2+/3+}$, the greater electron-hole distance also results in increased photocurrent. Specifically, RD1 coupled with $[Co(bpy)_3]^{2+/3+}$ exhibits 33% more photocurrent than when coupled with $[Co(DTB)_3]^{2+/3+}$. Barring this specific circumstance, observed photocurrents of

PTZ-containing sensitizers are generally lower than those without PTZ. This is tentatively attributed to inefficient hole transfer to the PTZ based on past studies with similar D-C-A complexes.¹ Additional studies are proposed to further elucidate the role and efficiency of PTZ in these dyes. The most promising of these experiments involves custom rotating disk electrodes that will allow the direct measurement of the mediator diffusion coefficient through the dyed TiO₂ film.

Chapter 5 References

- (1) Larson, S. L.; Elliott, C. M.; Kelley, D. F. *J. Phys. Chem.* **1995**, *99*, 6530–6539.
- (2) Cooley, L. F.; Larson, S. L.; Elliott, C. M.; Kelley, D. F. *J. Phys. Chem.* **1991**, *95*, 10694–10700.
- (3) Larson, S. L.; Elliott, C. M.; Kelley, D. F. *Inorg. Chem.* **1996**, *35*, 2070–2076.
- (4) Weber, J. M.; Rawls, M. T.; MacKenzie, V. J.; Limoges, B. R.; Elliott, C. M. *J. Am. Chem. Soc.* **2007**, *129*, 313–320.
- (5) Ashbrook, L. N.; Elliott, C. M. *J. Phys. Chem. C* **2013**, *117*, 3853–3864.
- (6) Hagfeldt, A.; Boschloo, G.; Sun, L.; Kloo, L.; Pettersson, H. *Chem. Rev.* **2010**, *110*, 6595–6663.
- (7) Nelson, J. J.; Amick, T. J.; Elliott, C. M. *J. Phys. Chem. C* **2008**, *112*, 18255–18263.
- (8) Daeneke, T.; Kwon, T.-H.; Holmes, A. B.; Duffy, N. W.; Bach, U.; Spiccia, L. *Nat. Chem.* **2011**, *3*, 213–217.
- (9) Klahr, B. M.; Hamann, T. W. *J. Phys. Chem. C* **2009**, *113*, 14040–14045.
- (10) Argazzi, R.; Bignozzi, C. A.; Heimer, T. A.; Castellano, F. N.; Meyer, G. J. *J. Phys. Chem. B* **1997**, *101*, 2591–2597.
- (11) Nazeeruddin, M. K.; Kay, A.; Rodicio, I.; Humphry-Baker, R.; Mueller, E.; Liska, P.; Vlachopoulos, N.; Grätzel, M. *J. Am. Chem. Soc.* **1993**, *115*, 6382–6390.
- (12) Sapp, S. A.; Elliott, C. M.; Contado, C.; Caramori, S.; Bignozzi, C. A. *J. Am. Chem. Soc.* **2002**, *124*, 11215–11222.
- (13) Wang, P.; Zakeeruddin, S. M.; Moser, J. E.; Nazeeruddin, M. K.; Sekiguchi, T.; Grätzel, M. *Nat. Mater.* **2003**, *2*, 402–407.

- (14) Ashbrook, L. N.; Elliott, C. M. *J. Phys. Chem. C* **2014**, *118*, 16643–16650.
- (15) Ondersma, J. W.; Hamann, T. W. *Langmuir* **2011**, *27*, 13361–13366.
- (16) Nusbaumer, H.; Moser, J.-E.; Zakeeruddin, S. M.; Nazeeruddin, M. K.; Grätzel, M. *J. Phys. Chem. B* **2001**, *105*, 10461–10464.
- (17) Boschloo, G.; Hagfeldt, A. *Inorganica Chim. Acta* **2008**, *361*, 729–734.
- (18) Boschloo, G.; Hagfeldt, A. *Chem. Phys. Lett.* **2003**, *370*, 381–386.
- (19) Tachibana, Y.; Moser, J. E.; Grätzel, M.; Klug, D. R.; Durrant, J. R. *J. Phys. Chem.* **1996**, *100*, 20056–20062.
- (20) Kuciauskas, D.; Freund, M. S.; Gray, H. B.; Winkler, J. R.; Lewis, N. S. *J. Phys. Chem. B* **2001**, *105*, 392–403.
- (21) Rawls, M. T.; Kollmannsberger, G.; Elliott, C. M.; Steiner, U. E. *J. Phys. Chem. A* **2007**, *111*, 3485–3496.
- (22) Cazzanti, S.; Caramori, S.; Argazzi, R.; Elliott, C. M.; Bignozzi, C. A. *J. Am. Chem. Soc.* **2006**, *128*, 9996–9997.
- (23) Bisquert, J.; Zaban, A.; Greenshtein, M.; Mora-Seró, I. *J. Am. Chem. Soc.* **2004**, *126*, 13550–13559.
- (24) Zaban, A.; Greenshtein, M.; Bisquert, J. *Chem. Phys. Chem.* **2003**, *4*, 859–864.
- (25) Hanss, D.; Wenger, O. S. *Inorg. Chem.* **2009**, *48*, 671–680.